A COLLISIONAL DAMPING INTERFACE FOR A TIME-OF-FLIGHT MASS SPECTROMETER WITH BOTH ELECTROSPRAY IONIZATION AND MATRIX ASSISTED LASER DESORPTION IONIZATION

BY

ANDREW KRUTCHINSKY

A Thesis
Submitted to the Faculty of Graduate Studies
in partial Fulfillment of the Requirements
for the Degree of

DOCTOR OF PHILOSOPHY

Department of Physics
University of Manitoba
Winnipeg, Manitoba, Canada

THE UNIVERSITY OF MANITOBA

FACULTY OF GRADUATE STUDIES

*****

COPYRIGHT PERMISSION PAGE

A COLLISIONAL DAMPING INTERFACE FOR A TIME-OF-FLIGHT MASS SPECTROMETER WITH BOTH ELECTROSPRAY IONIZATION AND MATRIX ASSISTED LASER DESORPTION IONIZATION

BY

ANDREW KRUTCHINSKY

A Thesis/Practicum submitted to the Faculty of Graduate Studies of The University of Manitoba in partial fulfillment of the requirements of the degree of

DOCTOR OF PHILOSOPHY

ACKNOWLEDGMENTS

I am very grateful to Dr. Standing, my advisor and my teacher, who taught me clear and logical thinking which helped me greatly in formulating the experiments. He responded to my wish to complete a Ph.D. program, invited me at his lab and supported me by many means during my education. I am very grateful for the fruitful idea of the collisional damping interface that was introduced to me by my advisor, the concept of which became the key part of my thesis. Being close to finishing my Ph. D. program, I am very proud to think that I belong to the Manitoba mass spectrometry school whose driving force has always been Dr. Standing.

I am also grateful to Dr. Ens who always supported my ideas and encouraged me to find the way to realize many of them. The discussions of many questions with him and his advice have clarified many problems.

I would like to thank Dr. Verentchikov, who was largely responsible for the design and coupling an ESI source to the existing TOF III mass spectrometer in orthogonal configuration. I also thank Dr. Chernushevich for sharing his experience accumulated during operating this wonderful instrument. The ion interface of the mass spectrometer has been modified several times - Dr. Chernushevich, Vic Spicer and Dr. Loboda helped me a lot in these modifications. Victor Spicer, my friend, has been always supportive - his ingenious computer and electronics skills are the part of successful operating of many instruments in the lab, including MANITOBA TOF III mass spectrometer.

Dr. Duckworth's valuable advice was directing and correcting our efforts in investigation of some large noncovalent complexes. I am thankful to my closest co-worker, Dr. Ayed and other colleagues - Dr. Donald, Dr. Potier, Gillian Sadler, for very efficient cooperation which resulted in series of interesting findings in the study of noncovalent complexes, the area of long mutual interest of both Dr. Standing's and Dr. Duckworth's laboratories at the Physics and Chemistry Departments.

Whenever something was broken and had to be repaired, replaced or built within very short period of time, Mr. Roy was irreplaceable. I am grateful to him for his constant readiness to help in this matter.

My very special thanks to all who are always in my heart - my beloved wife Marina and my newborn daughter Anastasia. I am indebted to my and my wife's parents for their love, support and prayers.

ABSTRACT

A collisional damping interface for orthogonal injection of either electrospray ionization (ESI) or matrix-assisted laser desorption/ionization (MALDI) ions into a reflecting TOF mass spectrometer (MANITOBA TOF III) has been designed. Ions produced by either ESI or MALDI are injected into an RF-quadrupole ion guide operating at pressure ~70mTorr. As they pass through the quadrupole their motion is constrained by the RF field. Meanwhile, they lose energy by collisions with the buffer gas molecules. Computer simulations and experiments performed in the instrument with the new interface indicate that collisional cooling of ions improves the quality of the primary ion beams orthogonally injected into the mass spectrometer. Important characteristics of the mass spectrometer, such as resolution and sensitivity were greatly improved. In addition, mass discrimination was reduced, providing an observable mass range greater than 1 MDa with an electrospray ion source and up to ~12,300 Da with a MALDI ion source. These improvements appeared to be very useful for the study of large biological compounds, noncovalent complexes in particular. The results of investigation of several noncovalent complexes are presented to illustrate the capabilities of the instrument with the new interface. The system studied consist of *Escherichia coli* citrate synthase dimers and hexamers interacting with an allosteric inhibitor, the reduced form of nicotinamide adenine nucleotide.

CONTENTS

II. MANITOBA TOF III MASS SPECTROMETER

III. COLLISIONAL DAMPING INTERFACE FOR AN ESI-TOF MASS SPECTROMETER

LIST OF FIGURES

LIST OF TABLES

I. INTRODUCTION

Background

Over the last ten years, mass spectrometry has emerged as one of the major analytical tools in biotechnology and biochemistry. This is mainly a result of the invention of two new ionization techniques for large and thermally labile biomolecules, electrospray ionization (ESI) and matrix-assisted laser desorption/ionization (MALDI) [Chait & Kent 1992; Andersen et al., 1996]. Both ESI [Fenn et al., 1989; Smith et al., 1991] and MALDI [Hillenkamp et al., 1991] have proven to be very effective for ionization and transfer into the gas phase of many biological compounds. However, the ion beams produced by the two methods have very different characteristics, and consequently different types of mass analyzer have been utilized to examine the ions. Since MALDI normally uses a pulsed laser to desorb the ions from the plane of the target, it is conveniently coupled to time-of-flight (TOF) mass spectrometers, which require a well-defined start time and well-defined initial ion position. On the other hand, ESI produces a continuous beam of ions. Like other continuous ion sources, it is more compatible with mass spectrometers that themselves operate in a continuous fashion, such as quadrupole mass filters and sector-field instruments; it was also coupled to quadrupole ion traps. Both methods have comparative advantages and disadvantages, and nowadays many laboratories have separate mass spectrometers configured with ESI and MALDI sources, which enable the mass specrometrists to obtain complementary information from ESI and MALDI mass spectra [see, for example, Yates, 1998].

ESI

Discovery and development of ESI

Spraying solutions in a strong electrical field is a well-known process [see, for example, Hines, 1966]. It was Dole and co-workers, who for the first time explicitly showed that it is possible to introduce intact ions of macromolecules into the gas phase directly from solution using an electrospray source and a simple vacuum system with a Faraday detector [Dole et al., 1968; Mack et al., 1970]. However, only after coupling ESI with quadrupole [Iribarne et al., 1983; Yamashita & Fenn, 1984; Aleksandrov et al., 1984; Covey et al., 1988], magnetic sector [Aleksandrov et al., 1984] and Fourier transform ion cyclotron resonance mass spectrometers (FT-ICR-MS) [Henry et al., 1991] was the potential of the technique for ionization of large non-volatile molecules explored in greater depth. Application of ESI to a wide variety of large molecules such as poly(ethylene) glycols with mass up to 17,500 Da and proteins up to 133,000 Da presented convincing experimental evidence of the power of the technique [Fenn et al.,1989; Covey et al., 1988].

An ESI source assembly

The essential details of a conventional atmospheric pressure ESI source are shown in Figure 1. A solution containing an analyte is delivered through a thin conducting capillary typically ~100 μm ID sharpened at its tip. A strong electric field on the order of ~ 10^4-10^5 V/cm is created at the end of the tip by applying high voltage (~ 2-5 kV) between to the capillary and a counter electrode distanced from the tip usually by ~ 1cm.

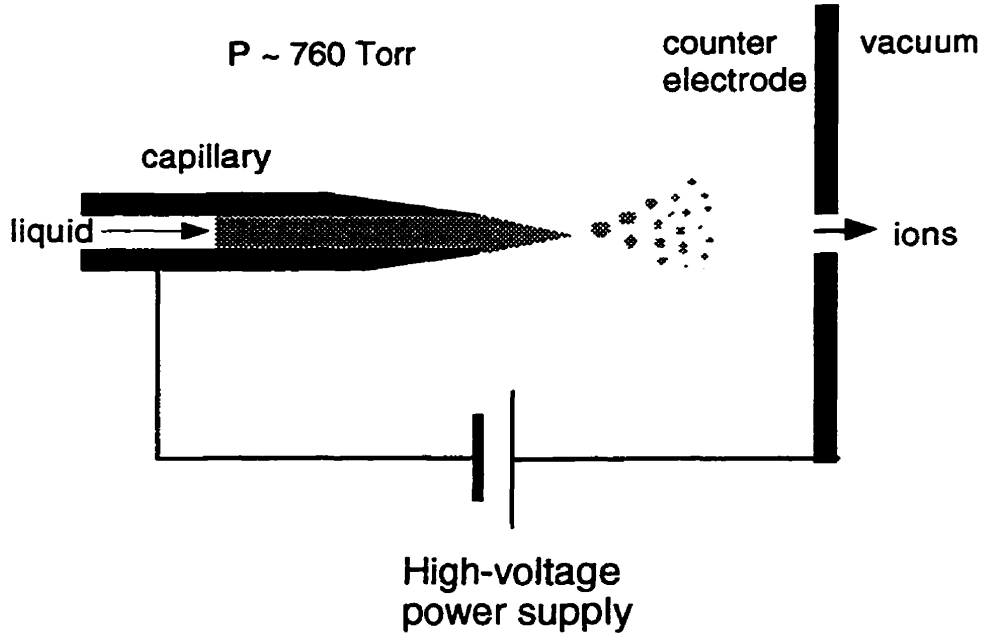

Figure 1. Schematic diagram of a typical electrospray ion source.

The polarity of the applied voltage determines the sign of the ions formed, i.e. positive or negative mode of ion source operation. The high electric field causes formation of a sharp meniscus of the liquid at the tip, which emits small droplets of the solution. These droplets undergo evaporation while moving towards a counter electrode, which may have a small orifice. If it does, it can be used to admit ions formed during evaporation process, together with unevaporated droplets and surrounding gas, into the first vacuum chamber of an atmosphere/high vacuum interface, coupling the ion source with a mass spectrometer.

Several modifications have been proposed to improve the performance of a conventional ESI source, which include pneumatically-assisted [Covey et al., 1988] ultrasonically-assisted [Banks et al., 1994], heat-assisted [Ikonomou & Kebarle, 1994], and liquid-sheath ESI sources [Smith et al., 1988]. An addition modification may be of interest - i.e. the heated capillary of Chowdhury et al. [1990]. However, the most interesting improvements have been achieved by scaling down the electrospray capillary. For example, in Dole's original electrospray set-up, the inner diameter of the capillary at the tip was ~180 μm and the operating flow rate of the sprayed liquid was ~ 300 μL/min [Dole et al., 1968]. When the inner diameter of capillary was reduced to a few tens of micro meters (micro-spray technique), this allowed less than one μL of the liquid to be consumed per minute without reduction of the total ion signal in electrospray spectra [Gale & Smith, 1993; Kriger et al., 1995]. However, it was only after introduction of the nano-spray technique [Wilm & Mann 1994], capable of spraying 0.5-1μL of the liquid with a flow rate less than 25 nL/min, that existing ESI sources began to be replaced by the

more powerful nano-spray ion source. Nano-spray sources have found a large area of applications in mass spectrometry of proteins from polyacrylamide gels [Wilm et al., 1996].

Mechanism of ESI

A number of theories have been proposed to explain the mechanism of ion formation from the droplets [see, for example, Kebarle & Tang, 1993]. The most famous among them are Dole's model [Dole et al., 1968], later significantly supplemented by Röllgen [Schmelzeisen-Redeker et al., 1989] and now sometimes referred as single ion droplet theory (SIDT), and the Iribarne and Thomson theory [Thomson & Iribarne, 1979]. The first theory suggests a mechanism in which the process of gradual solvent evaporation from a droplet alternates with a series of Coulomb explosions when the surface tension on the shrunken droplet becomes comparable with the repulsive forces due to the ions inside it. Eventually, in a series of such processes the solvent can be removed leaving an ion in the gas phase. The second theory assumes ion evaporation (emission) from very small and highly charged droplets. The question about the validity of these theories still remains controversial and more evidence for one or another theory is brought up time after time in the literature [Siu et al., 1993, Smith & Light-Wahl 1993]. Although sufficient data to verify any of these theories of ion formation are not yet available, ESI has became one of the most versatile ion sources widely used for mass spectrometry of biomolecules [see, for example, Cole, 1997].

The main properties of ions obtained from an ESI source

ESI is a gentle method of ionization that produces intact, multiply-charged gas-phase ions from solution. ESI of a particular compound usually results in a series of multiply-charged ion peaks which differ by a unit charge in the *m/z*-spectrum. In the positive mode of ion source operation, these peaks are usually formed by proton attachment to the basic sites of a molecule, whereas in the negative mode they arise by proton detachment from acidic sites. The attachment of cations or anions to the sites is a competitive mechanism of ionization but sometimes it seriously interferes with acquisition of meaningful spectra. For example, a large excess of salts in an analyzed solution may considerably spoil the quality of the spectra [Smith et al., 1991]. To avoid this, a sample is usually purified before analysis and the proper conditions are maintained in the solution by using appropriate solvents. However, the concentration of the analyte should be at least a factor of 10 higher than the concentration of non-volatile salts (an empirical requirement for yielding well resolved peaks in *m/z*-spectra). This practically limits the concentration of the analytes used for analysis to the range 10^{-5}-10^{-7} M.

ESI spectra are often obtained from strongly acidic (pH 2-3) or basic (pH 9-11) solutions in the presence of organic solvent denaturants [Mirza & Chait, 1994]. For proteins, such conditions usually cause their denaturation, i.e. the compact native conformation of the protein is destroyed. More sites become available for ionization in

the unfolded protein. A good correlation between the number of basic amino acid residues and the maximum charge state has been observed [Loo et al., 1989, 1990; Guevremont et al., 1991] which indicates, to some extent, the degree of protonation in solution. If the basic residues (Lys, His, Arg, plus the amino terminus) in a protein occurs with approximately equal frequency, the final charge-state will be approximately proportional to the total number of amino acid residues in a protein. Thus, the m/z distribution often remains within a 0-2500 window for a wide variety of proteins with mass up to 130,000 Da [Fenn et al., 1990; Smith et al., 1991]. Apparently these findings have convinced workers for a number of years that a quadrupole mass spectrometer with a corresponding *m/z* range (0-2500 *m/z*) is a suitable choice for analysis of electrosprayed ions. However, for many large proteins such as antibodies and plasma complement components with mass sometimes greater than 100 kDa, the *m/z* range of quadrupole spectrometers is not sufficient [Feng & Konishi, 1992]. Proteins that contain a large number of disulfide bonds may lack any signal in the above specified *m/z* range unless they are denatured by heating the solution in the spray capillary [Mirza et al., 1993] or treating with DTT [Loo et al., 1990; Smith et al., 1991]. Smith et al. hypothesized that causing protein-unfolding by breaking up the disulfide bonds destabilizes the protein native structure and promotes exposure of more ionization sites. The influence of denaturing vs. native conditions on the appearance of the signal in mass spectra of many proteins has been also demonstrated. The ESI spectra of proteins obtained from solutions maintaining non-denaturing conditions exhibit lower charge states and therefore higher m/z values, which reflects the more compact folded structure of a native form.

Observation of noncovalent complexes with ESI-MS

The formation of noncovalent complexes by macromolecules is one of the most important molecular processes in biology. It is intimately involved in such recognition phenomena as enzyme-substrate interaction, receptor-ligand binding, formation of oligomeric proteins, assembly of transcription complexes and formation of cellular structures themselves. Such an activity is very important in carrying out the biological functions.

It has been shown that ESI is gentle enough to preserve the higher order structure of biomolecules, enabling the observation of noncovalently bound complexes [Katta & Chait, 1991; Ganem et al., 1991]. The complexes are usually stable only at $5 < pH < 8$ (near physiological conditions). Many such complexes have high molecular weight, and the m/z produced in ESI sources increases with mass [Loo, 1997; Chernushevich et al., 1996, 1998]. Observation of electrosprayed ions with large m/z poses a problem for most types of mass analyzers. In particular, quadrupole mass spectrometers that are currently available commercially have stated m/z ranges up to 2000 or 4000. The use of a time-of-flight mass analyzer combined with ESI provides an attractive solution to this problem, since TOF instruments have in principle an unlimited m/z range. This is a significant advantage for measurements of ions of large mass, and noncovalent complexes in particular.

MALDI

The concept of using a matrix to assist laser desorption and ionization of large organic molecules was introduced almost simultaneously by two groups: Karas and Hillenkamp [Karas & Hillenkamp, 1988] and Tanaka with co-workers [Tanaka et al., 1988]. The technique allowed mass spectometrists to extend the mass range of the substances analyzed to well beyond 100,000 Da, circumventing many problems related to the original laser desorption experiments in which no matrix has been used [Cotter, 1987]

MALDI Ion Source

Unlike ESI, MALDI produces a pulsed beam of ions. A typical configuration of a MALDI source operating in a positive mode is shown in Figure 2. Samples for mass analysis are prepared on a target and placed into vacuum. Ions are produced by light of high intensity, of a pulsed laser, striking the sample surface. The preparation of a sample is a crucial component of the technique and many factors influence the final MALDI spectra [Cohen & Chait, 1996]. Essentially, a sample is prepared in a such a way that analyte molecules are embedded into a matrix substrate, which assists the ionization and transfer of the molecules into the gas phase during the laser desorption process. The matrix serves several major functions such as isolation of the biopolymer molecules from each other, absorption of energy from laser light, and plays an active role in the ionization process. A large variety of substances for the matrix preparation [Beavis & Chait, 1989; Beavis et al., 1992] including a frozen aqueous matrix [Williams, 1994], have been found

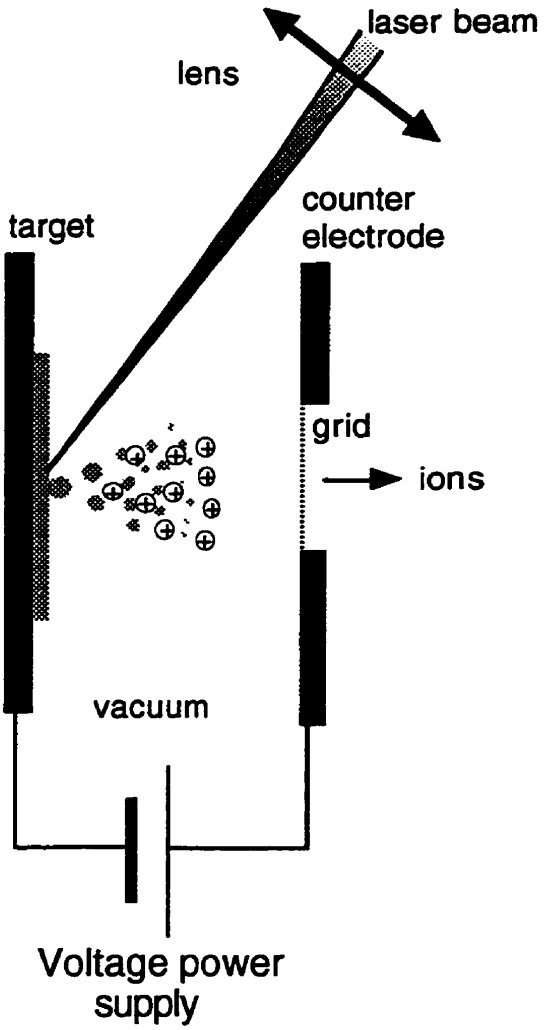

Figure 2. Schematic diagram of a typical MALDI ion source.
A positive mode of ion source operation is shown as an example.

to be suitable for successful MALDI of biomolecules (peptides, proteins, DNA, oligosaccharides etc.) utilizing lasers of different wavelengths: UV and IR [Overberg, et al., 1991; Hillenkamp et al., 1991; Niu et al., 1997; Cramer et al., 1996], and visible light [Williams, 1994].

Properties of MALDI ions and mechanism of ion formation

MALDI is a soft ionization technique capable of producing intact ions of analytes. Ions of relatively small biomolecules, for example peptides, are usually formed by the attachment of one proton in the positive mode or by a proton detachment in negative mode of the ion source operation. Some large organic molecules, such as proteins may acquire more charges in MALDI by multiple protonation or deprotonation [Cramer et al., 1996; Niu et al, 1997; Zhou & Lee, 1995]. The extensive formation of cationated ions can also be observed, especially when the concentration of sodium adducts in the analyte solution is high [Liao & Allison, 1995]. Nevertheless, a MALDI signal is rather tolerant towards the presence of salts and other contaminants with the exception of a number of non-volatile substances [Beavis et al., 1992].

Several mechanisms have been proposed to explain the mechanism of ion formation in MALDI [Hillenkamp et al., 1991; Wang et al., 1993; Vertes, 1992; Johnson et al., 1994]. Almost all theories consider the desorption and ionization processes separately. The key point of any desorption theory is the absorption of the laser energy by the matrix, which results in rapid heating of the sample [Johnson & Sundqvist, 1991]. This heating leads to the ejection of charged and neutral particles of matrix material

containing the analyte molecules [Quist et al., 1994; Ens et al., 1991]. These particles then lose all of their matrix molecules by evaporation, leaving the analyte molecules in the gas phase. Together with the products of desorption, analyte molecules expand into vacuum. It is believed that ion-molecular reactions in the expanding plume account for the ionization of analyte molecules [Wang et al., 1993]. The reactions of protonation or deprotonation are initiated by the photoradical matrix ions formed during the laser desorption process [Liao & Allison, 1995; Ehring & Sundqvist, 1995; Krutchinsky et al., 1995]. The yield of analyte ions produced was found to be very strongly dependent on the power density of the laser radiation, the matrix substrate and the matrix preparation procedure [Zhou et al., 1992].

As with ESI, MALDI has been combined with different types of mass analyzers such as magnetic sector [Annan et al., 1992], ion traps (IT-MS) [Cox, et al., 1992; Qin & Chait 1996], FT-ICR-MS [Buchanan & Hettich, 1993]. However, unlike an ESI source operating in the continuous fashion, a pulsed MALDI source most naturally couples to a TOF mass spectrometer, which is by far the most common analyzer used.

Time-of-Flight Mass Spectrometry

Time-of-flight mass spectrometers operate on the simple principle that ions of equal energy, when injected into a flight path, will separate according to their mass, if no collisions are involved, i.e. if the experiment is performed in vacuum. Starting a clock at the moment of their injection into the flight path and taking measurements at each time an ion packet arrives at the end of it, i.e. at the detector, gives the total flight time for ions of

a particular mass. These measured times can be easily converted to mass values. The first proposal for such a TOF mass spectrometer was made by Stephens [Stephens, 1946] and the experimental evidence for this type of mass spectrometer was given by Cameron and Eggers [Cameron & Eggers, 1948]. Since then, many physicists have contributed to development of TOF mass spectrometry, and "their name is legion" [see, for example, a book by Cotter, 1997 or the extended review on this topic given by Price & Milnes, 1990]. The efforts and the experience accumulated for many years have culminated in increasing performance of the commercially available instruments, combined with the two most important ionization techniques for the study of biopolymers: ESI and MALDI. The rapidly increasing number of TOF mass spectrometers in use by many laboratories worldwide indicates a true renaissance of TOF mass spectrometry.

Injection of ESI Ions into TOF Mass Spectrometers.

In spite of very different initial properties of ion beams produced in ESI and MALDI sources, both ionization techniques can be combined with a TOF mass spectrometer. Coupling is usually performed through different types of interface, which, to variable extent, decouples the ion production and the ion injection into a flight path. In general, ion beams, whether pulsed or continuous, may be introduced into a mass spectrometer in two directions - axial and orthogonal, relative to the axis of an instrument, as shown in Figure 3. It is informative to discuss the different ways of coupling ESI and MALDI ion sources with TOF mass spectrometers in the context of their relative orientations.

Injection of ESI ions in the axial configuration.

Considerable effort has been devoted to searching for efficient methods of coupling continuous ion beams to TOF mass spectrometers. A concept of pulse-time modulation of the continuous ion beam was first applied in a TOF instrument by Bakker [Bakker, 1973, 1974]. A beam of ions, continuously introduced from an ion gun along the axis of the instrument, was first accelerated and then modulated by pulses applied to various deflection plates, so only undeflected ions were detected. A resolution of ~700 was obtained for an instrument of about 1.5 m length, but the overall efficiency of such a technique is low [Yefchak et al., 1990].

To combine an ESI source with a TOF instrument in axial configuration, Boyle and co-workers utilized the concept of ion-storage before pulsing the ions into the flight path [Boyle et al. 1991]. The ions from a conventional ESI source were introduced from atmosphere into vacuum through several stages of differential pumping. In the vacuum chamber of a TOF mass spectrometer, they were decelerated to low kinetic energy in the electric field and then were allowed to fill the spacing between two grids installed at the entrance of a flight tube. After the storage cell between these grids was sufficiently filled up with the ions, an extraction pulse was applied to the end grid to extract ions into a flight path. Unfortunately, this mass spectrometer showed a poor mass resolution ~100 (though it had a short flight tube ~30 cm) because of the large energy spread in the primary ion beam. It is interesting to mention that the idea of axial injection was

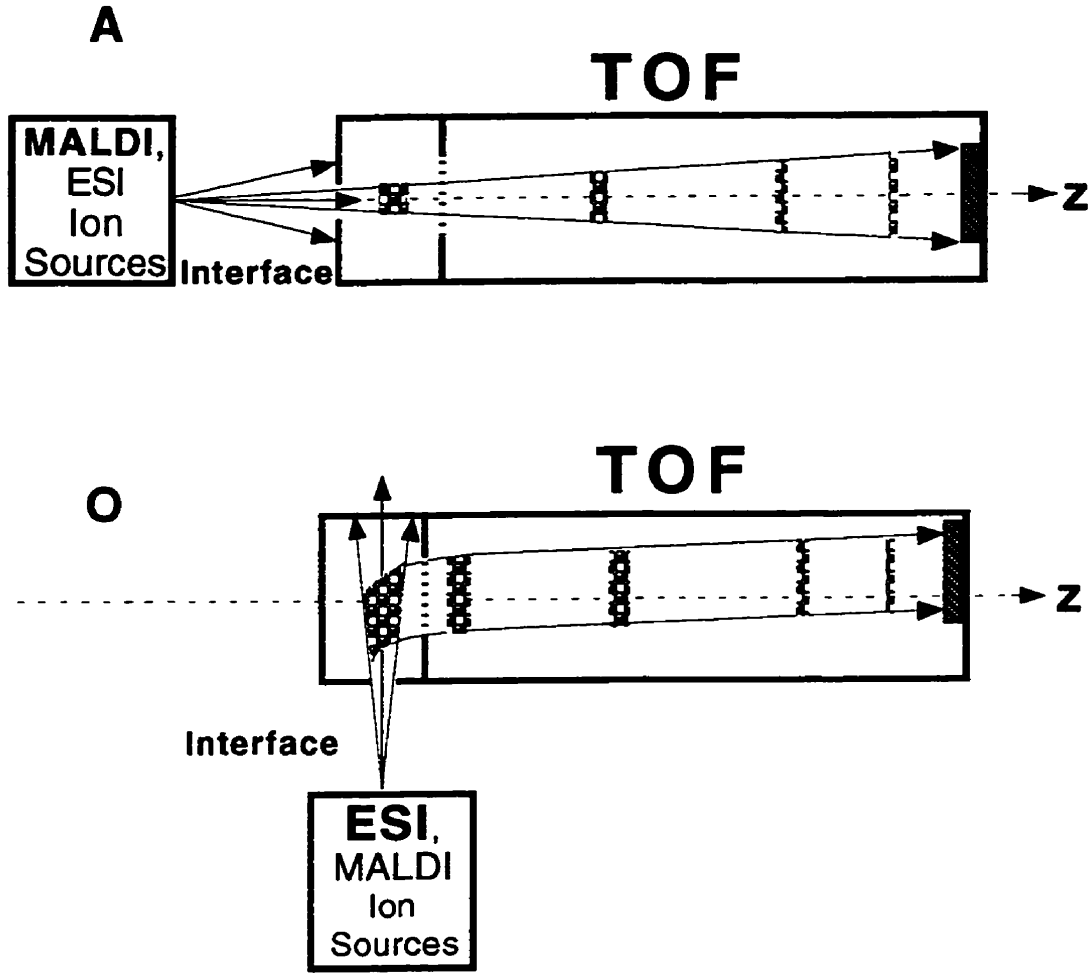

Figure 3. A schematical diagram showing the orientation of two ion sources, ESI and MALDI, relative to the z-axis of a TOF mass spectrometer.
A. - Axial configuration, in which ions from both ion sources are introduced into mass spectrometer along z-axis.
O. - Orthogonal configuration, in which ions are introduced perpendicularly to z-axis.

abandoned later by these authors in favor of an orthogonal configuration [Boyle & Whitehouse, 1992].

The concept of ion storage at the entrance of a flight tube has been utilized in a number of other instruments, in which a continuous ion source has been interfaced with a TOF mass spectrometer in axial configuration, through a quadrupole ion trap (IT) [Qian & Lubman, 1995]. In this configuration, ions from an ESI source are introduced through different stages of differential pumping into a quadrupole ion trap installed at the entrance of the flight path. A buffer gas (usually helium) is added to the trap so that the trap operates at an elevated pressure (~1 mTorr). Ions constantly filling the ion trap undergo multiple collisions with the molecules of buffer gas. As they lose their kinetic energy, they gradually fall to the center of the trap, being contained in the effective potential well created by the RF field of the trap. After collisional cooling (usually the process takes hundreds of milliseconds), ions are ejected from the trap into the flight path of a TOF spectrometer. One obvious advantage over the previous example is the ability to perform an MS/MS experiment with the stored ions before extraction into a TOF mass spectrometer. A resolution of up to 3000 and sensitivity in the picomole range has been achieved for leu-enkephalin-arg ions (712 m/z). Although the authors claim that the same resolution can be obtained in the MS/MS mode of operation, the example showing some melittin fragments definitely indicates poorer resolution. Unfortunately, no thorough analysis of this configuration was given in the multiple (and sometimes redundant) publications by Lubman and his collaborators.

However, Purves and Li have made an extended analysis of this technique [Purves & Li, 1997]. They conclude that there is a serious conflict that arises because the ion trap serves not only for ion storage, but also as an extraction device. The necessity to maintain a high pressure in the trap degrades the quality of the TOF spectra. Other authors, who have implemented the same approach to couple a MALDI source to a TOF spectrometer in this configuration [Kofel et al., 1996] point out that there are significant drawbacks in the technique arising from the limited ability of ion traps to accept the ions of large masses with a broad range of initial kinetic energy (acquired in the ion source) and from difficulties of finding optimum conditions for ion extraction from an ion trap into a TOF instrument. Nevertheless, the ability of this technique to couple both ESI and MALDI ion sources to the same TOF instrument and the possibility of performing MS/MS measurements appeal to many researchers, and the number of followers of this method is gradually increasing [Doroshenko & Cotter, 1998].

A quite new approach to coupling ESI in the axial configuration has been proposed recently by Benner [Fuerstenau & Benner, 1995]. It utilizes simultaneous measurements of the velocity and charge of a single ion as it passes through a charge sensing detector, which picks up the image current induced by an ion at the detector entrance and exit. The precision of such measurements is not high, but it is enough to be used to size large particles and intact DNA molecules, which may carry hundreds of charges.

All axial injection schemes for electrosprayed ions suffer from a series of significant drawbacks, and the most important among them arises because of the large

velocity and considerable spatial spread that the ions acquire in the supersonic jet during transportation from the atmosphere into vacuum. Big variations in the ion initial velocities and positions along the main axis of a TOF mass spectrometer affect the measured flight times and therefore limit resolution and sensitivity of the instrument. However, the influence of these factors can be greatly minimized, if the primary ion beam is directed orthogonally to the axis of a flight path.

Orthogonal injection of ESI ions into TOF mass spectrometer.

The first roots for the concept of orthogonal injection can be found at the Bendix company which constructed a TOF instrument in 1964 operating with a plasma gun continuous ion source. All the main elements of such a concept can be found in the drawings of the instrument presented in the technical documentary report [O'Halloran et al., 1964]. However, as frequently happens, the idea was abandoned, and only after about 20 years, was revived in a TOF mass spectrometer coupled with an atmospheric pressure ion source - ESI source in particular [Dodonov et al., 1987]. The development of orthogonal injection for continuous beams represents a great advance in the TOF mass spectrometry of gaseous ions produced at atmospheric pressures [Dodonov et al., 1994; Verenchikov et al, 1994; Boyle et al., 1992; Sin at al., 1991, Chernushevich et al., 1997].

In this technique, a continuous ion beam from a gas-dynamic interface enters the main vacuum chamber of a TOF mass spectrometer orthogonally to the axis of the instrument. It continuously passes through an ion storage region formed by two plane electrodes facing the entrance of a flight path (see Figure 3). Periodically, at a high

repetition rate, ions from the storage region are sampled into an accelerator column by a pulsed electric field between the plates. From the accelerator column, they enter the flight path. Between pulses, during the TOF analysis of the sampled ions, another portion of ions fills the ion storage region, and the procedure repeats. Such a scheme allows a relatively high duty cycle on the order of tens of percent. [Verenchikov et al., 1994].

The electrosprayed ions acquire a spread in velocity while entrained in the supersonic jet produced on entry into the vacuum system [Dole et al., 1968; Mack et al., 1970; Fenn et al., 1991], and from the declustering electric fields usually applied to remove adducts. These produce their largest effects in the longitudinal direction of the injected beam (i.e. perpendicular to the TOF axis), and the spatial width of the ion beam, caused by the transverse velocity spread, is relatively small. It is this width that limits the resolution of the TOF measurement so the advantage of orthogonal injection is clear.

The spread in flight time because of the spatial width of the primary beam in the ion storage region can be greatly reduced by a combination of Wiley-McLaren space focusing [Wiley & McLaren, 1955] and the use of an electrostatic ion mirror [Mamyrin et al., 1973]. By itself, space focusing provides limited improvement in mass resolution because it is most effective for short distances and good mass resolution requires relatively long flight paths. The electrostatic mirror provides energy focusing but not space focusing, so by itself it also offers limited improvement. However, in combination, these two methods are highly effective: the ions are spatially focused into a flat ion packet near the source and the mirror images the packet onto a detector, greatly increasing the flight-time without appreciably increasing the time spread. As a result, a mass

resolution of 5000 or more can be achieved for ions injected more or less directly from an electrospray ion source [Verentchikov et al., 1994].

Factors limiting performance of orthogonal injection of ESI ions.

Wiley-McLaren space focusing is not perfect even in the ideal case, the limitation being the so-called turn-around time of the ions, which is effectively determined by the divergence of the electrospray beam, manifested as a finite beam cross-section. If the beam width is reduced by collimation, it causes a drop in sensitivity. Thus performance still depends on the quality of the injected beam.

Another aspect of this problem concerns the rather uniform velocity distribution of electrosprayed ions introduced into vacuum. In the simplest picture, ions enter the storage region of the TOF mass spectrometer perpendicular to the spectrometer axis with an approximately constant velocity $v_{\perp}$ acquired in the supersonic jet expansion/ declustering process [Dole et al., 1968; Mack et al., 1970; Fenn et al., 1991]. Their corresponding kinetic energies may range from ~1 eV for ions of mass ~ 1kDa up to 1 keV for ions ~ 1MDa . When the ions are injected into the flight path they acquire an additional energy proportional to the accelerating voltage, so their axial velocity component v_{axial} is proportional to $(z/m)^{1/2}$. Thus the velocity after acceleration is the resultant of $v_{\perp}$ and v_{axial}, which depends on *m/z*. If the spectrometer is optimized for transmission of the ions of a given *m/z*, ions with other *m/z* values may miss the detector.

Although this has little effect on the flight time in a reflecting instrument, it does affect the ion transmission, producing mass discrimination.

Injection of MALDI ions into TOF spectrometers

Axial injection

In contrast to the complexity of the problem of how to inject electrosprayed ions into a TOF spectrometer, it is straightforward to inject ions from a MALDI source. As remarked above, the ion beam is already pulsed, so an axial geometry is suitable. A target is placed with its surface perpendicular to the axis of the TOF instrument, so the MALDI ion plume is ejected along the axis of the TOF instrument and can be easily extracted from the source along this axis by a constant electric field. The ion flight time is then measured at the end of a linear flight path.

Although this arrangement is simple, it imposes serious limits on the performance of the instrument. For any type of ion source, the resolution and accuracy of TOF instruments are usually limited by the initial space and energy spreads of the ions. In MALDI, the ions are ejected from a well-defined surface so the initial spatial spread is small. However, MALDI produces a plume of ions and neutrals which expands into the vacuum with a substantial energy spread. In the absence of an extraction field the ions have an average axial velocity in the range of 500 to 1000 m/s with velocity spreads comparable in magnitude [Beavis & Chait, 1991; Karas, 1998]. If the ions are ejected into a strong extraction field, the spread becomes still larger, probably because of collisions [Zhou et al., 1992]. An electrostatic mirror can provide energy focusing [Mamyrin et al.,

1973], but such a reflector does not correct for the spread in time that occurs during acceleration [Tang et al., 1988], and for this reason the resolution obtained in MALDI instruments with dc extraction has been rather modest.

A major advance in the performance of MALDI mass spectrometers came with the re-discovery of the virtues of "time-lag focusing", a technique first introduced long ago by Wiley and McLaren for extended gas sources [Wiley & McLaren, 1955]. In this method, often called delayed extraction, a delay is introduced between the laser pulse and the application of an extraction pulse, during which the ions drift in a field-free region. Consequently the ions have a spatial spread in addition to their velocity spread when the extraction pulse is applied, and the faster ions, being closer to the end of the accelerating column, receive a smaller accelerating impulse. Ions of a given mass then arrive at the plane of the detector at the same time, if the time delay and the amplitude of the accelerating pulse are adjusted properly. The method is particularly successful for MALDI because the ions start from a well-defined target plane. Moreover, the time delay allows the ion plume to expand before the extraction field is applied, greatly reducing the number of collisions and the resulting energy spread.

Delayed extraction can produce remarkably good performance in MALDI even with a linear TOF instrument [Brown & Lennon, 1995; Colby et al., 1994], but the best results are achieved in combination with a reflector [Vestal et al., 1995]. In this case the experimental parameters are adjusted so that ions arrive at a plane near the source at approximately the same time, but with a considerable variation in velocity. The velocity

dispersion is then compensated by the mirror. Resolutions higher than 15,000 have been obtained with this configuration [Vestal, 1998].

In spite of the significant progress made with the introduction of delayed extraction, it has some limitations. On leaving the MALDI plume, ions have approximately the same velocity distribution independent of mass. The resulting dependence of the energy on mass means that the optimum time-focusing conditions have some mass dependence, so resolution can only be optimized for part of the spectrum at a time. For the same reason there is a small perturbation in the mass vs. time formula and so high accuracy requires a more complex calibration procedure [Beavis, 1998]. Delayed extraction partially decouples the ion production process from the mass measurement, but there is still some dependence of the necessary focusing conditions on the type of matrix, the method of sample preparation, and the laser fluence. Moreover, because of the large number of ions that are normally produced in a single shot, they must be measured by a transient recorder. Even so, it is necessary to match the detector gain carefully to the laser fluence to avoid saturating the analogue-to-digital converter on intense peaks, and to avoid detector-shadowing problems produced by intense matrix signals.

Orthogonal Injection of MALDI ions into a TOF mass spectrometer

Orthogonal injection of MALDI into a TOF spectrometer [Spengler & Cotter 1990; Ens et al., 1995; Mlynski & Guilhaus, 1996] has some potential advantage over the usual axial injection geometry. In particular, it serves to decouple the ion production process from the mass measurement to a greater extent than it is possible even in delayed-

extraction MALDI. Thus there is a greater freedom to vary the target conditions without affecting the mass spectrum, and the plume of ions has more time to expand and cool before the electric field is applied to inject the ions into the spectrometer. Some improvement in resolution can also be expected because the largest spread in velocities is along the ejection axis normal to the target, which in this case is perpendicular to the TOF axis.

In the early experiments on orthogonal injection, the ion plume is allowed to expand toward the mass spectrometer axis and fill an extraction region. At a particular time after a laser shot, some ions are extracted from the storage region into a mass spectrometer, quite analogously as ESI ions are extracted. The ions are detected with a microchannel plate detector and recorded with a transient recorder as in the usual MALDI experiments. The detector is usually placed at the spatial focus plane. A resolution ~700 has been achieved in the 35-cm long linear TOF mass spectrometer used to test a limit on the possible resolution for any given length of flight path [Ens et al, 1995]. This characteristic can be improved, and a resolution ~3000 for orthogonal injection of small MALDI ions into a linear TOF spectrometer with a 1.5 m flight path was reported by Mlynski and Guilhaus [Mlynsky & Guilhaus, 1996].

Factors limiting performance of the orthogonal injection of MALDI ions without collisional cooling.

Experience accumulated in our laboratory [Ens, 1998] has shown that orthogonal injection of MALDI ions without collisional cooling suffers from several problems that

appear to make the configuration undesirable for measurements with both high resolution and high efficiency:

1. The velocity component of the ions in the primary beam $v_{\parallel}$ (along z-axis), while much smaller than the longitudinal velocity $v_{\perp}$, is still large enough to cause substantial widening of the beam as it expands toward the axis of the TOF instrument. The beam divergence limits the resolution. The effect can be reduced by collimation, but only at a significant sacrifice in sensitivity. The collimating slit must be placed at a considerable distance from the TOF axis to avoid distorting the extraction field, so the target must be placed far enough from the slit to produce a reasonably parallel beam.
2. Since the longitudinal velocity $v_{\perp}$ of the ions in the plume is largely independent of mass, the corresponding energy $1/2mv_{\perp}^2$ is mass dependent. As a result, the direction of the trajectory in the TOF spectrometer depends on the mass, yielding a mass-dependent instrumental acceptance, i.e. there is mass discrimination. The same effect is observed when ESI ions are injected directly from a gas-dynamic interface as described previously.

As the primary ion beam reaches the extraction region of a TOF mass spectrometer, it spreads out along its axis by an amount comparable to the separation between the target and the TOF axis. The size of the aperture which admits ions from the storage region into the spectrometer must clearly be much smaller than this spatial spread to maintain a uniform extraction field, particularly if a slit is placed between the target and the TOF axis. This further reduces the sensitivity.

Improving the Ion Beam Quality in a Collisional Damping Interface.

Despite the fact that electrospray and MALDI produce quite different ion beams, there are common problems limiting the performance of a TOF mass spectrometer coupled to either of the ion sources in an orthogonal configuration:

1. mass discrimination of the TOF instrument because of the approximately uniform velocities $v_{\perp}$ that the ions acquire in the supersonic jet formed when either electrospray ions or the MALDI plume expands into vacuum.
2. resolution and sensitivity of a TOF instrument are limited because of the difficulties in producing narrow primary ion beams. Although, the component of the velocity $v_{\parallel}$ of the ions in the ion beam is much smaller than the longitudinal one $v_{\perp}$, it is still enough to cause a substantial divergence of the primary beam as it fills the ion storage region. This causes bigger turn-around times which affect the resolution. This can be minimized by collimation but at the expense of sensitivity.

It is easy to see that these problems arise in connection with the initial characteristics of the ions of the primary ion beam. These characteristics may be improved by a sequence of steps, which are:

1. minimization of the initial velocities of ions in the primary beam (ideally to zero values) without considerable ion losses or spreading of the ion beam.

2. 2D spatial focusing of the beam on the axis along the direction of the orthogonal injection, and
3. re-acceleration of the ions across a given potential difference in the direction of orthogonal injection so that the component $\upsilon_{\parallel}$ will be small (zero in an ideal case), and the longitudinal velocity $\upsilon_{\perp}$ will be proportional to $(z/m)^{1/2}$.

These steps will produce a narrow beam of ions which enters the flight path in the same direction independent of *m/z*. The direction can be optimized for any particular instrument geometry, so no mass discrimination is observed.

In practice, the improvement in the ion beam quality can be obtained by damping the initial velocities of the injected ions in the gas dynamic interface between the source and the TOF spectrometer. This can be carried out by collisional cooling in an RF ion guide operating at an intermediate pressure between an ion source and a spectrometer [see, for example, Gerlich, 1992]. Such devices have been successfully implemented in different types of instruments - RF quadrupoles operating at ~5 mTorr [Douglas & French, 1992] and 20 mTorr [Wachs & Henion, 1991] for injection into a quadrupole mass filter, RF hexapoles operating at 100 mTorr [Xu et al., 1993] and a higher pressure [Van der Bergh et al., 1997] as a velocity damping device for ions, or a "molecular ion reactor" operating at a pressure ~1 Torr [Dodonov et al., 1997].

Ions passing along the axis of an RF multi pole ion guide lose their kinetic energy as the result of collisions with the molecules of buffer gas presented in the ion guide compartment. Their radial motion is constrained in the effective potential well created by

the RF electrical field [Gerlich, 1992; Tolmachev et al., 1997]. As ions lose their kinetic energy, they gradually "fall" to the bottom of the effective potential, slowly drifting along the potential valley, i.e. along the axis of the guide. In the ideal case, collisional cooling in a RF multi-pole ion guide produces a very narrow beam with very small $v_{\parallel}$ and $v_{\perp}$ components of the ion velocity, close to the mean of the thermal velocity distribution. At the output of the guide, the ions acquire a constant energy as they are reaccelerated towards the mass spectrometer axis so that the component $v_{\parallel}$ remains small and the longitudinal velocity $v_{\perp}$ is proportional to $(z/m)^{1/2}$. Thus, the collisional damping RF ion guide can be considered as a device for improving the quality of the ion beam orthogonally injected into a TOF mass spectrometer.

Overview of the thesis

This thesis describes the implementation of a collisional damping quadrupole ion guide in the gas dynamic interface connecting ESI and MALDI ion sources with the time-of-flight mass spectrometer. The purpose of using such a guide is to decrease the initial kinetic energy of the ions obtained from both ion sources in order to improve the quality of the beam orthogonally injected into the TOF mass spectrometer. The results of this implementation are discussed, and the improvements in the performance of the TOF instrument are shown. In addition, several methods providing an efficient way of coupling both sources, ESI and MALDI in one instrument are proposed.

The thesis is divided into five chapters. In the *Introduction*, the importance of both ion sources, ESI and MALDI, for mass analyses of biological molecules has been briefly discussed. The different methods of combining these ion sources with TOF mass spectrometers have been reviewed. When mentioning shortcomings, the emphasis has been made on the quality of the primary ion beam introduced into a TOF mass spectrometer.

The second chapter provides detailed information about the MANITOBA TOF III mass spectrometer. This chapter is necessary to introduce the mass spectrometer operating with an ion source in orthogonal configuration and to show the importance of initial beam quality on the overall performance of the instrument. In order to improve it the gas dynamic interface of the TOF III has been modified.

The third chapter describes the results obtained from the addition of a collisional damping RF quadrupole ion guide to the TOF mass spectrometer with orthogonal injection of electrosprayed ions.

The concept of cooling of the ions prior to their orthogonal injection into a TOF mass spectrometer has been implemented for orthogonal injection of MALDI ions and the fourth chapter describes the results.

The last chapter shows some applications of the mass spectrometer with a collisional damping interface.

In the *Final Conclusions and Perspectives*, the results are briefly summarized, underlining the problems, their possible solution and further perspectives.

II. MANITOBA TOF III MASS SPECTROMETER

Background

The TOF III mass spectrometer with orthogonal injection of ESI ions was constructed at the Time-of-Flight Laboratory at the Physics Department of Manitoba University in 1993 and the first results obtained were published in 1994 [Verentchikov et al., 1994]. The prototype for this spectrometer was the TOF II instrument operating with a secondary ion emission source [Tang et al., 1988]. High performance characteristics have been demonstrated by analysis of a variety of biological samples [Poppe-Schriemer et al., 1995] and resolution of up to 13,000 has been achieved for some inorganic clusters [Tang, 1991].

The design of the MANITOBA TOF III mass spectrometer is based on the construction elements of the previous instrument: a simple one-stage accelerator, a single-stage mirror mounted on the top of a vertically positioned flight tube and a detector built of two micro-channel plates in a chevron configuration. However, coupling a continuous ion source, such as ESI, to the new mass spectrometer has demanded a quite new approach to the design of the ion interface. Orthogonal injection of ions into the mass spectrometer has been considered as the best solution for the problem. The conceptual part of the orthogonal injection has been discussed in the previous chapter, but for closer understanding the operational principles and the possible limitations of the instrument it is necessary to provide a mathematical model.

Mathematical Model of the Mass Spectrometer.

The general mathematical treatment of the theory of orthogonal injection can be found in many articles [Dodonov et al., 1994; Laiko & Dodonov, 1994; Cotter, 1997]. Probably, the simplest and the most elegant mathematical model has been proposed by Vestal [Vestal, 1998]. As a special case, this model describes a mass spectrometer consisting of a simple one-stage accelerator, a field-free region and one-stage mirror. The TOF III mass spectrometer (schematic diagram in Figure 4) satisfies these criteria.

To illustrate the operational principles of the instrument, it is convenient to start with an equation describing the total flight time of an ion in the mass spectrometer:

$$t = (Df_0 / v_a)\left[1 + f_1 p / f_0 + f_2 p^2 / f_0 + ... + (2d_a / D)(v_\parallel / v_a)\right] \quad (1)$$

where, D is the length of the field-free region,

d_a is the length of the ion acceleration region measured relative to the origin, which coincides with the center of the orthogonally injected beam.

$v_\parallel$ is the initial velocity component of the ion along the axis of the mass spectrometer,

v_a is the velocity of an ion after acceleration process if it starts its movement at the plane $z=0$ with zero initial velocity component along the z-axis, and

$$p = z / d_a - (v_\parallel / v_a)^2 \quad (2)$$

is the relative initial energy deficit of a particular ion produced within the acceleration region at the particular distance z from the origin (center of the ion

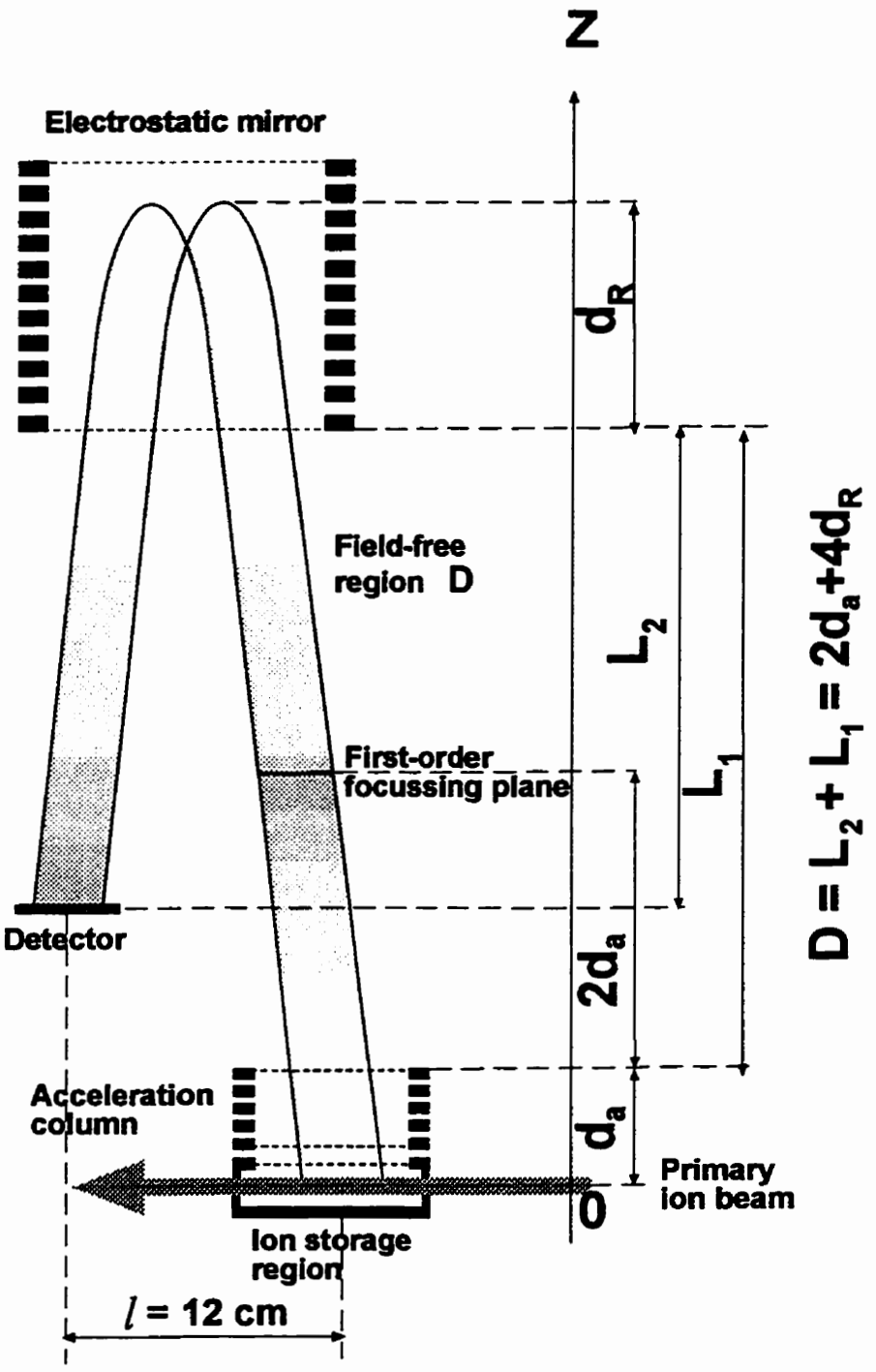

Figure 4. Schematic diagram of TOF IIII mass spectrometer illustrating the geometrical conditions in the instrument.

beam), with an initial velocity $v_{\parallel}$. This energy deficit is relative to the kinetic energy of the ion starting its movement at $z=0$, with zero initial velocity component along z-axis.

$f_0 = 1 + (2d_a + 4d_R)/D$, and d_R is a depth of ion penetration into the electrostatic mirror (see Fig. 4).

$$f_1 = \frac{1}{2}\left[1 - (2d_a + 4d_R)/D\right]$$

$$f_1 = \frac{1}{8}\left[3 - (2d_a + 4d_R)/D\right]$$

This equation has been derived without taking into account a post-acceleration region and the derivation can be found in the Appendix I.

The uncertainty in the arrival times of the ions of a particular m/z at the detector can arise because of the spatial spread of the ion beam ($z \neq 0$ for all ions) and some initial velocity ($v_{\parallel} \neq 0$) along z-axis. Mathematically, this is manifested in small, but finite values of p. This uncertainty can be minimized by demanding that the second term in the equation (1) is zero.

$$pf_1 / f_0 = 0 \Rightarrow f_1 = 0, \qquad (3)$$

This is a condition for so called first order focusing, and it can be achieved when it is satisfied by the geometrical conditions in the instrument,

$$2d_a + 4d_R = D \qquad (4)$$

which are also shown in Figure 4. The rest of the coefficients can be also found from this condition, and

$$f_0 = 2$$
$$f_1 = 1/4 \qquad (5)$$

This geometrical condition was taken into account while constructing the TOF III mass spectrometer. However, it is the combination of this geometrical condition with other operational conditions that enables one to achieve the high performance characteristics of the instrument.

Operational Conditions

Interface

Ions produced in the conventional ESI source enter the ion storage region in the main vacuum chamber of the mass spectrometer through a gas-dynamic interface. The main function of the original gas dynamic interface was to transfer the ions from the atmosphere through several stages of differential pumping, and to collimate the passing ion beam through different apertures in each stage. The schematic diagram of this interface is shown in Figure 5. The extensive collimation of the primary ion beam considerably decreases the number of ions transferred from the atmosphere into the mass spectrometer and a few pA (~10^7 ions/s) is a typical ion current through the first skimmer [Verentchikov et al., 1994].

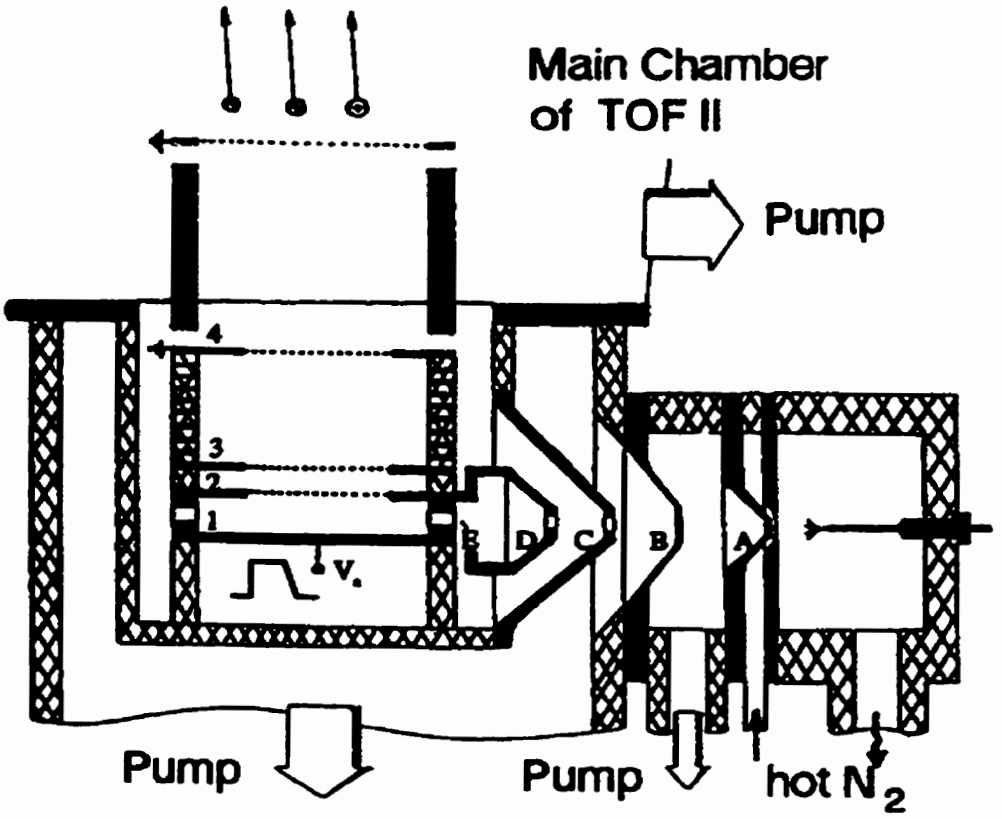

Figure 5. Schematic diagram of the gas -dynamic interface that was originally installed in the TOF III mass spectrometer [Verentchikov et al., 1994] and the acceleration region. A, nozzle; B and C, first and second skimmer; D and E, slits; 1-4, extraction electrodes.

Extraction and Acceleration

After the interface, a narrow beam of ions enters the main vacuum chamber of the mass spectrometer through another stage of differential pumping. It is further collimated first by a horizontal 1.5 x 6-mm slit and then by a 1.5-mm gap between the upper and the lower plates of the ion storage region (shown by letters D and E in Figure 5). The schematic diagram of an ion storage region and an accelerator column of TOF III illustrating the process of orthogonal extraction of ions into a flight path is also shown in Figure 6. The ions from the interface continuously fill the ion storage region. However, at any instant there are only a few ions in this region. This can be evaluated by calculating the linear density of ions in the beam: $\rho = i / \upsilon_{\perp}$, where i is the ion current and, $\upsilon_{\perp}$ is the ion velocity perpendicular to the axis of mass spectrometer. Assuming that only a small portion of ions from the interface reach the ion storage region, say 10^5-10^6 ions/s (~ 0.01-0.1 pA), and their velocity retained in the supersonic expansion/declustering process is of the order of ~1000 m/s gives $\rho \sim 10^2$-10^3 ions/m. The diameter of the electrodes of an acceleration column is ~5 cm and thus only 5-50 ions are present in the storage region compartment. But again, only a portion of these ions can be extracted into a flight path through a ~2-cm aperture in the upper electrode of the ion storage region (Fig. 6).

To extract the ions, a pulse (1) is applied to the bottom plate of an ion storage region. It has an amplitude of +425V, a rise time of ~50 ns, and duration of ~27 μs. At the same time, a pulse (2) is applied to the third (from the bottom) electrode supporting a grid. It has an amplitude of -395V, a rise time of ~50 ns and duration of ~25 μs. This

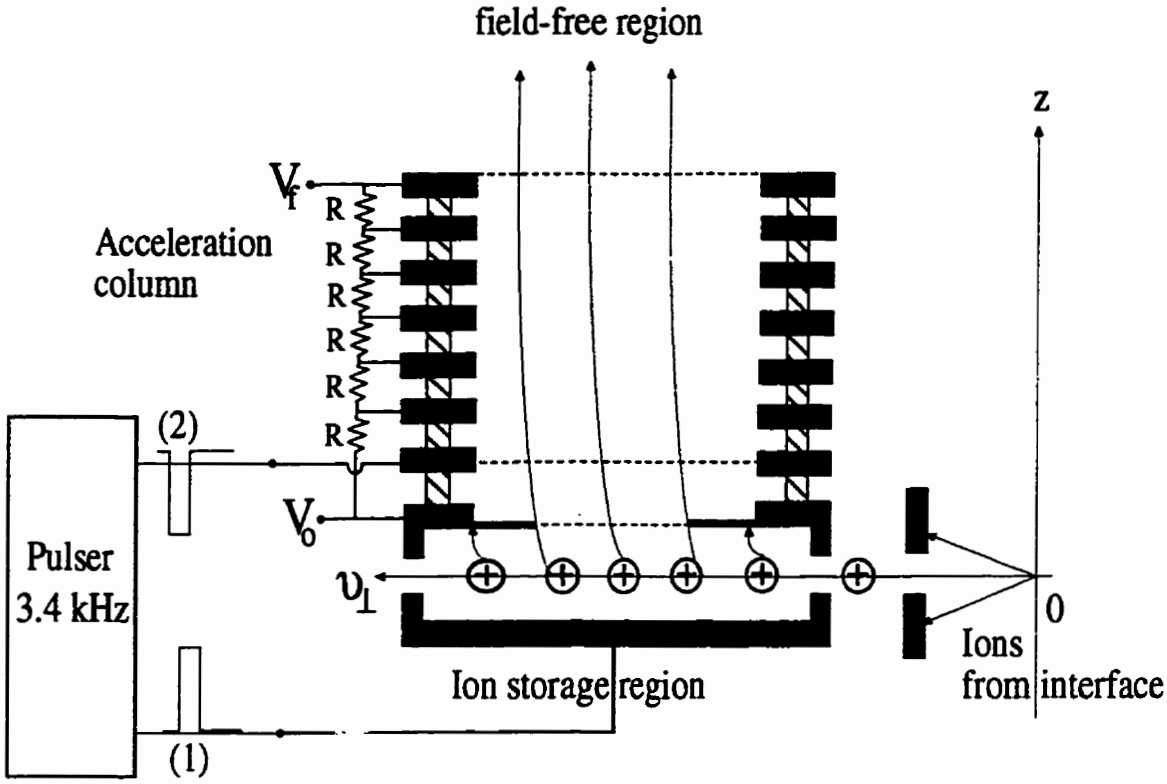

Figure 6. Schematic diagram of an ion storage region and an acceleration column of the TOF III mass spectrometer illustrating the process of orthogonal extraction of ions into the flight path (see explanations in the text)

electrode is also offset to a small potential (+9V) to compensate the electric field penetrating into the ion storage region from the other electrodes of the acceleration column [Dodonov et al., 1994]. When the pulses are applied, the electric field becomes approximately uniform throughout the ion storage region and the acceleration column. Ions are accelerated across a given potential applied either to the storage region (V_0) or the grid at the exit of the acceleration column (V_f). In the first case, the flight path is kept at ground, but the ion interface and the pulser are floated to the same potential. Another option includes keeping the ion storage, and hence the interface and the pulser, at ground, but elevating the flight path to a high negative potential (to operate with positive ions). In either case, in the existing TOF III ions acquire the energy ~ 4000 eV per charge, which slightly varies (2-3%) according to the ion initial position of an ion in the ion storage region.

Reflector

The ions extracted into the flight path of the mass spectrometer have different initial positions along the z-axis because of the spatial width of the primary beam in the ion storage region. However, under the conditions discussed previously, according to the Wiley-McLaren space focusing condition [Wiley & McLaren, 1955], all ions will be focused onto a horizontal plane lying above the exit of the acceleration column at the distance twice the length of the acceleration path of the ions in the acceleration column measured from the center of the ion beam (this is shown in Figure 4). This plane can be treated as a virtual "object plane" at which the ions of a particular *m/z* have a very small

spatial spread, but a large velocity spread along the z-axis. This axial velocity spread is corrected to the first order by an electrostatic mirror which reflects the ions from the "object plane" onto an image plane. The depth of the ion penetration into the electrostatic mirror can be regulated by varying the voltage applied to create the retarding potential. Thus, the condition (4) discussed in the previous chapter can be satisfied so that the image plane will coincide with the surface of the detector. A more extended discussion of the theory and design of the electrostatic mirror used in TOF III instrument can be found in [Tang et al., 1988; Verentchikov et al., 1994].

Detector and Acquisition System.

The detector consists of two 40-mm in diameter micro-channel plates (MCP) in chevron configuration [Wiza, 1979]. The amplified signal produced in the detector is applied through a constant-fraction discriminator and another discriminator (~20-mV threshold) to the input of a time-to-digital converter (TDC, Model CTN-M2, Institute de Physique Nucléaire, Orsay, France). Since only a few ions are extracted at a time, it is very convenient to use a pulse-counting technique. [Ens et al., 1994]. The data collection is controlled by a Power PC Macintosh computer running a spectral acquisition program "TOFMA" developed in-house.

Factors Limiting Performance of the Mass Spectrometer.

An extended analysis of factors that influence the performance of a TOF mass spectrometer with orthogonal injection of ions has been made by Dodonov and co-workers [Dodonov et al. 1994, Laiko & Dodonov 1994]. Precision of the TOF assembly, transmission through the grids, orientation of the micro-channels in an MCP relative to the direction of ion movement and many other factors were thoroughly investigated. However, the following analysis will be mostly focused on the influence of the initial properties of the orthogonally injected beam on the main characteristics of the instrument, since the only element of the mass spectrometer that has been modified for the measurements reported here is the ion interface.

Mass Discrimination.

In TOF III, the accelerator column and the detector for the reflected ions are positioned approximately 12 cm apart (l = 12 cm, see Figure 4). As discussed earlier, this constructional feature puts some restrictions on the simultaneous transmission of ions with different m/z values.

It can be easily noticed from the equation (1) that the effective flight path is just

$$Df_0 = 2(2d_a + 4d_R) \qquad (6)$$

Let's substitute the length of the acceleration column ($\approx$ 6.6 cm) instead of the exact value of d_a and the length of the mirror ($\approx$ 32 cm) instead of the exact value of d_R. This gives

an effective flight path ≈ 2.8 m. (The effective flight path can also be found from a time-of-flight spectrum of a compound with a given mass. This approach gives a similar value). Thus an ion will strike the detector if the ratio of the components of its velocity is

$$\upsilon_{\perp} / \upsilon_{a} \approx 12/280 \qquad (7)$$

The previous interface did not provide the means to satisfy this condition for ions of all values of m/z because of the rather uniform velocities $\upsilon_{\perp}$ acquired in the supersonic jet. Instead, the steering plates, positioned right after the acceleration column, were used to correct the angle at which the ions entered the flight path. Although this arrangement allowed an operator to adjust the transmission of ions through the TOF mass spectrometer to some extent so that they will strike the detector, it still produced a considerable mass discrimination [Verentchikov et al., 1994]. However, the solution for this problem can be obtained with the damping of the initial ion velocities to a very small value and then re-accelerating them across a given potential, say V_0. Just as in the acceleration process this also introduces an *m/z*-dependence of $\upsilon_{\perp}$ so that:

$$\upsilon_{a} = \sqrt{2zV_{a}/m}$$

and, (8)

$$\upsilon_{\perp} = \sqrt{2zV_{0}/m}$$

This removes m/z-dependence in the ratio (7). Using the geometrical conditions, V_0 can be easily found from:

$$V_{0} = (12/280)^{2} V_{a} \qquad (9)$$

and, for an acceleration potential ~ 4000 *V*, V_0 is equal to ≈ 7 *V*. In the following chapters, it will be shown that the use of this approach in the collisional damping interface allows the ion transmission to be optimized without producing any mass or *m/z* discrimination.

Resolution

Uncompensated terms in the equation (1) put some limits on resolution, which can be defined as:

$$R = t_0 / 2\Delta t \tag{10}$$

where t_0 is the flight time for an ion with $z = 0$ and $\upsilon_{\parallel} = 0$ and, $\Delta t = t(z, \upsilon_{\parallel}) - t_0$, where z and $\upsilon_{\parallel}$ are the extreme values.

Substitution of the conditions (4) and (5) into the equation (1) and then into (10) gives

$$R^{-1} = p^2 / 4 + ... + 2(d_a / D)(\upsilon_{\parallel} / \upsilon_a)] \tag{11}$$

and, substitution of the expression (2) for p and into the equation (11) and separating into parts gives

$$\begin{aligned} R_z^{-1} &= (z / d_a)^2 / 4 \\ R_\upsilon^{-1} &= 2(d_a / D)(\upsilon_{\parallel} / \upsilon_a) + (\upsilon_{\parallel} / \upsilon)^4 / 4 \\ R_{z\upsilon}^{-1} &= (z / d_a)(\upsilon_{\parallel} / \upsilon_a)^2 / 2 \end{aligned} \tag{12}$$

Neglecting the smaller terms in (12) leaves only two terms:

$$\begin{aligned} R_z^{-1} &= (z / d_a)^2 / 4 \\ R_\upsilon^{-1} &= 2(d_a / D)(\upsilon_{\parallel} / \upsilon_a) \end{aligned} \tag{13}$$

which are necessary to discuss.

The first term describes the limit in resolution because of the spatial width of the primary ion beam only. The width of the beam must be reduced in order to minimize the difference in the arrival times for the ions starting their motion from the different planes adjacent to *(z=0)*-plane. The second term shows the limit because of non-zero axial component of the initial ion velocity. This term is commonly referred as turn-around time [Wiley & McLaren, 1955]. If it is assumed that the axial component of ion velocity is a small portion of the orthogonal component: $\upsilon_{\parallel} = \beta\upsilon_{\perp}$ (where β is a small opening angle of the collimated ion beam "cone"), the second equation of (13) can be re-written as:

$$R_{\upsilon}^{-1} = 2(d_a / D)\beta(\upsilon_{\perp} / \upsilon_a) \qquad (14)$$

Again, if the orthogonal velocity component $\upsilon_{\perp}$ is approximately uniform for all ions, this produces m/z-dependent resolution. In fact, this was observed in the TOF III mass spectrometer with the old interface [Verentchikov et al., 1994]. However, it may be expected, that *m/z*-dependence may be removed if firstly, the initial ion velocities are decreased, and then ions are re-accelerated across a given potential (V_0 ~7 V in TOF III). Thus, the second equation becomes:

$$R_{\upsilon}^{-1} = 2(d_a / D)\beta\sqrt{V_0/V_a} \qquad (15)$$

It will be shown in the next chapter that resolution of up to 10,000 can be obtained not only for the ions of insulin (5,734 Da average molecular weight), but also for the ions citrate synthase hexamer with the molecular mass ~ 287,320 Da, when the TOF III mass spectrometer is coupled to an ESI source via a collisional damping interface.

Sensitivity

Sensitivity of the instrument for the ions of some particular compound depends on many factors such as the ion current produced by an ion source, efficiency of this current transmission through the interface and the mass spectrometer, plus the detection efficiency of a detector. One of the major factors limiting sensitivity of the instrument, at least for the ions with considerable low m/z, is the efficiency of ion transmission through the interface. For example, typical losses in ion current of the electrosprayed ions through the old interface of the TOF III were in the order of 10^4-10^5 ions per ion transmitted into an ion storage region [Verentchikov et al., 1994] . Such losses were mainly the result of the extensive collimation of the primary ion beam.

Incorporation of a collisional damping stage improves the ion transmission through the interface because of ion focusing onto the beam axis. Although a collimating step prior to ion injection into an ion storage region is still necessary, the overall losses are less not only because of the focusing effect , but also because of the improved transmission through the mass spectrometer itself, as was discussed earlier. These features will be demonstrated in the following chapters.

III. A COLLISIONAL DAMPING INTERFACE FOR AN ELECROSPRAY IONIZATION TIME-OF-FLIGHT MASS SPECTROMETER.

Experimental

Atmosphere/high vacuum interface

The original ESI atmosphere-vacuum interface used for orthogonal ion injection into our TOF III mass spectrometer has been described previously. A heated metal capillary has now been now added to provide another stage of pumping and desolvation, and a new section containing a small RF quadrupole has been installed. A schematic diagram of the main elements of the instrument and the new interface is shown in Fig. 7.

The results reported here used a conventional electrospray ion source. In this device a solution of an analyte is delivered to the sharpened tip of a stainless steel needle (1) (0.45 mm OD, 0.11mm ID) by a syringe pump (Model 55 1111, Harvard Apparatus, Holiston, MA) with a typical flow rate of 0.17-0.25 μL/min. Electrospraying of the analyte against a counter-flow of hot (50-70^0 C) nitrogen is performed at 3 - 3.5 kV potential difference between the tip of the needle and the inlet of a metal heated capillary (2) (0.5 mm ID, 12 cm long). Along with nitrogen, the ions and droplets produced are sucked into the capillary where they undergo some additional desolvation as they pass through [Chowdhury et al., 1990].

Expansion of this mixture into the next region produces a supersonic jet. This region is pumped to a pressure ~2.5 Torr by an Edwards 5.7 L/s (342 L/min) mechanical pump. A declustering voltage is applied to a focusing electrode (3) installed ~10mm downstream from the end of the heated capillary to which it has an electrical connection. Up to 300 V potential difference can be maintained between the focusing electrode and the flat aperture plate (4) 3 mm further downstream. The 0.35-mm diameter aperture in the plate connects this region to the second pumping stage containing the RF quadrupole (5); it

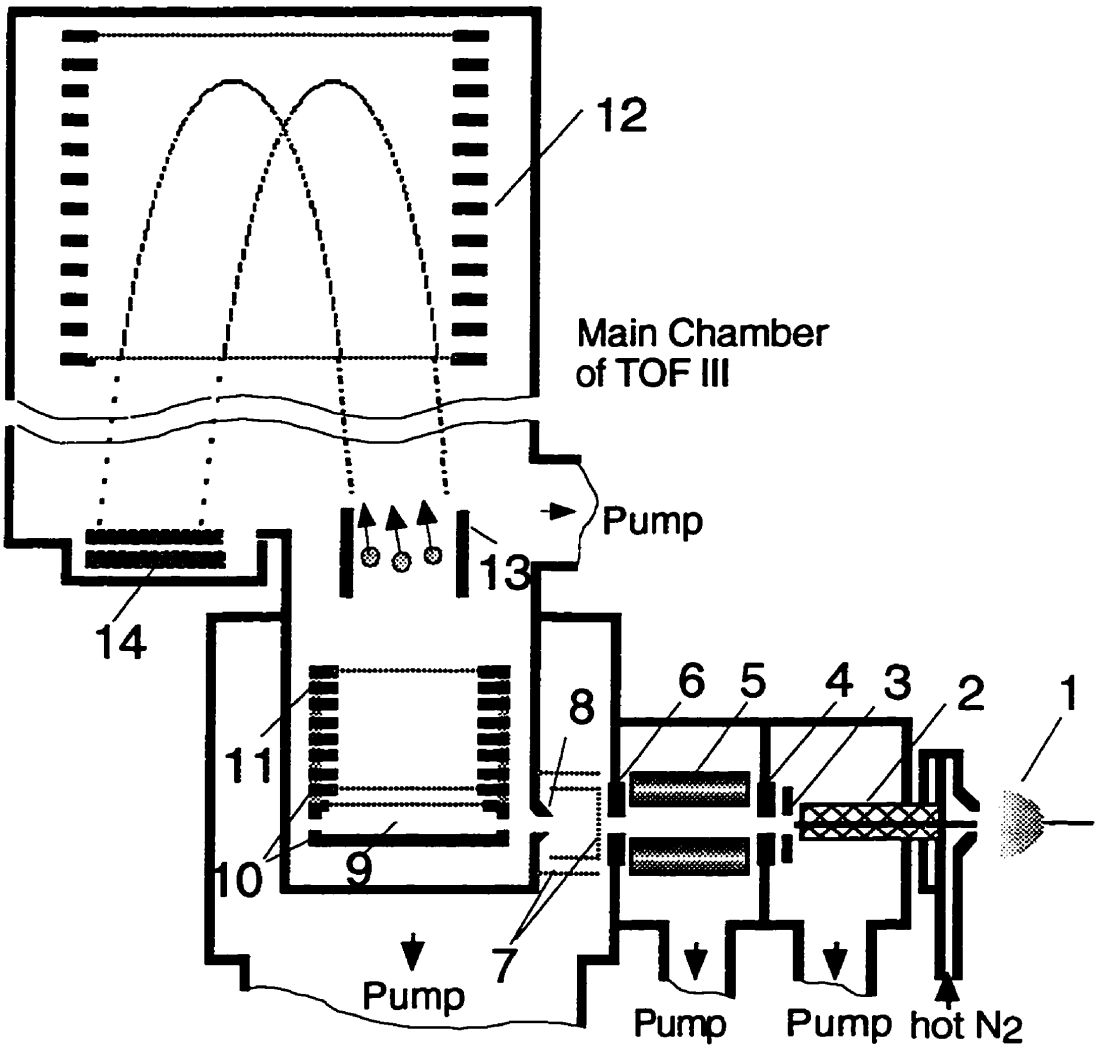

Figure 7. Schematic diagram of the time-of-flight instrument TOF III.
1 - ESI ion source; 2 - heated capillary; 3 - focusing electrode; 4 - first aperture plate; 5 - RF quadrupole; 6 - second aperture plate; 7 - grids; 8 - slit; 9 - the storage region; 10 - extraction electrodes; 11- acceleration column; 12 - electrostatic mirror; 13 - deflection plates; 14 - detector.

is evacuated to a pressure ~ 0.1 Torr by a Leybold-Heraeus 12.6 L/s (760 L/min) mechanical pump.

After passing through the quadrupole the ions enter the third region through a 0.75 mm-diameter aperture in the flat plate (6). This region is pumped to a pressure ~10^{-5} Torr by an Edwards 450 L/s turbomolecular pump. The electrical field between this aperture plate and the grids (7) form an ion lens used to shape the ion beam prior to its entry through the horizontal slit (8) (6 mm width, 1.5 mm height) into the main chamber of the mass spectrometer.

At the beginning of the injection cycle the electric field in the gap of the storage region (9) is zero. After a group of ions has filled the storage region, the process of ion acceleration starts by applying pulses to the extraction electrodes (10) of the accelerator column (11). Ions then leave the acceleration column in the direction of the electrostatic mirror (12) with ~ 4 keV kinetic energy. The direction of ion motion can be corrected, if necessary, by the deflection plates (13), so as not to miss the detector (14). The pressure in the main chamber is kept at ~3×10^{-7} Torr by an APD cryopump (~1000 L/s).

The voltages applied to the aperture plates and slits, as well as the RF quadrupole, are adjusted to obtain optimum ion transmission through the interface. A typical potential distribution is shown in Figure 8.

The quadrupole rods (0.8 cm diameter and 3.5 cm long) are supported by an insulator whose surfaces are screened from the ion beam. The quadrupole is driven by a small sine-wave signal generator (Model GFG-8016G, Instec Co, City of Industry, CA) coupled through a broadband RF power amplifier (Model 240L, ENI, Rochester, NY), which exhibits flat gain for a wide range of operating frequencies from 20 kHz to 10 MHz. An RF coupling transformer constructed in our laboratory gives an output voltage range from 0 to 1000 volts peak-to-peak. The transformer also provides the required 180 degree phase difference between the pole pairs. The quadrupole rods are "offset" to some DC potential intermediate between the potentials on the first and second aperture plates when

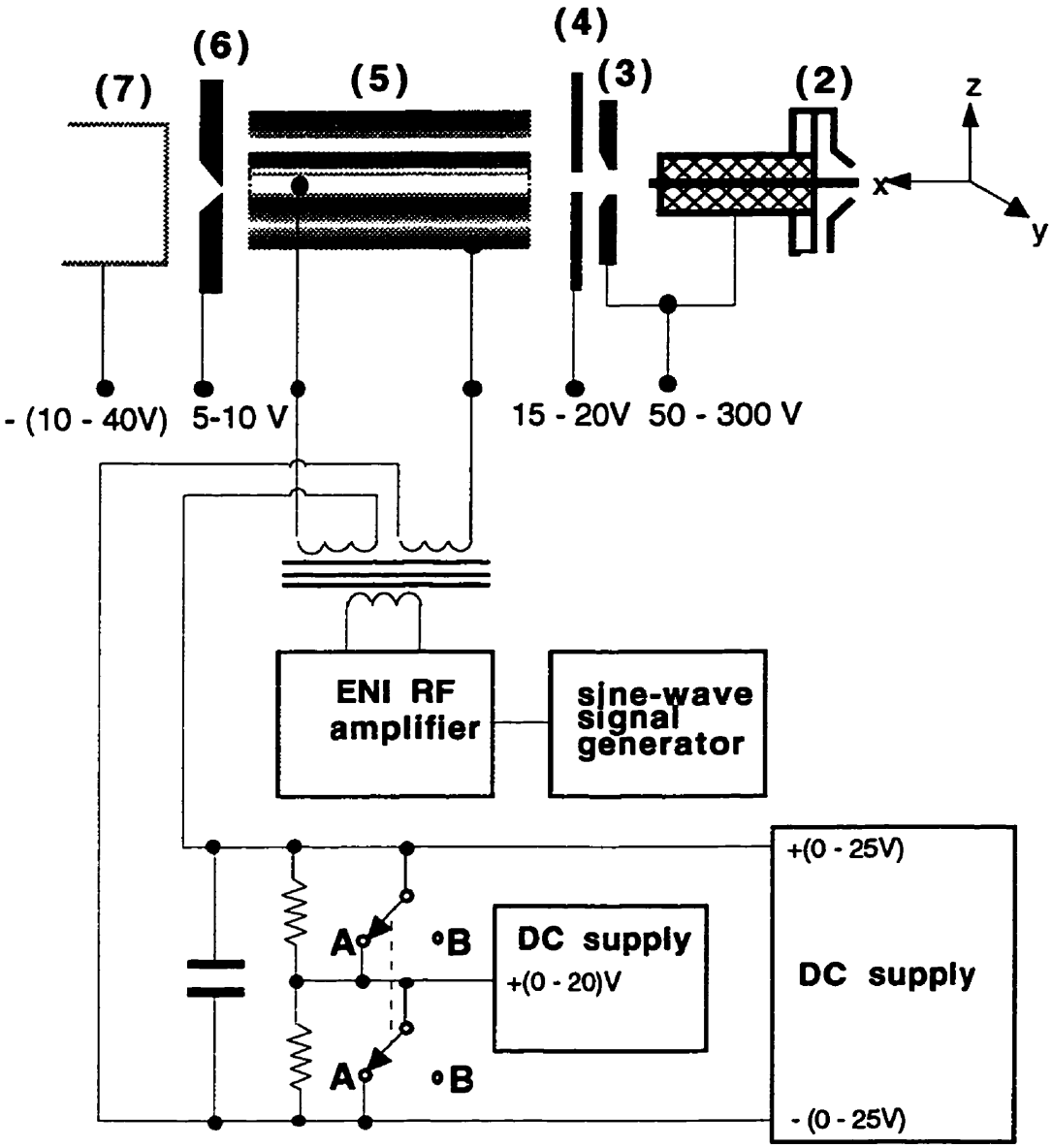

Figure 8. Distribution of the typical potentials on main elements of the new interface.

the switch is in position "A", as shown in Figure 8. For operation as a mass filter, small positive and negative voltages are applied in addition to each pair of rods to provide a non-zero Mathieu parameter a [Dawson, 1976]. For this operational mode, the switch is in position "B".

In its original configuration, the whole ESI interface assembly was elevated to 4 kV DC acceleration potential so that the flight path of the mass spectrometer was at ground. In this case the relatively high pressure in the first stage inhibited discharges to the grounded mechanical pump; a 1 m length of plastic hose was sufficient. The pressure in the third and fourth regions was low enough to prevent discharges. The section containing the quadrupole was more of a problem. Here it was necessary to run both internal and external voltage dividers (each consisting of 27 1MW resistors) along the ~1.5 m polyethylene hose; these were sufficient to prevent electrical arcing. However, the spectrometer has been modified recently [Shevchenko et al., 1997] by the insertion of an internal shield enclosing the flight path. The shield is now electrically floated at the acceleration potential so that the ESI source operates at near ground potential. This modification makes it much easier to operate, but it does not change the essential features of the ion guide operation.

Chemicals

Solutions of proteins were prepared in deionized water, reagent grade methanol and glacial acetic acid (up to 5% in 1/1 methanol/water) when it was not necessary to preserve the protein native structure. To create conditions close to physiological ones, buffer solutions of 5 mM ammonium acetate (99.99% purity, Aldrich Chemical Co., Milwaukee, WI) or ammonium bicarbonate (J. T Becker, Phillisburg, NJ) were used to keep the pH values either at ~ 6 for ammonium acetate or at ~ 7.5 for ammonium bicarbonate. Substance P, des-Arg-bradykinin, bovine pancreas insulin, horse heart cytochrome c, horse skeletal muscle myoglobin and bovine serum albumin were purchased from Sigma Chemical Co. (St. Louis, MO) and were used without further purification.

Soybean agglutinin was prepared at Albert Einstein College of Medicine, N.Y. [Tang et al., 1994] and *E. coli* catalase HP II was obtained from P. C. Loewen (Microbiology department, University of Manitoba). Both samples were purified by centrifugal filtration of the aqueous solutions, using ultrafree-MC filters with 30,000 Da molecular weight cutoff (Millipore Co., Bedford, MA). Recombinant citrate synthase from *E. coli* was prepared by A. Ayed in H. W. Duckworth's laboratory [Ayed et al., 1998] (Chemistry department, University of Manitoba) and supplied as solutions in 20 mM ammonium acetate or ammonium bicarbonate; these solutions were diluted by a factor of four with water and analyzed without further purification.

Results and Discussion

Calculations

Several approaches based mainly on Monte Carlo models have been developed to simulate the processes taking place for ions passing through a relatively high pressure RF ion guide. The results of numerical calculations that utilize some elements of two models [Douglas & French, 1992; Xu et al., 1993], adapted for our operating conditions are presented in this chapter. The details of the computational algorithm are given in the Appendix II.

A simulation of the ion motion of myoglobin ions was performed with the initial parameters indicated in Table I. The initial coordinates of the input ions were set randomly within a circle of a 3.5 mm radius at the entrance of the quadrupole. The initial velocity vectors were generated within a cone of opening angle ~80^0, while the velocity vector amplitudes followed a binomial distribution with a mean ~1,000 m/s. This choice of ion velocity is based on our experimental finding that optimum ion transmission requires a small accelerating voltage ~ 6 ± 2 volts between the first aperture plate and the quadrupole. For ions of m/z =1000 this corresponds to a velocity ~1000 m/s. The actual ion velocity is

Parameter	Value
Ion mass	16,951 Da
Number of charges, z	15
Collision cross-section [a]	4040 $Å^2$
Pressure inside the rods	0.1 Torr
Amplitude of RF field	150 V
Frequency of RF field	2 MHz

[a] Taken from [Covey & Douglas, 1993]

Table I. Parameters used for calculations of ion motion.

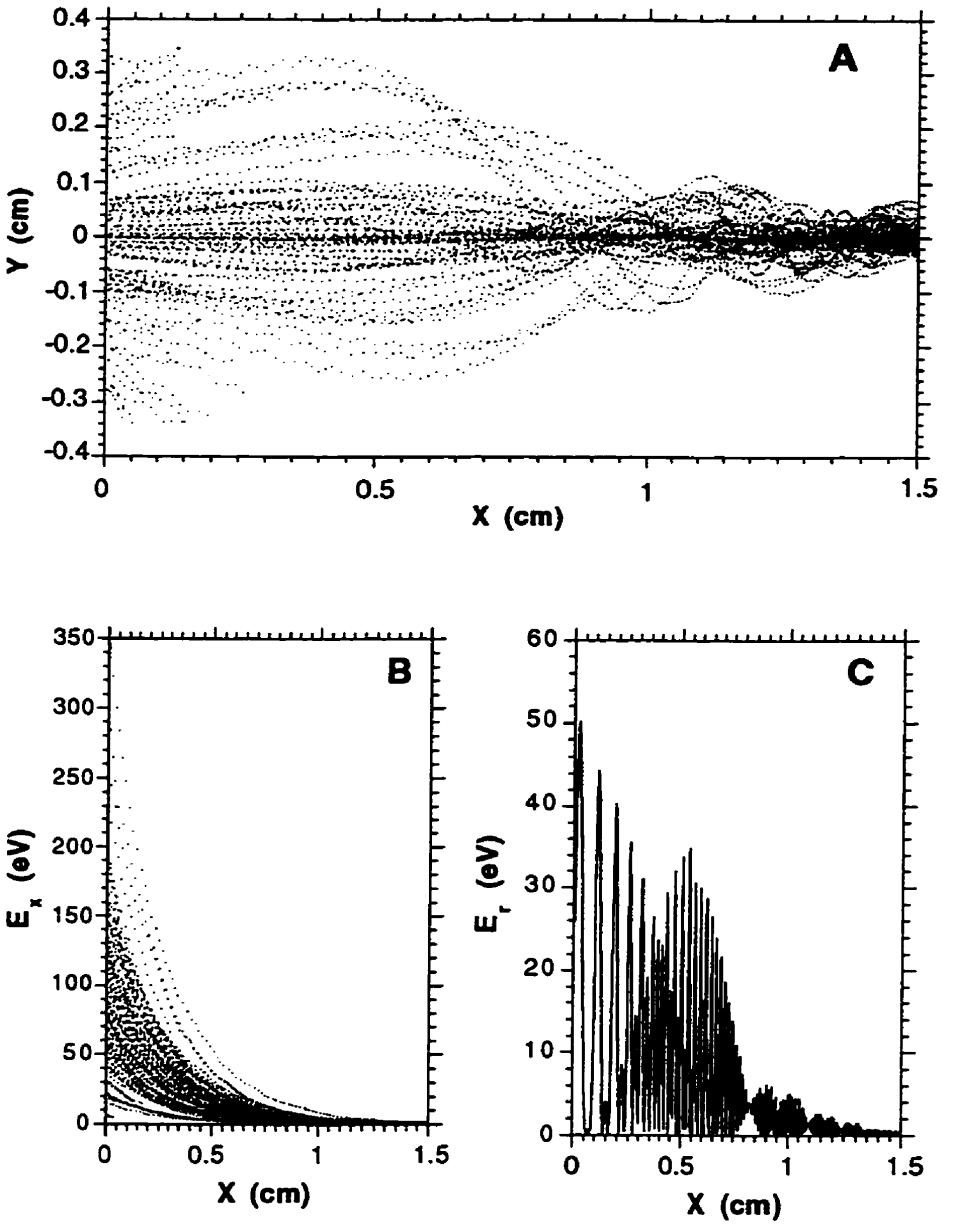

Figure 9. Computer simulation of ion motion in the quadrupole ion guide for myoglobin ions.
(**A**) Projection of ion trajectories on a cross section plane along the x axis of the quadrupole.
(**B**) Energy E_x of the ions as a function of position along the quadrupole x axis, where $E_x = 1/2mv_x^2$
(**C**) The energy E_r of the ions as a function of position along the quadrupole x axis, where $E_r = 1/2mv_r^2$

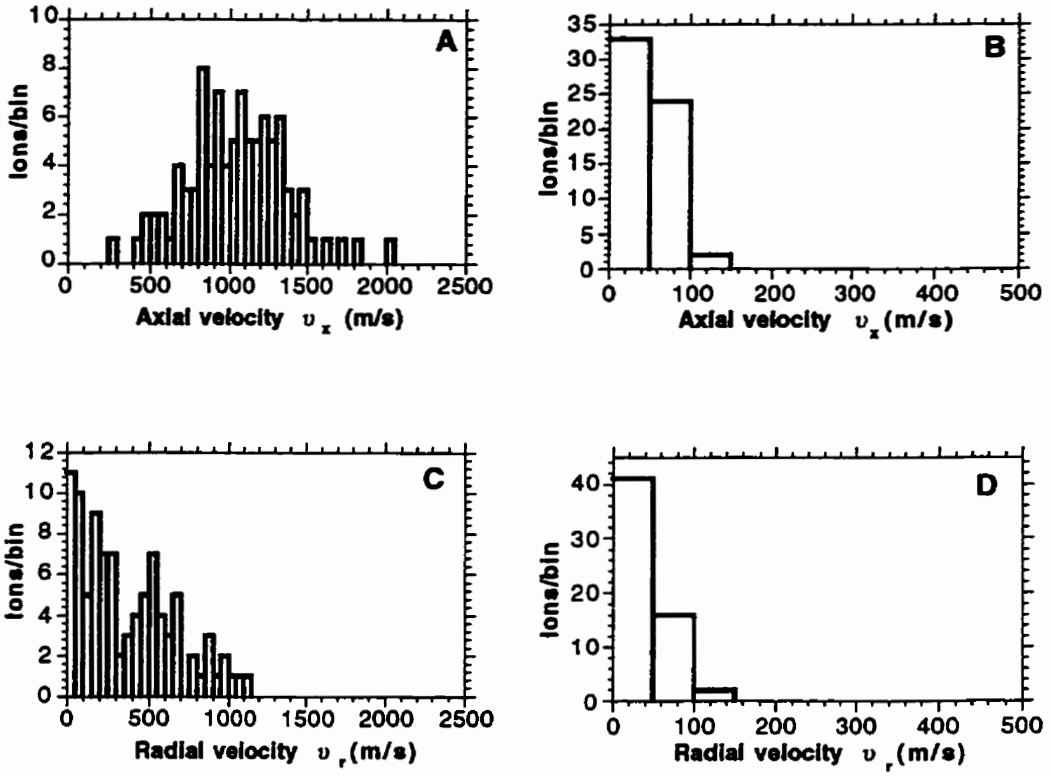

Figure 10. Histograms of the ion velocity components.
(**A**) Axial velocities at the input of the quadrupole ion guide.
(**B**) Axial velocities at a distance of 1.5 cm inside the quadrupole ion guide.
(**C**) Radial velocities at the input of the quadrupole ion guide.
(**D**) Radial velocities at a distance of 1.5 cm inside the quadrupole ion guide.

probably considerably higher than this, because the ions retain some of the velocity (<1000 m/s) acquired in the supersonic jet expansion, as mentioned in the introduction above. However, the conditions assumed in the calculation (Table I) should be adequate to give a good qualitative picture of the processes taking place.

Projection of the myoglobin ion trajectories onto the *yx*-plane are shown in dotted lines in Figure 9A. Strong position focusing is evident. The truncated trajectories represent ions lost due to collisions with the rods. As the ions pass through the buffer gas they lose energy, as can be seen in Figures 9B and 9C. It was found that the kinetic energy of almost all the injected ions approached the mean energy of the collision gas molecules (3/2 kT ~ 0.03 eV) at $x = 1.5 \pm 0.5$ cm, so the calculation was terminated at $x = 1.5$ cm. Several theories have been proposed to explain the mechanism of ion motion past the thermal threshold [Xu et al., 1993; Tolmachev et al., 1997].

Of most interest is the change in velocities. The velocity histograms in Figures 10 A and B, show that the average axial velocity 1069 m/s for input ions is reduced to 74 m/s average axial velocity for the ions at $x = 1.5$ cm. Similarly Figure 10D shows a reduction in the radial velocity to 67 m/s from 396 m/s (Figure 10C).

Thus, the computations show that by $x = 1.5$ cm:

1. There is a strong radial focusing of ions and radial velocity damping at least by a factor of ~ 6.
2. There is axial velocity damping by a factor of ~ 14.

Calculations performed for ions of different masses and charge states gave rather similar values for the damping factors. Although ions of larger mass lose less energy in a single collision, such ions have larger collision cross-sections [Covey & Douglas, 1993; Chen et al., 1997], so it appears that these effects tend to cancel each other. However, it is difficult to draw any certain conclusions because of the non-analytical character of the Monte Carlo method. The analytical model of the process proposed recently [Tolmachev et al., 1997] may help to elucidate these questions.

Time delay measurements

The time delay distribution for ions passing through the ion guide was measured experimentally in order to estimate the average velocity of the ions and to investigate the factors that determine this value. The experimental setup is shown in Figure 11.

In normal operation electrosprayed ions pass through the interface and arrive at the storage region of the mass spectrometer as a continuous beam. Pulses from a digital delay generator (DDG) are amplified and applied to the extraction electrodes of the accelerator column to inject ions into the flight path of the mass spectrometer at a repetition rate of 3300 Hz, i.e. a pulse every ~ 300 μs. These pulses also supply start signals for an Orsay time-to-digital converter (TDC) that can accept up to 255 stop signals from the detector within an observation time 255 μs after the start signal, i. e. the contents of the storage region (up to 255 mass values) are sampled every ~ 300 μs.

In the experiment on time delay measurement, the continuous beam of electrosprayed ions is gated to modulate the ion intensity. Marker pulses are then obtained from a frequency divider that divides the operating frequency of the pulses coming from the DDG (3300 Hz) by a given number (usually 33). A short positive pulse ~100 μs long, generated by each marker pulse (at 100 Hz = 3300 Hz /33), is applied to the focusing electrode (see Fig. 11) to allow ions to pass through the first aperture plate into the quadrupole. Otherwise a negative DC voltage applied to the focusing electrode prevents ions from going through the first aperture plate. The TDC continues to sample the contents of the storage region every ~300 μs but the ion intensity in this region is now modulated by the time delay of the ions in the interface.

The marker pulse is also applied to a second input on the TDC, which results in the production of a characteristic signal at the TDC output. Recognition of this signal by the computer starts a sequence of integrations that yield the time distribution of the ions in the storage region. First the ion signals in a specified *m/z* range acquired within the first

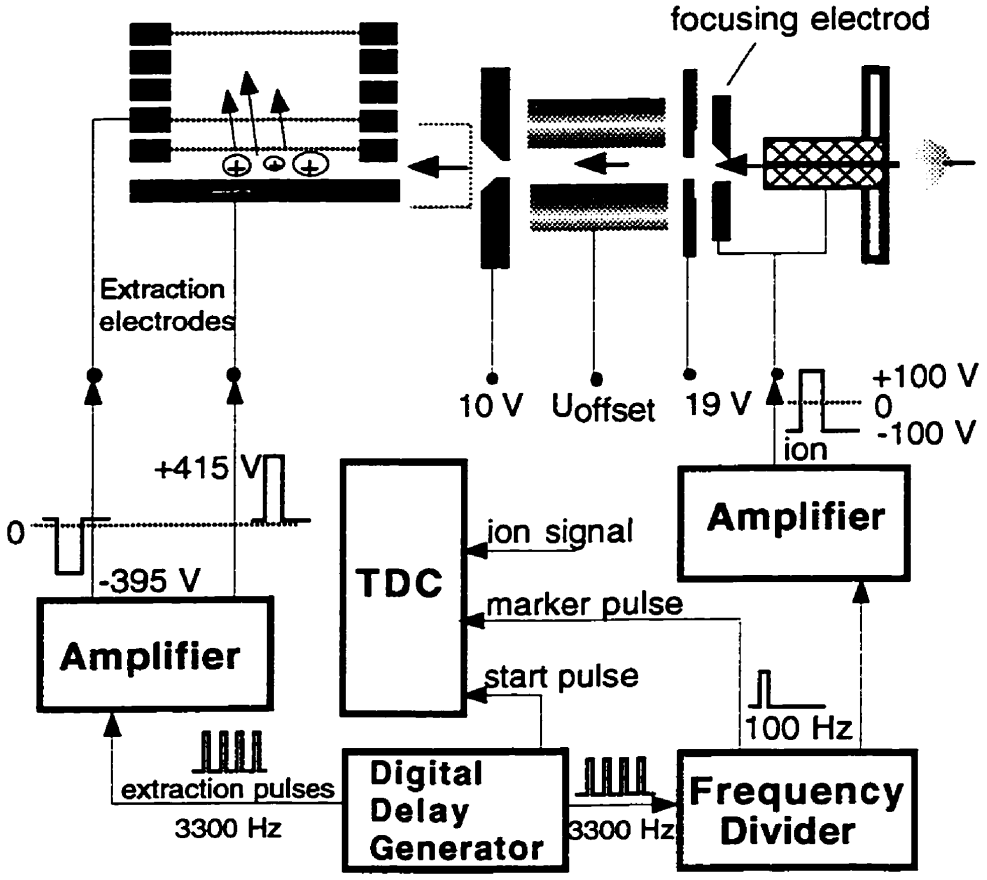

Figure 11. Experimental set up for measurements of time delays. The computer (Power Macintosh 7300/180) connected to the TDC is not shown.

observation period are recorded, integrated and the value obtained is placed in a first histogram channel. The ion signals from the next sampling ~ 300 μs later are stored in a second histogram channel, and so on. In the present measurements this process of integration and storage was repeated until 33 channels were filled, representing a total sampling time of ~10 ms.

When the next marker signal is recognized the histogramming process is repeated and the new values are added to those already stored in the histogram. This technique allows us to minimize the effect of ion signal instability in the ES source on the final flight-time distribution. A typical measurement lasted for ~10 min.

The average transit time measured for several peptide and protein ions with masses from 1347 to 66,500 Da turned out to be nearly the same: 1.4 ± 0.2 ms (Figure 12) when the "offset" voltage on the quadrupole was approximately equal to the average of the voltages on the first and second aperture plates. We have not found any large difference in transit times for myoglobin ions sprayed from solutions in which the native structure is presumably preserved (pH 6-7.5, average z ~ +8) or not preserved (pH 2-3, average z ~ +15), which indicates that ions spend approximately equal times in the quadrupole over a considerable m/z range. The average time that the ions need to go through the quadrupole gives a measure of the *average* velocity with which they move through the quadrupole ion guide: $<v>$ ~ 25 m/s for all measured ions. This value for an *average* ion velocity is about the same order of magnitude as the velocity calculated for thermal equilibrium *(3/2kT)* with the molecules of the buffer gas (for example, ~70 m/s for ions with m/z ~1000 m/z). Since the ions start with velocities ~1,000 m/s, it suggests that most of the transit time occurs after the ion velocity has reached thermal values.

The flight-time increases substantially when the 'pulling' voltage at either end of the quadrupole is decreased to zero, indicating that the axial ion motion is strongly influenced by penetration of DC electric fields into the quadrupole. Figure 13 shows that when there is no potential difference between the first aperture plate and the quadrupole, or

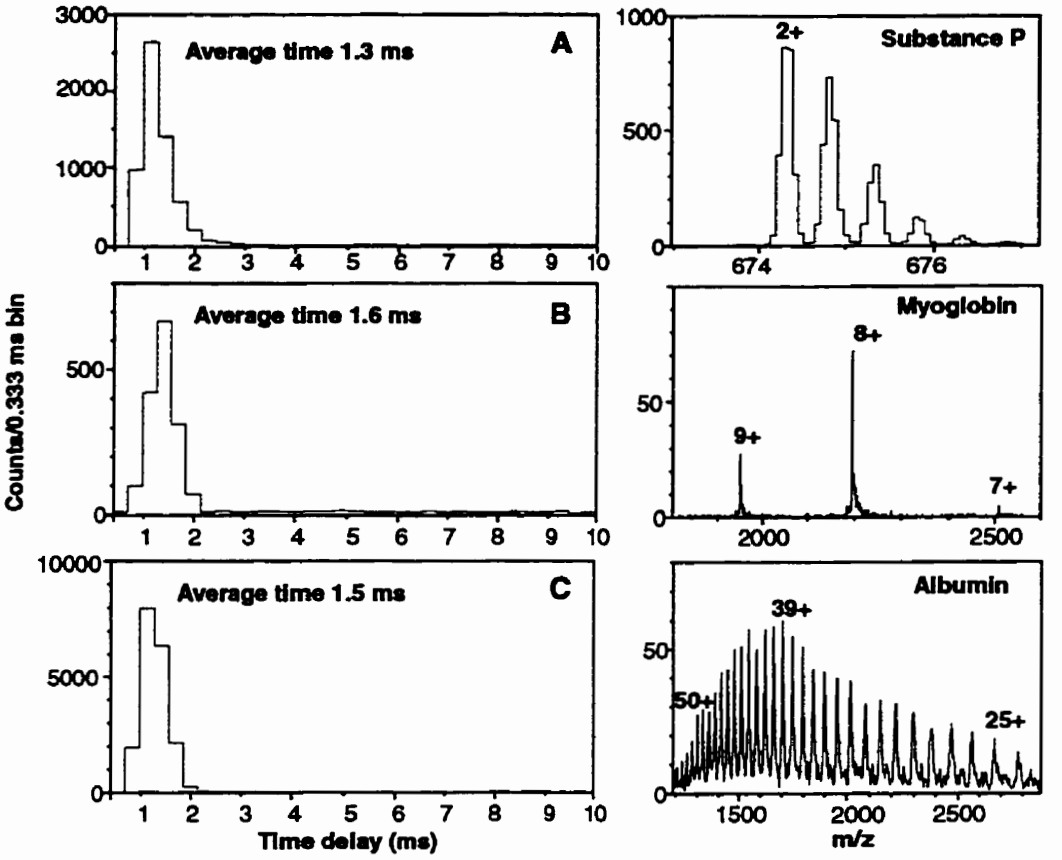

Figure 12. Distribution of time delays for different ions with a quadrupole offset voltage ~13 V. (**A**) For double charged ions of substance P (1347.74 Da). (**B**) For ions of myoglobin (17,951 Da) (native state). (**C**) For ions of albumin (~66,500 Da) (denatured state).
Right: corresponding spectra of m/z regions in which the ion signals were recorded and integrated (see explanations in the text).

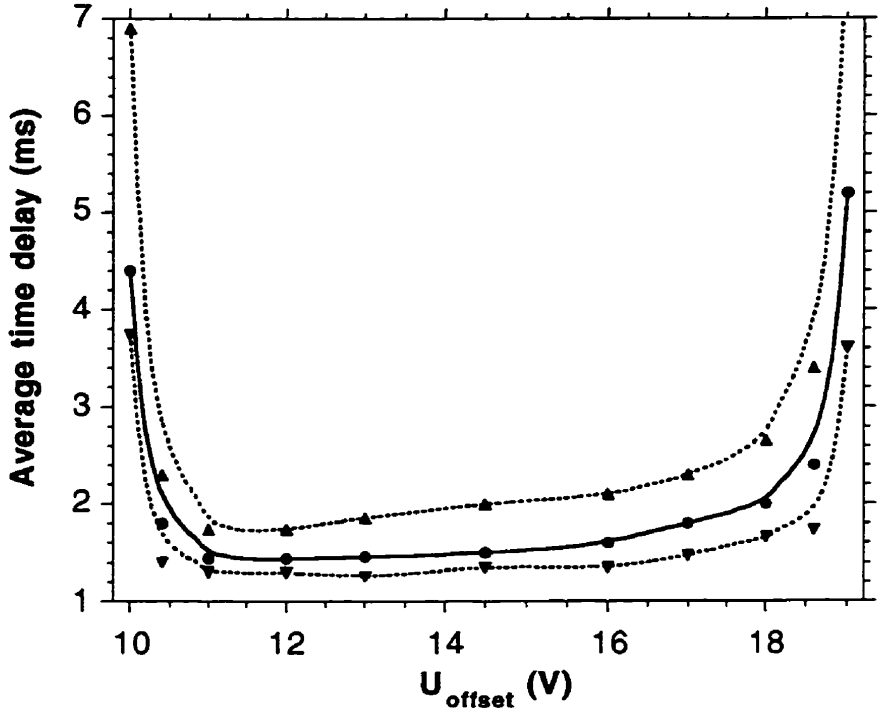

Figure 13. Average time delay plotted as a function of the potential on the quadrupole U offset. When U offset approaches the values of the potentials on the first (19 V) or the second (10 V) aperture plate, the time that the ions of substance P spent in the quadrupole increases. The dotted lines above and below the time delay curve correspond to the width of the time delay distributions

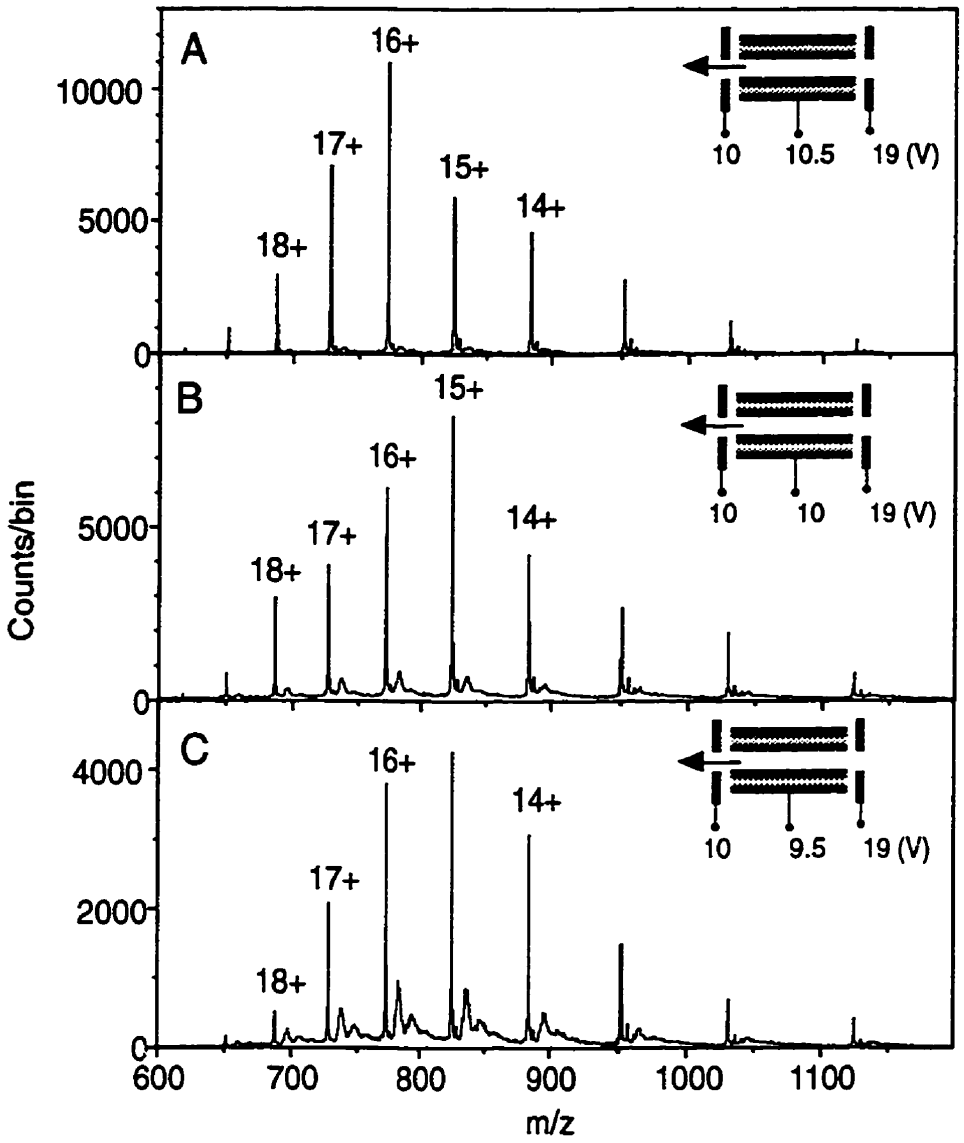

Figure 14. m/z spectra of cytochrome c recorded with:
(A) A small accelerating potential at the output of the quadrupole (ΔU=0.5V).
(B) No accelerating potential.
(C) A small decelerating potential (ΔU = - 0.5V) at the output.

between the quadrupole and the second aperture plate, the flight-time distribution for substance P ions becomes very wide, indicating the transformation of the pulsed ion beam into an almost continuous one.

A long residence time of ions in the quadrupole may result in undesirable chemical reactions giving increased formation of adducts, as shown in Figure 14 for cytochrome c. This process is observed in our instrument when the buffer gas contains impurities.

The flight-time distributions measured for the ions of different compounds show that the penetration of DC electric fields (fringing fields) from both ends of the high pressure RF-quadrupole ion guide plays an important role in the ion motion. After this finding we have incorporated fringing fields in the computer program discussed above, but the simulations show that there are still some regions inside the quadrupole where the ions move with drift velocities less than the threshold velocity determined by thermal equilibrium conditions. Whether it is gas dynamic "wind" or space charge that makes the ions move under these conditions is still an open question.

Mass Measurements

Decreased m and m/z Discrimination

The new interface allows complete control over the energy of the orthogonally injected ions by applying an appropriate voltage to the second aperture plate. The optimum deflection potential no longer depends on the mass of the ion, and is in fact the same for a wide range of m or m/z and declustering potentials. This enables us to examine different compounds over a large range of m/z without appreciable discrimination.

Figure 15 shows the m/z spectrum of a mixture of four compounds, substance P (1346.74 Da, 1 μM concentration in the solution), cytochrome C (12,360 Da, 1 μM), the tetramer of soybean agglutinin (SBA ,~116,000 Da, 3 μM) and the tetramer of catalase HP II (~ 339,100 Da, 5 μM) prepared in a water/0.08% acetic acid solution. The slightly acidic condition of the solution has partially denatured the catalase HP II tetramer so it appears

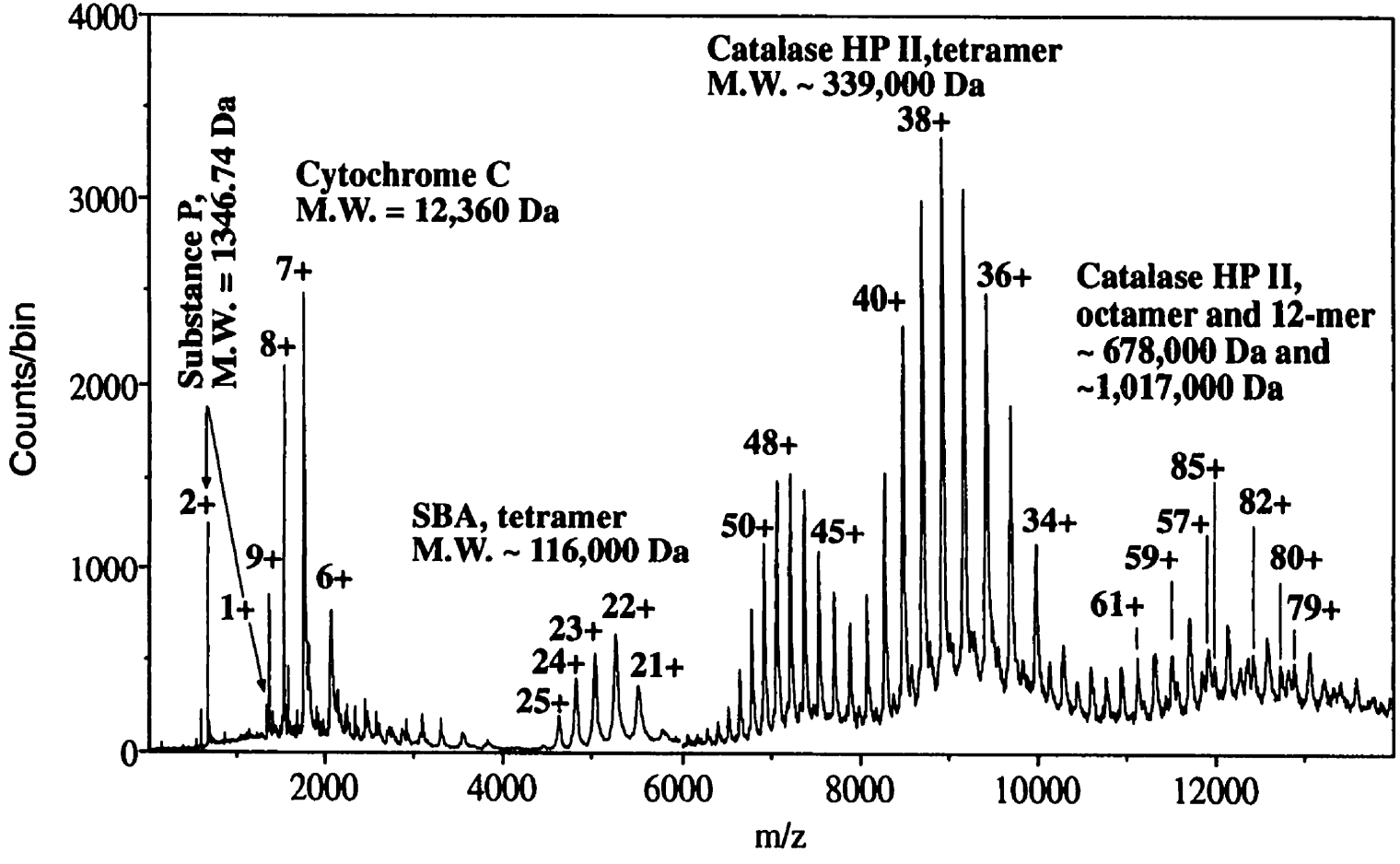

Figure 15. The m/z spectrum of a mixture of four compounds: substance P, cytochrome c, SBA tetramer and catalase HP II tetramer.

with a bimodal charge distribution. The multiple small peaks in the cytochrome c m/z range are impurities from the catalase HP II sample.

Because the observation time for our TDC is limited to 255 μs the first part of the spectrum was obtained for an *m/z* range 0 - 6380. After introducing a 200 μs delay in the start signal we were able to measure the mass spectrum over the m/z range 4165 - 20300. Both parts of the *m/z* spectrum were obtained with the same distribution of voltages in the ion interface and the two parts were joined together at ~6000 *m/z*.

The spectrum shows the capability of our TOF III instrument with the new interface to cover a large mass range. The m/z peaks of the 12-mer of the catalase HP II with a mass more than 1 MDa are as easy to identify as the doubly charged peak of substance P.

An even higher *m/z* range (up to ~30,000 m/z) has been examined recently on the mass spectrometer in an initial attempt to detect the intact brome mosaic virus (MW ~ 4.65 MDa). Although we were able to detect a signal that presumably arises from the intact virus [Chernushevich et al., 1996], the charge distribution was not resolved because of the high heterogeneity of the sample.

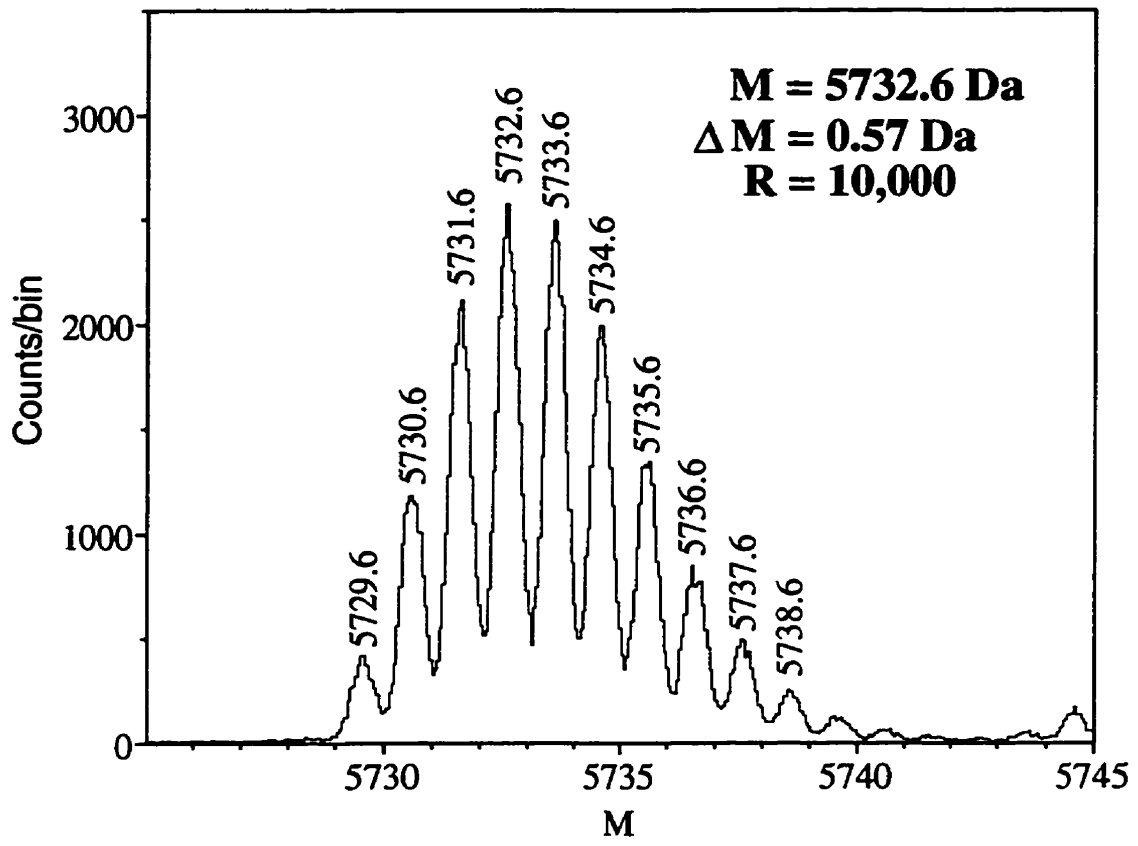

Figure16. Deconvoluted mass spectrum of bovine insulin with isotopic peaks resolved.

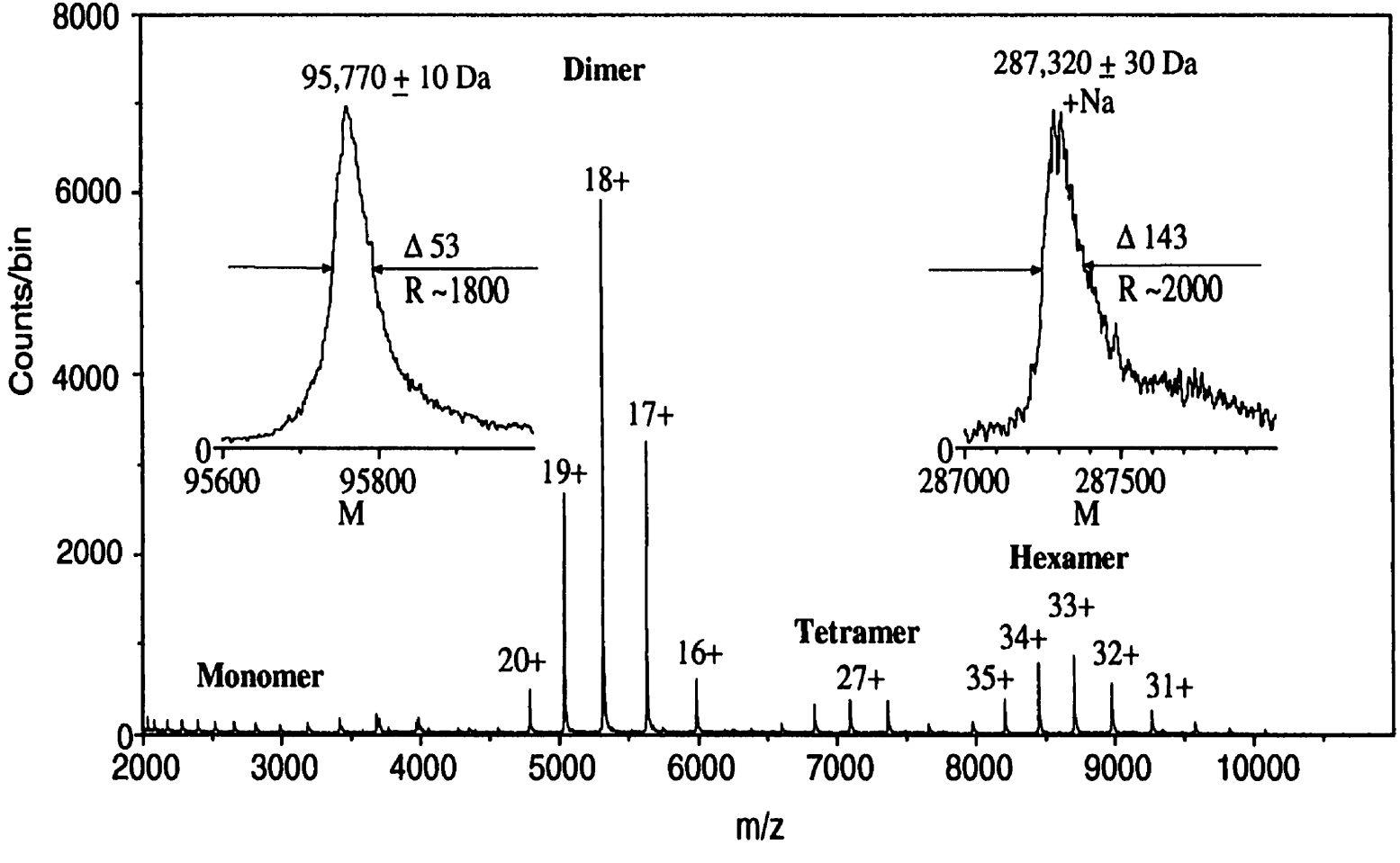

Figure17. m/z spectrum of citrate synthase and deconvoluted mass spectra of the citrate synthase dimer and hexamer. The resolution for both mass peaks (FWHM) is about 2000. Partially resolved sodium in the hexamer peak suggests higher resolution ~10,000 at mass 287,320 Da; declustering potential ΔU = 300 V.

about 7,000-8,000 evaluated for the singly- and doubly-charged peaks of substance P.

The resolution remains reasonably high for a broad mass range. Figure 17 shows the spectrum of *E. coli* citrate synthase obtained from a 10^{-5} M solution of the protein in 5 mM ammonium bicarbonate buffer. The measured masses of both dimer and hexamer agree well with the theoretical masses 95,770 Da and 287,310 Da, calculated on the basis of mass of the monomer 47,885 Da, derived from the known amino acid sequence. The mass resolution for the dimer ~1800 is slightly less than for the hexamer (~2000), apparently because the dimers start fragmenting at high declustering potential (ΔU=300 V, in this experiment), which may lead to the broadening of the peak. The partially resolved peak due to the sodium adduct in the fine structure of the hexamer peak suggests that a somewhat higher resolution (~ 10,000) could be achieved if the sample were sufficiently purified. In any case, the resolution achieved was sufficient to resolve separate additions of the NADH ligand to the CS dimer and the hexamer [Krutchinsky et al., 1998; Ayed et al., 1998].

Sensitivity

The RF quadrupole significantly increases the sensitivity of the TOF III mass spectrometer. Figure 18 shows a comparison of two cytochrome c spectra obtained before (a) and after (b) installing the new ion interface. Both spectra are plotted on the same scale. The amount of the sample consumed in the latter case was ~ 350 times less. This is one especially favorable case, but on average, the ion interface gives us now from 2 to 10 times better sensitivity for a variety of samples. The improvement appears to be larger for higher masses and yields a sensitivity in the femtomole range for proteins of M.W. ~ 100,000 Da. Figure 19 shows the spectrum of soybean agglutinin (SBA, M.W. ~116,000 Da) recorded in 10 seconds. 120 femtomoles of the glycoprotein was consumed using a conventional

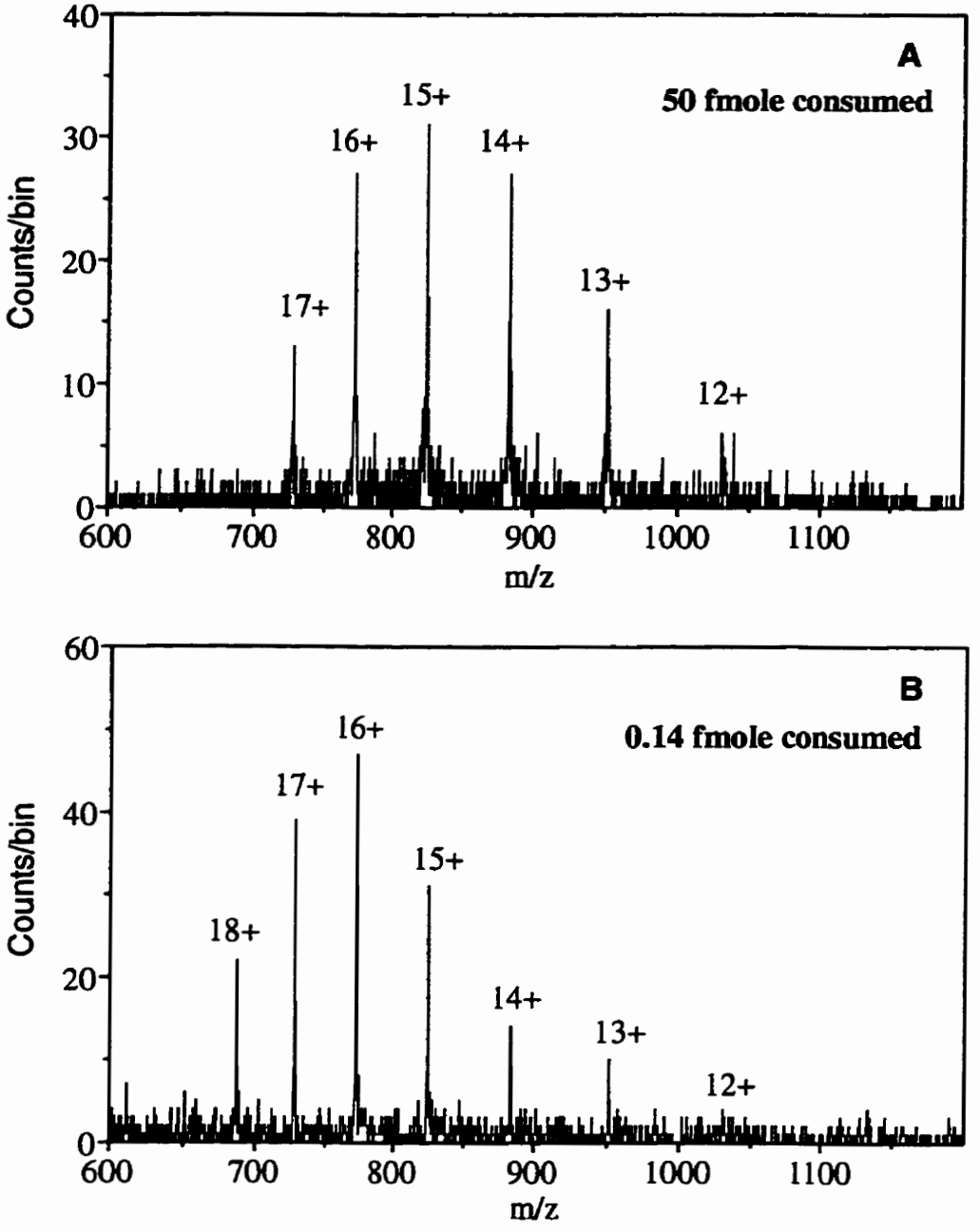

Figure18. Comparison of the sensitivities of the TOF spectrometer for cytochrome c. (**A**) Before installing the new interface. A 10^{-6} M solution of cytochrome at a flow rate of ~0.01 μL/s in 5 s recording time. Total number of counts of cytochrome c ions ~2150. (**B**) After the quadrupole ion guide was installed in the interface. A 10^{-7} M solution of cytochrome c at a flow rate of ~1.4 nL/s in 1 s recording time. Total number of counts of cytochrome c ions ~1500.

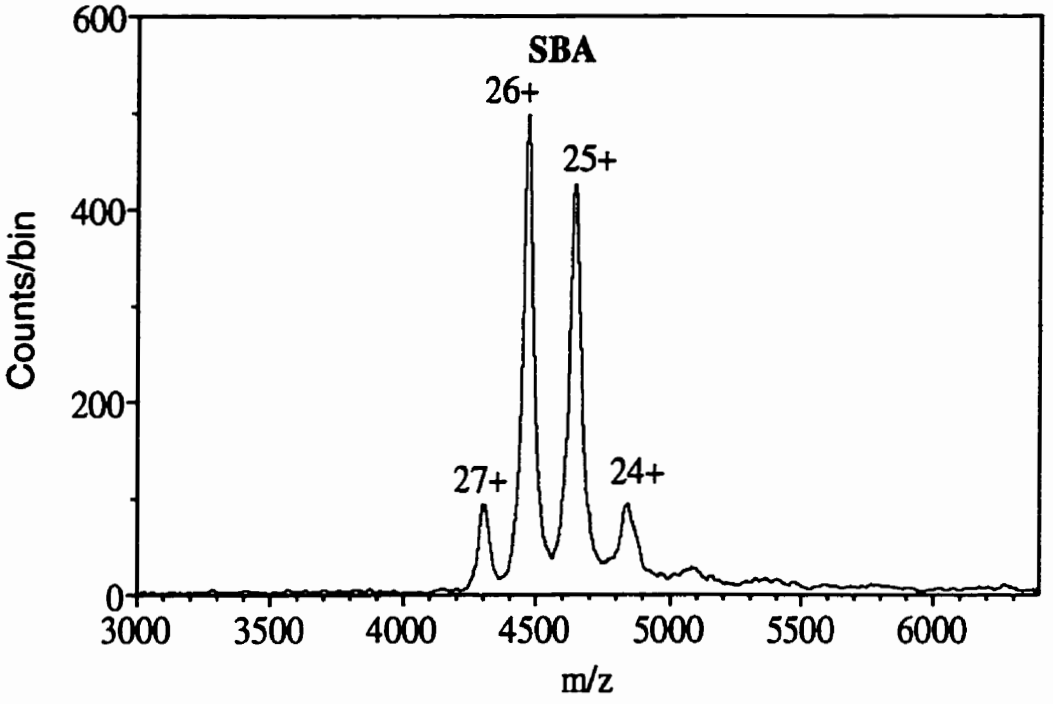

Figure 19. The m/z spectrum of SBA tetramer (M.W. ~116,000 Da) recorded in 10 s. A $4x10^{-5}$ M solution of SBA at a flow rate 2.8 nL/s. Approximately 120 fmole of the glycoprotein was consumed to obtain the spectrum. The total number of counts of SBA ions ~17,000.

electrospray. The mass spectrometer has higher sensitivity (in the attomole range) for the same sample using a nanospray technique [Chernushevich et al., 1995].

Manipulation of Electrospray Ions prior to Injection

Mass filtering mode of operation.

Figures 20 B and 20 C show the possibility of using the ion guide for filtering particular masses even though the quadrupole operates at very high pressure. Cytochrome c was electrosprayed from a weak acetic acid solution (0.05%) so that both denatured and native forms are presented in the spectrum in Figure 20 A. The filtering was performed by adjusting the frequency and small positive and negative voltages applied to each pair of rods (up to +-30V). Mathieu parameters a and q were changed independently [Dawson, 1976]. Although the ~80 m/z window used corresponds to rather poor resolution, it allows us to filter each charge distribution. The losses by filtering the ion peaks using the 80m/z window appeared to be less for substances with bigger m or m/z and vary from ~100 for doubly-charged peak of substance P to ~10 for cytochrome c.

Collision-Induced Dissociation

In order to cover the maximum m/z range for ion transmission through the quadrupole ion guide, the operating frequency is set to be ~2 MHz, the maximum value provided by the signal generator. It gives a cutoff at m/z 70 by applying a peak RF voltage of ~500 V to the ion guide. Figure 21 A shows the mass spectrum of leucine enkephalin (M.W. 555.28 Da) obtained at a low declustering potential (ΔU=100V). The group of peaks in the low m/z range is not caused by sample fragmentation but by "chemical noise", impurities that are always present in any sample. It is possible to filter out this noise either in filtering mode of operation or, by increasing the amplitude of the RF driving voltage or by decreasing its frequency. In the second case, decreasing the frequency is preferable to avoid a discharge between the quadrupole rods. When the operating frequency equals 320

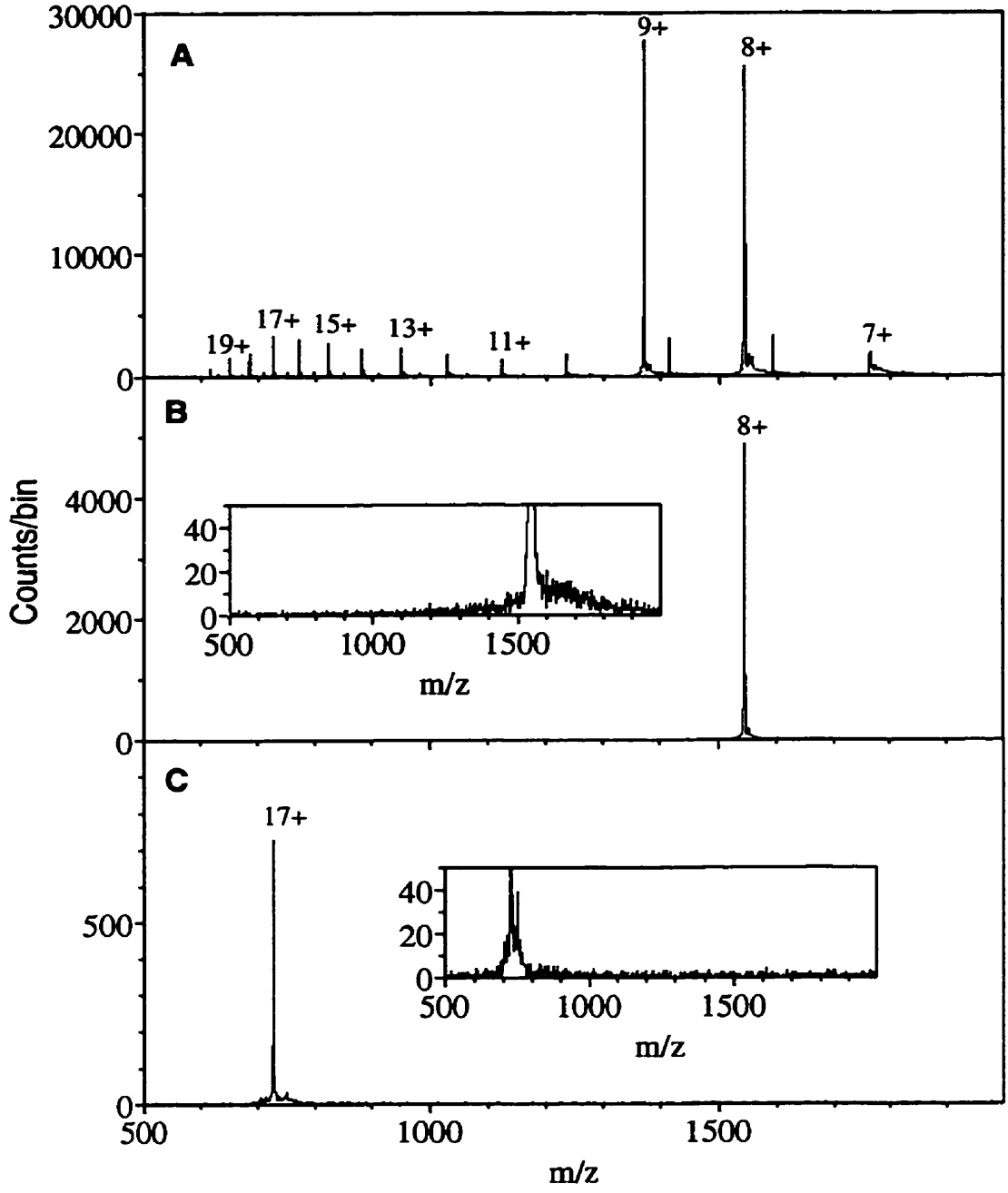

Figure 20. (A) The m/z spectrum of cytochrome c from weak acidic solution (water/methanol (1/1 v/v) +0.05% acetic acid). (B) Mass filtering of the 8+ peak of cytochrome c from the charge distribution by the quadrupole ion guide operating as a mass filter. A zoomed spectrum is shown to evaluate the signal to noise ratio around the ~80 m/z filtering window. (C) Mass filtering the 17+ peak and the corresponding zoomed spectrum around the filtering window.

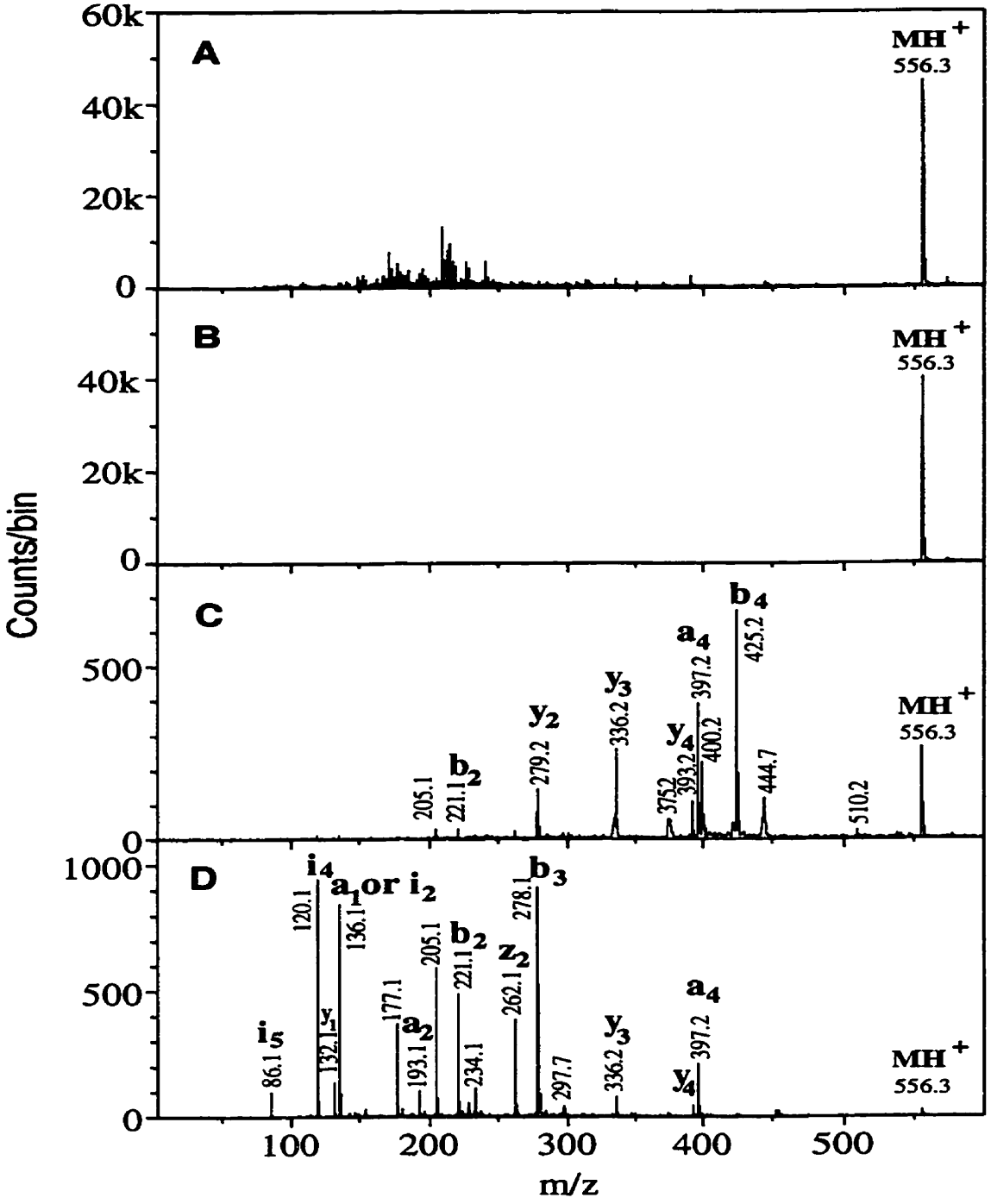

Figure 21. The m/z spectra of leucine enkephalin (555.28 u)
(A) f_{RF} =2 MHz, U_{RF} =500V, ΔU=3V at the exit of the quadrupole
(B) f_{RF} = 320 kHz, U_{RF} =500V, ΔU=3V at the exit of the quadrupole
(C) f_{RF} = 320 kHz, U_{RF} =500V, ΔU=34V at the exit of the quadrupole
(D) f_{RF} = 320 kHz, U_{RF} =500V, ΔU=64V at the exit of the quadrupole. The excess kinetic energy that the ions gain in collisional induced dissociation was compensated by proper adjustment of the voltages on the steering plates

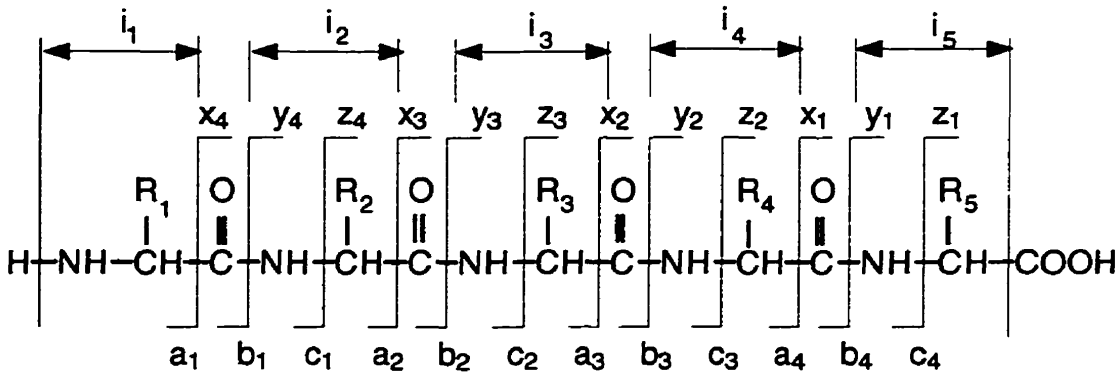

Figure 22. The assignment of the major backbone fragments and the immonium ions of a pentapeptide according to Roepstorff's nomenclature [Roepstorff & Fohlman, 1984].

kHz the mass cutoff is ~550 Da so that no noise signal is observed up to the quasi-molecular ion peak, the most abundant one in the spectrum in Figure 21 B. This mode of operation is convenient for performing collision-induced dissociation at the exit of the quadrupole. Figures 21 C and 21 D show two fragmentation spectra of leucine enkephalin obtained at 34V and 64V difference between the offset of the quadrupole and the second aperture plate (5mm gap). All fragment ions were identified, but only the immonium and backbone fragment ions have been labeled in these and other spectra, according to Roepstorff's nomenclature (Fig. 22). The fragmentation pattern obtained in this region with a collision gas thickness ~$3.5 \times 10^{15}/cm^2$ is similar to that described previously for some small peptides [Thomson et al., 1995]. To the author's knowledge, this is probably the first collision-induced dissociation spectrum of a parent ion obtained in a quadrupole-TOF mass spectrometer system in the orthogonal configuration. Later, the technique has evolved in the so called QqTOF or Q-TOF instruments developed by Micromass [Morris et al., 1997] and by our laboratory in co-operation with SCIEX [Shevchenko et al., 1997].

Selective Collision-Induced Dissociation of Ions in the Quadrupole Ion Guide.

Selective collision-induced dissociation is a well-known technique of tandem mass spectrometry, and it is mostly utilized in quadrupole ion traps [Kaiser et al., 1991; Vachet & Glish, 1996]. However, it is also possible to implement this technique in a quadrupole ion guide.

Ion motion in a quadrupole is described by a Mathieu type equation [Dawson, 1976, see also Appendix II]. The analytical solution for this equation is difficult to obtain, but with a number of assumptions it is possible to find an approximate solution. According to some of the solutions [for reference here and further see: Gerlich, 1992], ions perform a fast oscillatory motion (wiggling motion with the frequency of an RF-field), superimposed on slow oscillations around the quadrupole axis with the so called secular frequency. Those

can be recognized from the ion trajectories plotted in Figure 9A. The frequency of secular motion can be found from an equation of motion in an effective potential V^*, which in the case of the quadrupole ion guide increases in proportion to $\sim r^2$, where r is the distance from the center of the guide. Since the effective potential V^* is a harmonic potential, the solution gives a unique value of the secular frequency for ions with a particular *m/z* value.

It was shown previously in the *Calculation* section that the amplitude of secular oscillations decreases as ions move along the quadrupole ion guide, i.e. there is a strong radial focusing of ions and radial velocity damping (see Fig. 9A and Fig. 23A). However, the secular oscillations of the ions with a particular *m/z* can be excited again by a small RF-signal with a corresponding frequency, added to the main RF-signal driving the quadrupole. This is schematically shown in Figure 23B. Ions whose oscillations are excited collide with the molecules of a buffer gas and eventually may undergo collision-induced dissociation.

A few spectra illustrate this technique. To begin with, the electrospray spectrum of a mixture of two peptides, substance P (M.W. =1346.74 Da) and des-Arg-bradykinin (M.W. =903.47 Da), shown in Figure 24A, was obtained in the single MS mode. In this case, the collisional quadrupole ion guide was driven by an RF signal with a frequency 1.93 MHz and an amplitude 760 V. The most abundant peaks in the spectrum are the doubly- and triply-charged peaks of substance P (674.37 *m/z* and 449.91 *m/z*) and a doubly-charged peak of des-Arg-bradykinin (452.73m/z). When a small RF-signal (f_{exc} = 405 kHz, U_{exc} = 14V) is added to the main driving signal, it causes the resonance excitation of ions in the region ~450 *m/z*. The triply-charged ions of substance P and the doubly-charged ions of des-Arg-bradykinin become excited producing the collision-induced dissociation (CID) spectrum shown in Figure 24 B. (The spectrum was obtained by subtraction of the spectra obtained with and without excitation).

In general, CID of doubly-charged ions of des-Arg-bradykinin produces a ladder of y-fragments, whereas CID of triply-charge ions of substance P results mainly in two

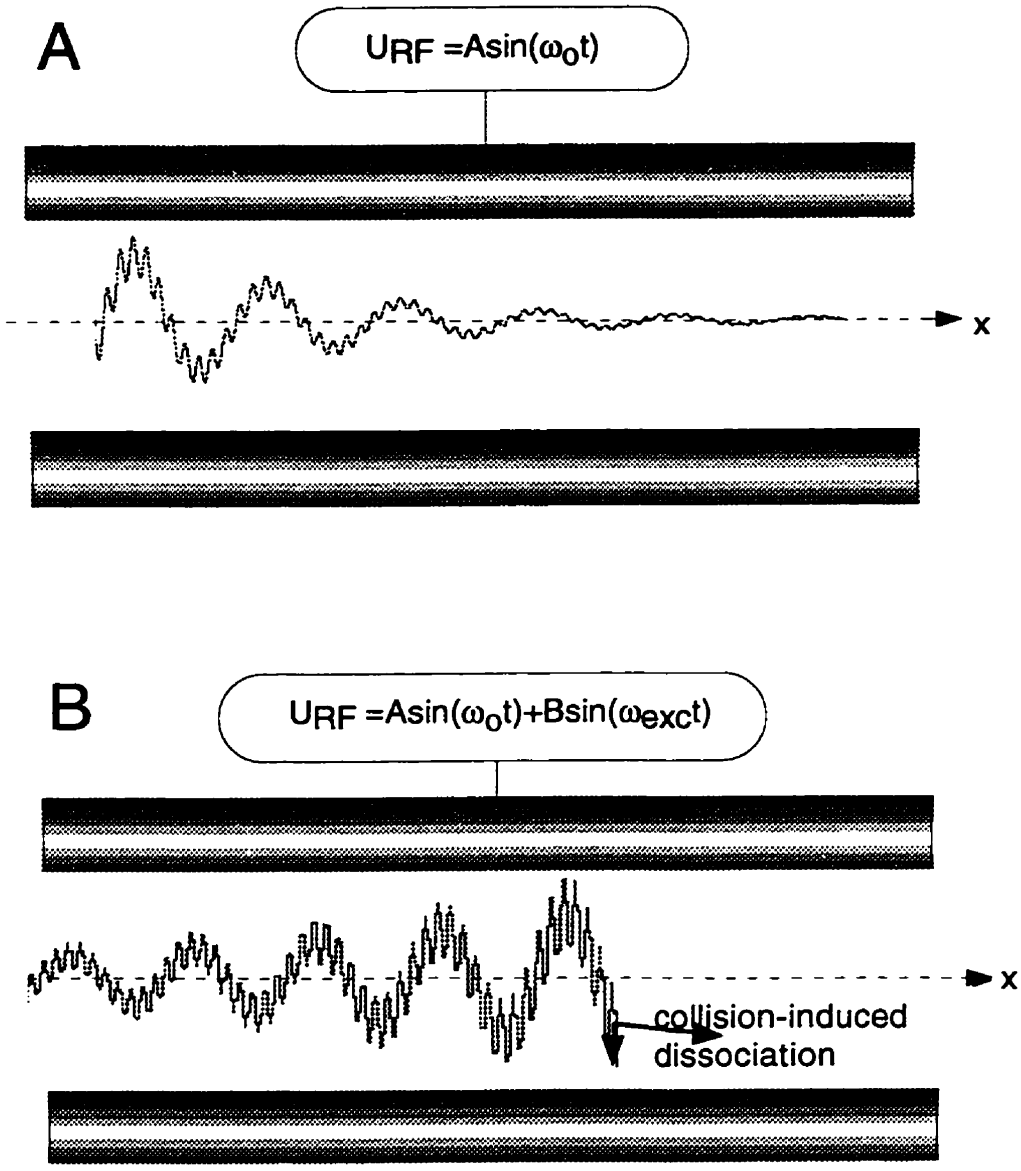

Figure 23. (**A**) Typical ion trajectory in a collisional quadrupole ion guide. An ion collides with buffer gas molecules and loses kinetic energy. The amplitude of ion oscillations decreases as the result of collisions. (**B**) The oscillations can be excited again if a small RF signal with a frequency ω_{exc} corresponding to an ion with particular m/z is added to the main RF signal. Collision-induced dissociation may occur as the result of resonance excitation.

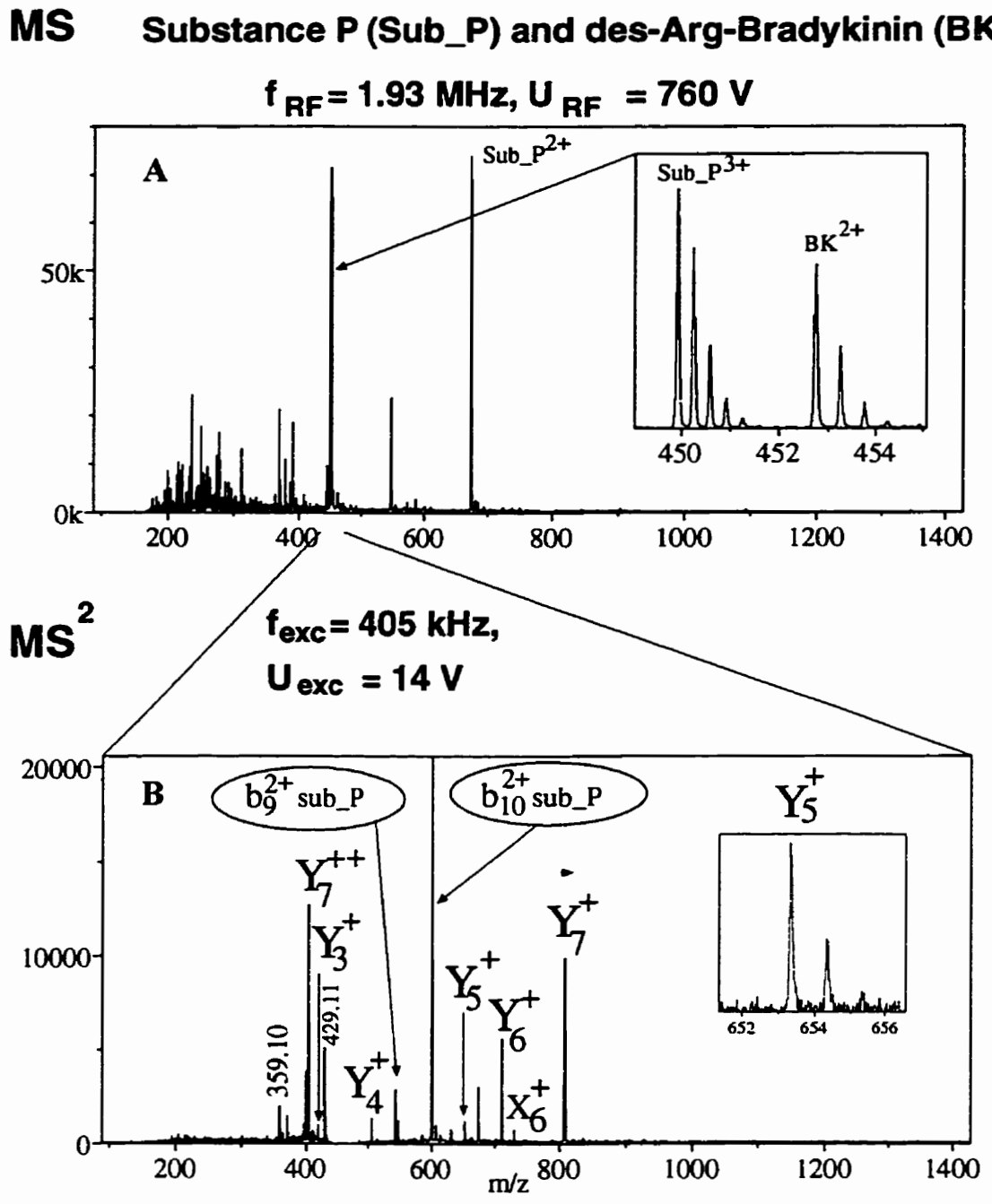

Figure 24. (A) Electrospray spectrum of a mixture of two peptides, substance P (1346.74 Da) and des-Arg-bradykinin (903.47 Da). (B) CID spectrum of doubly-charged ions of des-Arg-bradykinin (452.73 m/z) and triply-charged ions of substance P (449.91 m/z) obtained by resonance excitation of ions in the m/z region ~430-480. The peaks are assigned according to Roepstorff's nomenclature (see Fig. 22)

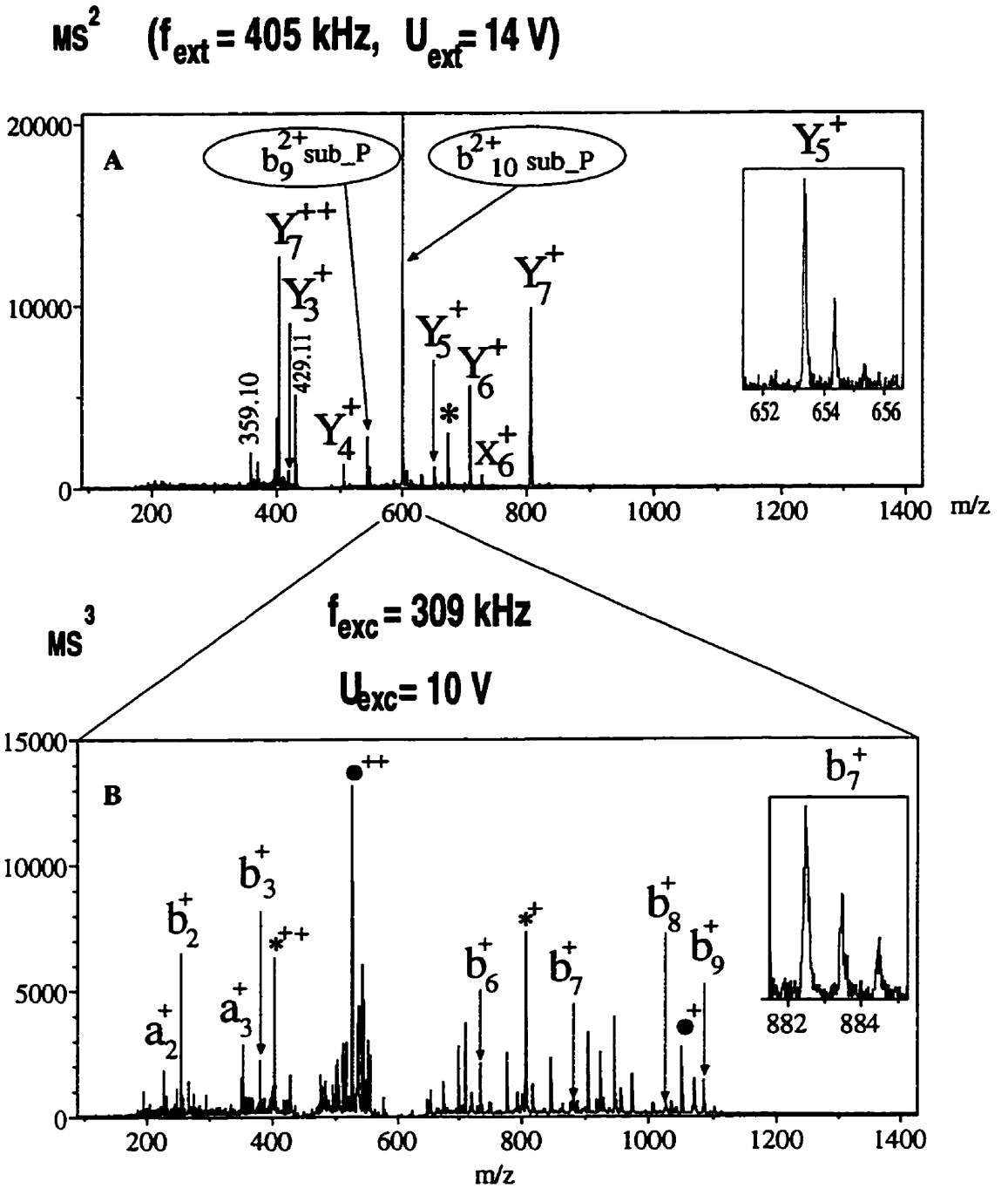

Figure 25. (A) CID spectrum of doubly-charged ions of des-Arg-bradykinin (452.73 m/z) and triply-charged ions of substance P (449.91 m/z) obtained by resonance excitation of ions in the m/z region ~430-480. (B) Resonance CID spectrum of doubly-charged b_{10}-fragments of substance P. Some prominent internal fragments are labeled with asterisks and filled circles.

peaks, the doubly-charged fragments b_9 and b_{10}. It is possible to extend this approach and to add another excitation signal. For example, addition of another small RF signal (f_{exc} = 309 kHz, U_{exc} = 10V) to the previous ones causes the resonance excitation of the doubly-charged b_{10}-fragment ion of substance P, the CID spectrum of which is shown in Figure 25 B. CID of doubly-charged b_{10}-fragments produces a ladder of clearly identifiable singly-charged b-fragments labeled in the spectrum. Some internal fragments are left unlabeled. Thus, it is possible to perform an MS^3 experiment using a single collisional-damping quadrupole ion guide.

Preliminary results on this technique have been reported [Loboda et al., 1998] and, a provisional patent application has been submitted by the authors. More detailed results will be published in the future as a separate paper.

Conclusions

Mass range, sensitivity, and resolution of our ESI/TOF III instrument have been considerably improved by installing a quadrupole collision ion guide in the atmosphere/ high vacuum interface. These three most important characteristics of any mass spectrometer were improved at the same time. Measurements on time delays and the results of simulations of the ion motion inside the collisional ion guide confirm the main ideas underlying its operation. Both transverse and axial velocities that the ions acquire in the free expansion/declustering processes are damped to very low values while the ions are constrained close to the quadrupole ion guide axis. These effects enable us to obtain a highly focused beam of ions with a well-defined kinetic energy prior to its injection into the storage region of the mass spectrometer. Several techniques of ion manipulation in the collisional quadrupole ion guide before the orthogonal injection of ions into the mass spectrometer have been demonstrated.

IV. ORTHOGONAL INJECTION OF MALDI IONS INTO A TIME-OF-FLIGHT SPECTROMETER THROUGH A COLLISIONAL DAMPING INTERFACE

The successful incorporation of a collisional quadrupole ion guide in the ESI-TOF III mass spectrometer has encouraged us to implement the concept of collisional cooling of MALDI ions for the orthogonal injection into the same mass spectrometer. Based on our experience and findings accumulated in the experiments with electrospray ions as well as some simulations of ion motion using the computer program described above, a new collisional damping interface capable of operating with a MALDI source has been built.

Experimental

The collisional damping interface

A schematic diagram of the new interface installed on the TOF III mass spectrometer is shown in Figure 26. In this interface, a MALDI target can be inserted on the end of a probe that fits through a probe inlet port, then through a valve into the quadrupole compartment, where it is held in position by a supporting ring. A more detailed diagram of the probe is shown in Figure 27; its tip is electrically insulated from the rest of the shaft.

A mixture of the sample to be investigated and a suitable matrix applied to the tip of the probe is irradiated by the beam of a pulsed N_2-laser (Model VSL-337ND, Laser Science Inc., Franklin, MA), which is focused on the target surface by a lens, and is run at a repetition rate up to twenty pulses per second. Each laser shot normally produces a

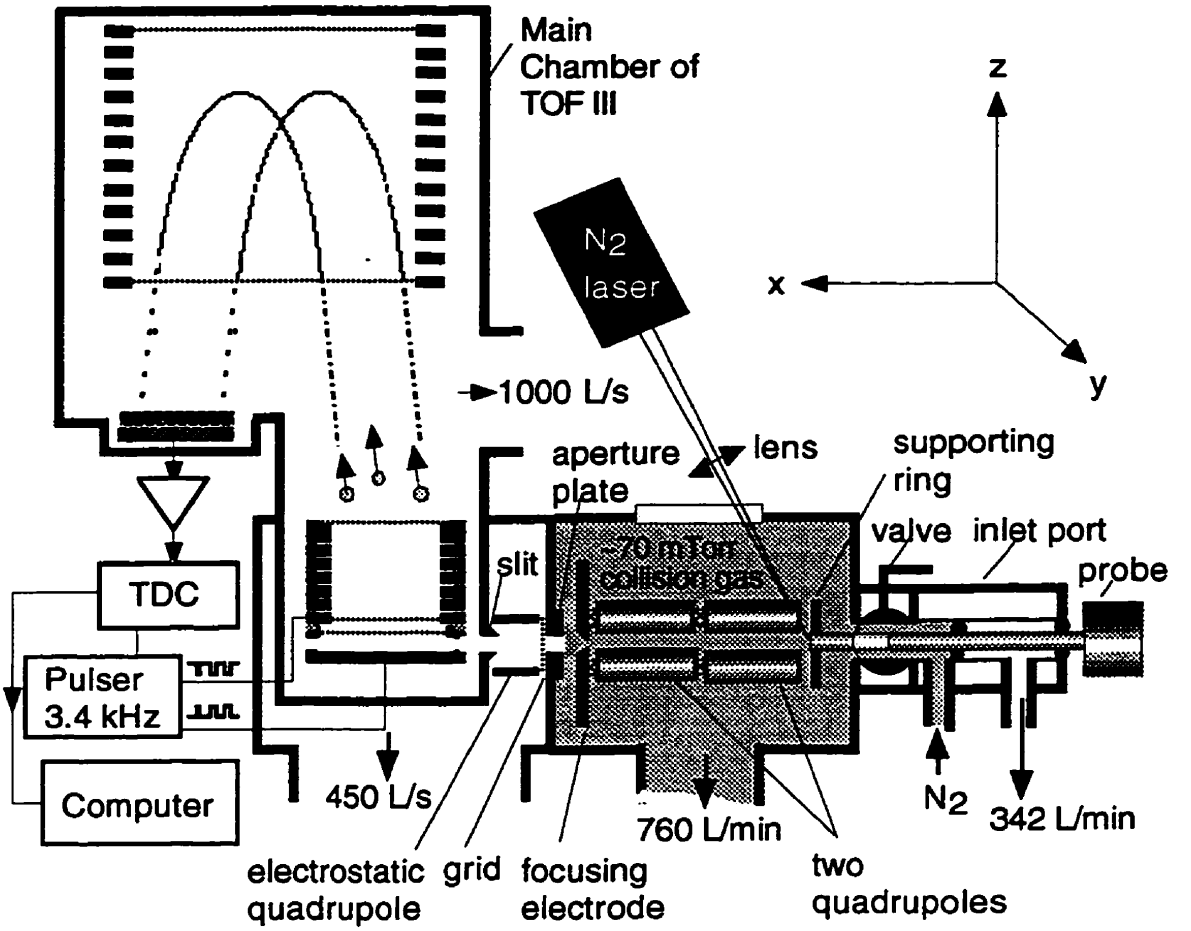

Figure 26. Schematic diagram of the orthogonal injection TOF mass spectrometer coupled to a source of MALDI ions through a collisional damping interface. The quadrupole compartment contains N2 as a buffer gas. The ion guide consists of two sets of quadrupoles made of cylindrical rods 4.45 cm in length and 1.1 cm in diameter supported by a focusing electrode. The TOF instrument has a total length ≈1.2 m and a total equivalent flight path ≈2.8 m.

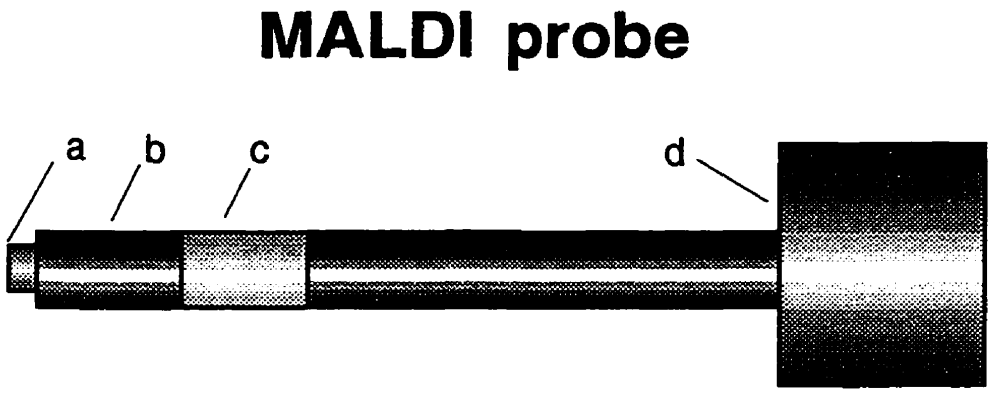

Figure 27. The MALDI ion probe. It consists of a 0.76 cm diameter tip (a) at the end of the probe shaft (b), separated by insulator (c) from the rest of the shaft , which is mounted in the knob (d). When the probe is inserted the tip makes an electrical connection to the supporting ring.

plume of neutral and charged molecules, which expands into the quadrupole compartment. This chamber contains two sets of quadrupole rods supported by a focusing electrode. The pressure inside is determined by a balance between an inlet flow of nitrogen and the pumping is provided by a Leybold-Heraeus 760 L/min mechanical pump. A typical pressure in the chamber is ~ 70 mTorr N_2, but it can be varied over a substantial range by adjusting the flow of nitrogen through a leak valve. After passing through the quadrupole and suffering collisional damping through collisions with the gas, the ions have very low energy, probably close to thermal, as in the case of electrosprayed ions. The ions (mass m and charge q) pass through a focusing electrode and an orifice (1.1 mm in diameter) in an aperture plate into the next vacuum chamber. They are accelerated to an energy $1/2\, mv_{\perp}^2 = qV_0$ by a small potential V_0 applied to the aperture plate.

This chamber is pumped to a pressure ~10^{-5} Torr by an Edwards 450 L/s turbomolecular pump. Here the ions are focused by a grid and an electrostatic quadrupole lens through a slit (6 mm width, 1.5 mm height) into an ion storage region. Segments of the ion beam are extracted from the storage region by pulses applied to the extraction electrodes, then accelerated to an energy $1/2\, mv_a^2 \approx 4000q$ electron volts by a conventional DC accelerating column. A detailed description of the accelerating process and the pulses applied to the extraction was given in the second chapter. After acceleration, ions travel at an angle θ to the axis of the TOF spectrometer given by $\tan\theta \approx v_{\perp}/v_a$. In the present case, setting $V_0 \approx$ 6-7 volts optimizes the transmission for ions having a wide range of *m/z* values as they travel through a single-stage electrostatic

ion mirror and onto a detector. With this setting, no steering voltages are necessary to deflect the ions.

At the detector, ions undergo post-acceleration through ~ 1 kV, so their total energy when they strike the first micro-channel plate is ~ 5000q electron volts. The ions are detected using single-ion counting and recorded with a time-to-digital converter (TDC Model CTN-M2, Institut de Physique Nucléaire, Orsay, France). The electrodes of the storage region , accelerating column , mirror and detector are contained in the main TOF chamber, which is pumped to a pressure ~$3x10^{-7}$ Torr by an APD cryopump (~1000 L/s).

Both sets of quadrupoles are driven by an RF coupling transformer with two secondary coils, providing output voltages from 0 to 1000 volts peak-to-peak when driven by a broadband RF power amplifier (Model 240L, ENI Rochester, NY), which exhibits a flat gain for a wide range of operating frequencies from 20 kHz to 10 MHz. The amplifier is excited by a small sine-wave signal generator (Model SG-100, Telulex Inc, Mountain View, CA). Typical operating frequencies are 200 kHz to 1 MHz, and typical operating voltage amplitudes are 100 to 1000 V peak-to-peak. Bias or offset potentials are applied to the rods of the quadrupoles and to various other components by a multiple-output power supply (Model TD-9500, Spectrum Solutions Inc., Russellton, PA). When the collisional quadrupole ion guide is run in an RF-only mode, as shown in Figure 28A, it serves to damp the initial velocity of the MALDI ions and focuses them toward the center of the quadrupole axis. The first quadrupole can also be run in a mass-

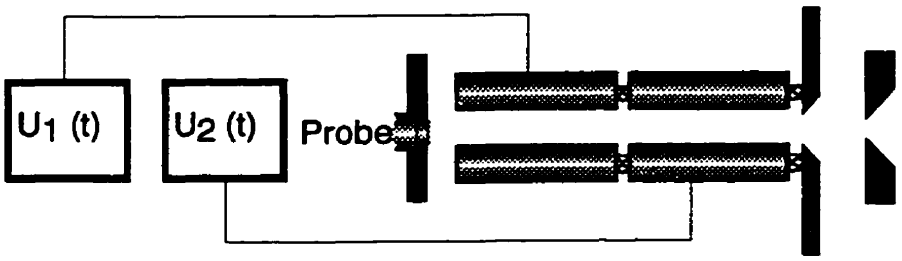

A. RF-only mode

$U_1(t) = A_1\sin(\omega t)$

$U_2(t) = A_2\sin(\omega t)$

$A_2 = A_1$

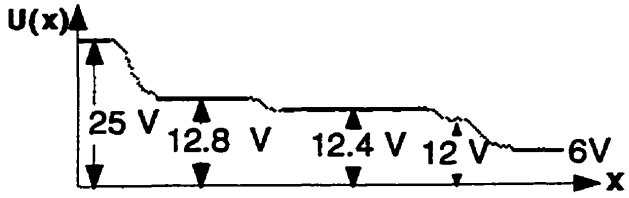

B. Mass selection mode

$U_1(t) = A_1\sin(\omega t)+V$

$U_2(t) = A_2\sin(\omega t)$

$A_2 = 1/3A_1$

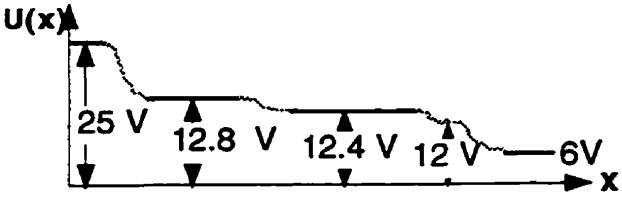

C. MS/MS mode

$U_1(t) = A_1\sin(\omega t)+V$

$U_2(t) = A_2\sin(\omega t)$

$A_1 = 1/3A_2$

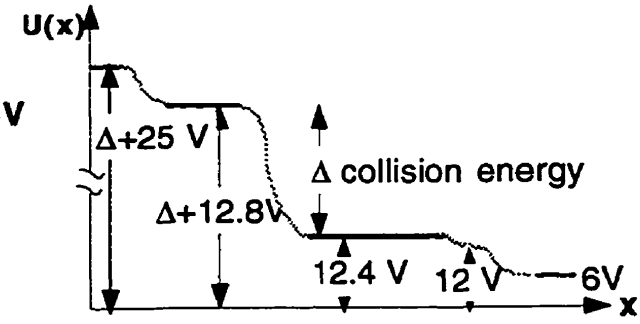

Figure 28. Typical distribution of DC and AC voltages applied to the electrodes of the collisional damping interface when the quadrupoles are operating in the different modes.
(A) RF- only mode; (B)- mass selection mode; (C) MS/MS mode

filtering mode by applying an appropriate dc voltage to the rods, as shown in Figure 28B. Then, the second quadrupole can be used as a collision cell (and as quadrupole ion guide) in collision-induced dissociation experiments (MS/MS mode, Figure 28C).

Target preparation

Solutions of peptides were prepared as for conventional electrospray experiments, in deionized water/reagent grade methanol (1/1 v/v) with an addition of glacial acetic acid (5-10% in solution). The concentration of analyte ranged from 10^{-4} to 10^{-9} M. D-Ala^2-leucine enkephalin-Arg (dalargin), substance P, melittin, bovine pancreas insulin, horse heart cytochrome c, and horse skeletal muscle myoglobin were purchased from Sigma Chemical Co. (St. Louis, MO) and were used without further purification.

Recombinant citrate synthase from *E. coli* was prepared in the University of Manitoba Chemistry department [Duckworth & Bell, 1982]. The tryptic digestion of citrate synthase was performed in 20 mM ammonium bicarbonate by adding TPCK-treated trypsin (Sigma) (1:100 w/w) to the sample and incubating for 30 min, 1 hour, or overnight (12 hours). Digestion was stopped by addition of acetic acid and diluted four times with methanol and water to give a final protein concentration of approx. 0.5 mg/mL ($\sim 10^{-5}$ M) in 1:1 methanol/5mM ammonium bicarbonate, 3% acetic acid. Then the samples were used without further purification.

Two methods of matrix preparation have been used. In one, similar to the method described by Vorm [Vorm et al., 1994], a saturated solution of α-cyano-4-

hydroxycinnamic acid (also from Sigma Chemical Co., St. Louis, MO) was prepared in reagent grade methanol/acetone (1/1 v/v). A fairly thick layer of the matrix was created by depositing 5 to 10 μL of this saturated solution onto the tip of the probe so that the whole area of the probe tip (7.6 mm in diameter) was covered. That solution was allowed to dry quickly to form a rather smooth homogeneous matrix layer . Then 1 μL of the analyte was applied to the top of the matrix surface and allowed to dry. In some cases, the sample was "washed" by placing a droplet of 10 μL of water on top of the sample spot, and leaving it there for ~10 s before blowing it off by a stream of air.

In the other method [Xiang & Beavis, 1994], a saturated solution of a-cyano-4-hydroxycinnamic acid was prepared in aqueous 0.1% TFA/acetonitrile (2:1, v:v). 1μL of the matrix solution was applied to the tip of the MALDI probe to form a smaller spot (~2 mm in diameter). Then an analyte was mixed with the same matrix solution and 1μL of the solution was applied on the top of the matrix layer created previously. This procedure gave better sensitivity for analytes in the low femtomole range.

Experimental results and discussion

Collisional cooling of ions in an RF quadrupole ion guide produces an approximately parallel ion beam of a small cross section. The beam has a small energy, independent of mass, as well as a small energy spread. Thus cooling helps to avoid earlier discussed problems connected with the orthogonal injection of MALDI ions into a TOF

mass spectrometer directly from the ion source. This and other advantages are illustrated in the experimental results that follow:

Resolution and mass accuracy

Figure 29 shows the spectrum of an equimolar mixture of several peptides desorbed from an α-cyano-4-hydroxy cinnamic acid matrix (4HCCA). The spectrum was acquired in a single 60 s run at 20 Hz laser repetition rate, and shows mass resolution ($M/\Delta M_{FWHM}$) between 4000 and 5000 for all components. Resolutions consistent with this value were also observed for small proteins (see below). In the present interface, the entrance orifice in the second aperture plate was made slightly larger than normally used in ESI in order to make adjustments easier in the preliminary experiments. The resolution obtained is close to that found with an ESI source under similar conditions. However, a resolution ~10,000 has been observed for ESI ions in the same instrument with a smaller apertures, as shown previously, and a resolution of up to 15,000 in a SCIEX ESI QqTOF mass spectrometer with a similar interface has been reported recently [Chernushevich, 1998]. Some preliminary results obtained in our laboratory with a QqTOF instrument configured with a MALDI ion source show that resolution of more than 10,000 can be readily achieved when the internal geometry of the interface is optimized [Loboda et al., 1998, preliminary results]

The near-uniform energy of the ions after collisional cooling removes any mass dependence on the optimum extraction conditions and allows the simple quadratic relation

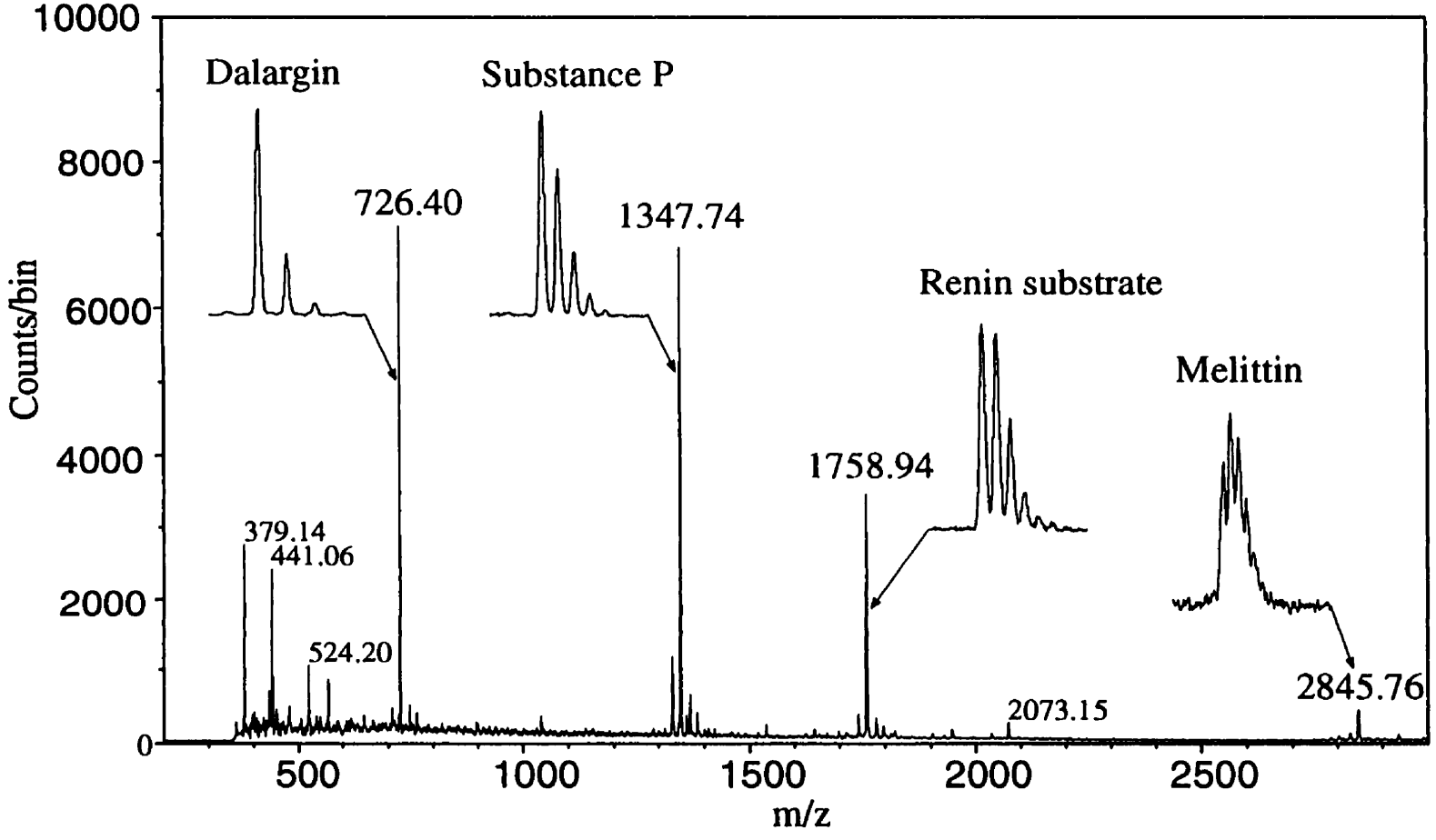

Figure 29. MALDI spectrum of an equimolar mixture of four peptides (dalargin, substance P, renin substrate, and melittin from a matrix of α-cyano-4-hydroxycinnamic acid. 1μL of a 10^{-6} M solution of each peptide was applied to the target. The repetition rate of the N_2-laser was 20 Hz and the spectrum was acquired for 1 min. Expanded views of the protonated ion peaks show a uniform resolution ($M/\Delta M_{FWHM}$) of 4000 to 5000. Substance P and melittin were used as internal calibrants, so the numbers over those peaks are theoretical values. Labels over the other peaks indicate experimental masses.

between flight time and mass to be used for calibration with two calibrant peaks. Using a simple external calibration with substance P and melittin, the mass determination is accurate to within about 30 ppm for ions up to a mass of at least 6000 Da. Such a two-point external calibration is stable for several weeks if the mirror voltage supply is left on. The calibration is largely insensitive to the distribution of the voltages in the quadrupole interface. In our experiments with a variety of voltage settings, the accuracy always remained within 50 ppm using an external calibration and ~ 30 ppm using an internal calibration.

Mass range

As already demonstrated for electrospray ions, collisional cooling also removes mass and *m/z* discrimination in the TOF mass spectrometer. In previously described experiments, a wide range of masses (up to bovine insulin) have been analyzed at the same time. At present the observable mass range is limited by the detection efficiency, which decreases with mass for singly-charged ions at a given energy because of the strong dependence of efficiency on velocity [Westmacott et al., 1996]. In the present configuration, the energy of singly-charged ions at the detector conversion surface is only about 5 keV (compared to 30 keV in typical MALDI experiments), and this results in a substantial decrease in the relative intensities of the molecular ions with increasing mass. These measurements are consistent with the relative intensities observed from the same sample when analyzed in a conventional MALDI experiment using 5 kV acceleration.

In spite of the reduced efficiency for larger ions, we have been able to obtain a mass spectrum from cytochrome C (M.W.= 12,359.2 Da) by using the maximum laser repetition rate (20 Hz), an increased amount of sample and 10 min recording time. The spectrum shown in Figure 30 was obtained with the same instrumental settings as in Figure 29, emphasizing the mass-independence of the optimum extraction conditions. The observed peak width is the same as that obtained using electrospray ionization, limited in this mass range by the width of the isotopic distribution. The mass determination was made using an external calibration obtained more than a month earlier.

The 5 kV potential difference between the injection electrodes and the detector surface is the same as used previously for electrosprayed ions. There it was sufficient for observation of the entire mass range because of the higher charge states produced in ESI. However, the efficiency for MALDI ion detection suffers from the low charges (typically one or two) produced in the MALDI process. The obvious solution to the problem is to accelerate the MALDI ions to a higher energy.

Time profile after cooling

An additional effect of the collisional cooling is to spread the ion beam out along the quadrupole axis. Our simulations of the ion motion in the collisional ion guide, using a computer program based on a Monte Carlo method, indicate that ions are cooled down rather quickly (see, for example, Fig. 9). After the kinetic energy reaches thermal values, the ions continue their motion with a small drift velocity. The drift velocity and

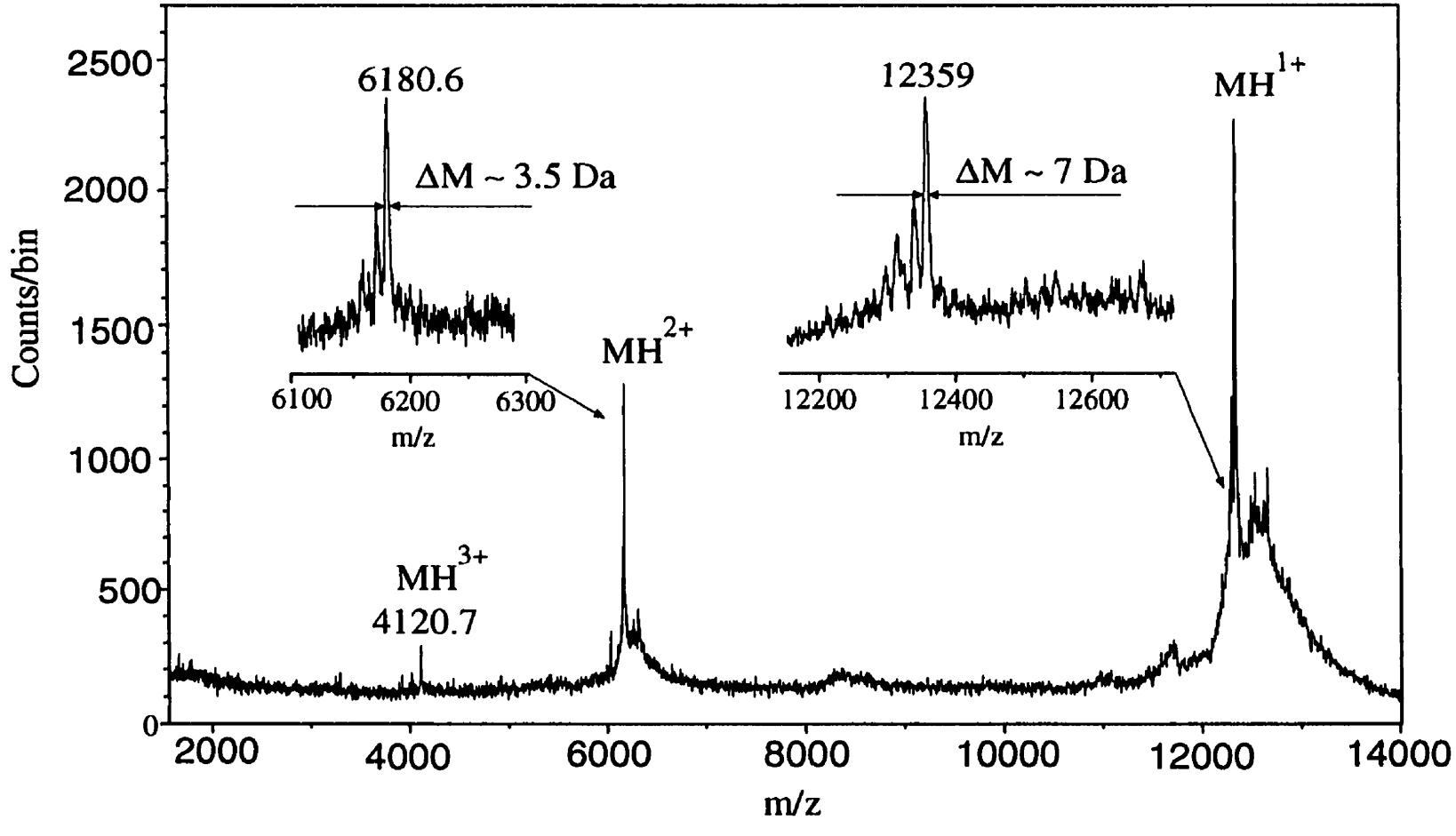

Figure 30. MALDI spectrum of cytochrome c from an α-cyano-4-hydroxycinnamic acid matrix. 100 picomole of the protein was applied to the probe. The repetition rate of the N_2 laser was 20 Hz and the spectrum was acquired for 10 min. The insets show expanded *m/z* regions around the singly and doubly charged peaks with an indication of their widths at half maximum.

consequently the transit time are strongly influenced by the fringing fields that are present near the edges of the various electrodes in the ion guide. The time the ions spend in the quadrupole increases dramatically when the fringing fields are minimized, as shown previously for electrosprayed ions.

Using the voltage settings indicated in Figure 28A, in which the fringing fields are small, collisional damping changes the initial beam pulsed at 13 Hz into a quasi-continuous beam. This is illustrated in Figure 31, which shows the distribution of transit times through the quadrupole ion guide at a pressure of 70 mTorr for ions of various peptides. In this measurement, the counting rate for an ion selected by the mass spectrometer is recorded as a function of time after the laser pulse (for the detailed explanations see section *'Time Delay Measurements'* of the third chapter). The transit times strongly depend on the operating pressure, as shown in Figure 32 for ions of substance P. When the operating pressure is higher than 40 mTorr, the width of the time distribution is ~20 ms, about 25% of the time interval between laser pulses. This may be compared to the subnanosecond duration of the original laser pulse; i.e. it represents an increase in the time spread by a factor of at least 10^7.

At first sight it would seem counter-productive to convert the original pulsed MALDI beam into a quasi-continuous one, and then convert it back into a series of pulses for the flight time measurement in the TOF spectrometer. Nevertheless, this procedure provides a number of advantages, since the properties of the final pulsed beam are quite different from those of the original beam. Multiple injection pulses - 160 to 256 in our

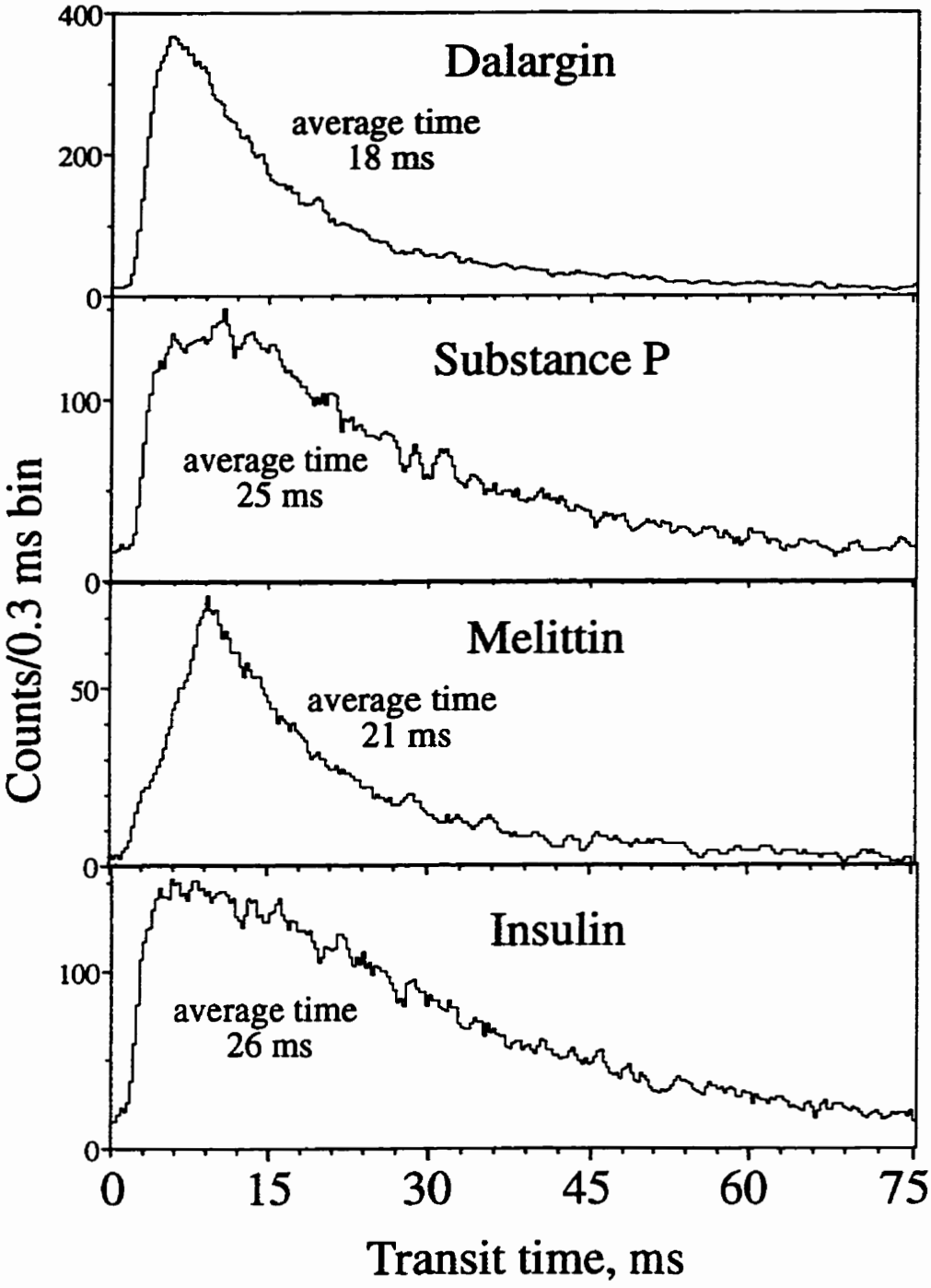

Figure 31. Distribution of transit times through the collisional damping interface for different MALDI ions. The interface was operated as a quadrupole ion guide with collisional damping. The gas pressure in the guide was about 70 mTorr and the repetition rate of the laser was ~13 Hz.

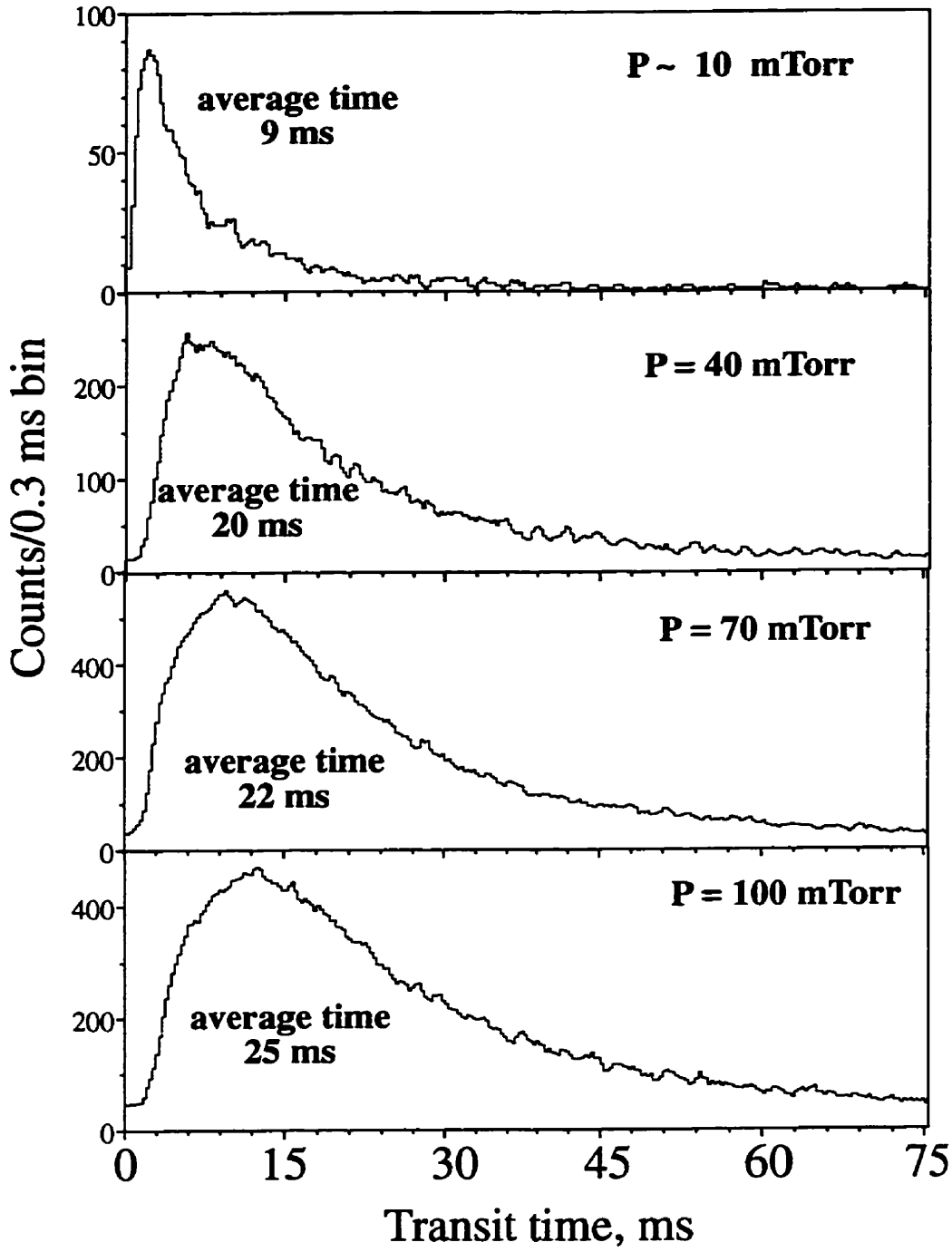

Figure 32. Distribution of transit times for substance P MALDI ions passing through the collisional damping interface operating at different pressures. The average transit times found from the distributions and the pressures are indicated.

case - can be used for every laser shot, because the time-of-flight measurement is no longer correlated with the laser pulse. This reduces the number of ions in a single time measurement by at least the same factor, and thus eliminates problems of peak saturation and detector-shadowing from intense matrix signals. In the present configuration, an average of 3 to 5 ions are detected for each injection pulse, and this is easily compatible with single-ion counting methods with a time-to-digital converter (TDC). Single-ion counting makes the combination of high timing resolution (0.5 ns) and high repetition rate (essential for maximum duty cycle) technically much simpler than using a transient recorder, which is necessary in conventional MALDI experiments. Single-ion counting also places much more modest demands on the detector and amplifier time resolution because the electronic reduction and digitization of the pulse is quite insensitive to the detector pulse shape [Ens et al., 1991].

Sensitivity

The spreading out of the ion beam along the quadrupole axis has advantages as mentioned above, but it involves some losses because of imperfect transmission of the ion guide, and from the 20% duty cycle in our instrument. The transmission of the ion guide has not yet been optimized or measured carefully but preliminary measurements indicate that the practical sensitivity is in the femtomole range for substance P as shown in Figure 33. Five femtomoles of the analyte were applied to the target from a 5 nM solution using 4HCCA as the matrix in water/acetonitrile (2:1) with 0.1% TFA. The spectrum was

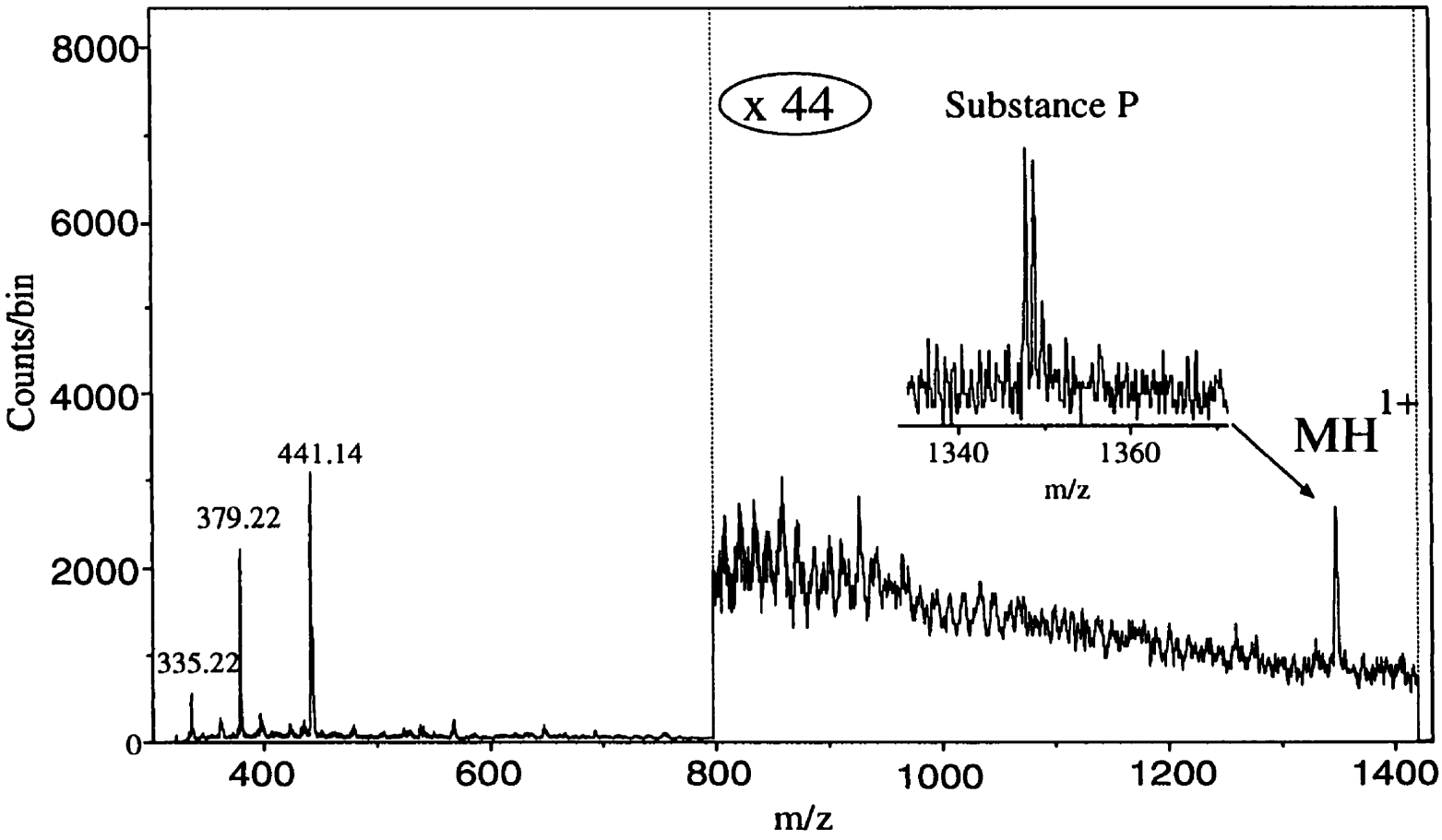

Figure 33. Sensitivity of the instrument. Five femtomoles of substance P were applied to an α-cyano-4-hydroxycinnamic acid matrix. The MALDI spectrum was acquired for 1 min at a laser repetition rate ~13 Hz.

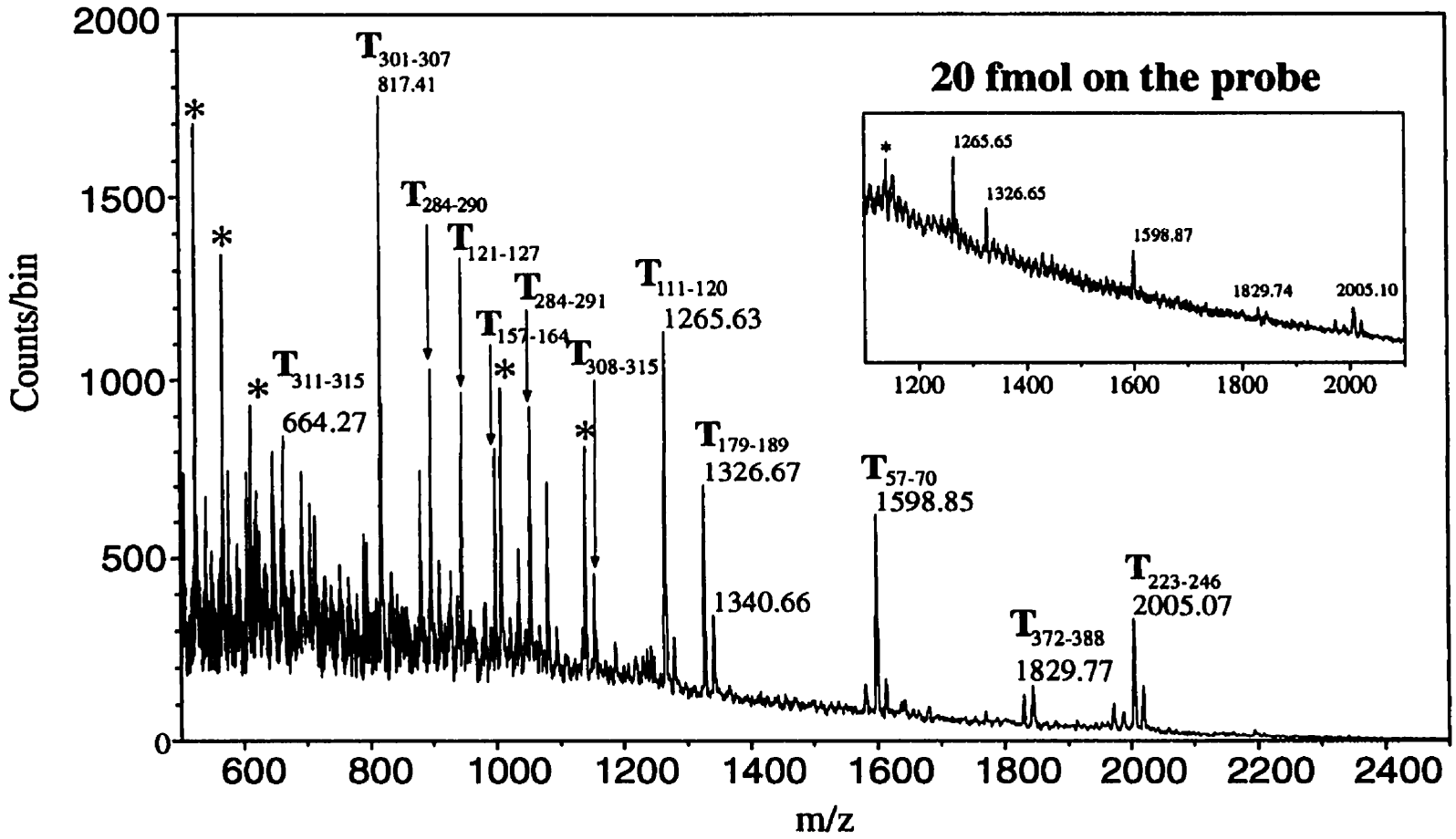

Figure 34. MALDI mass spectrum from a one hour tryptic digest of citrate synthase. The most prominent peaks identified as digestion fragments are indicated by the usual notation. Some abundant background peaks (impurities, cluster matrix ions, and self-digestion peaks of trypsin) are marked with asterisks.

obtained in one minute, although enough sample was present for several more minutes of accumulation. Figure 34 shows the spectrum obtained from a tryptic digest of citrate synthase, again showing the uniform mass resolution over the mass range; the inset shows the spectrum obtained from 20 femtomoles applied to the target. This sensitivity is similar to the typical sensitivity with conventional MALDI. Even better sensitivity for the same sample, in the range of a few hundreds of attomoles, has been achieved on our QqTOF mass spectrometer with a MALDI ion source [Loboda et al., 1998, preliminary results].

Although there are losses compared to the conventional axial MALDI experiment, the data rate can be compensated to a large extent by the higher repetition rate and higher fluence of the laser. In these experiments, the repetition rate was 13 Hz, but it can easily be increased to 20 Hz with the current laser (as for Fig. 29). A laser giving rates up to at least 100 Hz could be used before the counting system becomes saturated. In contrast, the usual MALDI experiment is run at about 1 or 2 Hz. The laser fluence in a conventional MALDI experiment must be kept close to threshold to achieve the best performance, but in the present configuration it can be increased to any convenient fluence up to the point where the ion production process saturates.

The ion losses in the orthogonal interface might be expected to give lower absolute sensitivity than obtained by conventional MALDI but it seems that the lack of dependence of the spectrum on the irradiation conditions (see below) allows more efficient usage of the sample deposited on the target. Use of a fluence several times higher

than threshold continues to produce ions until the matrix is completely removed from the target probe. Figure 35 shows the dependence of the signal for substance P ions on the number of laser shots on one spot. Here one pmole of the sample was applied on top of a 4HCCA matrix, and a single spot was irradiated by a series of shots from the laser, running at 13 Hz. The laser intensity was two or three times the "threshold" intensity.

During the first few hundred shots the signal of the analyte increases, consistent with previous observations that irradiation of a target with high laser fluence increases the signal, possibly as a result of surface cleaning. After the initial increase of the signal it begins to decrease, indicating the gradual exhaustion of the analyte-matrix deposit. Using matrix layers thicker than normal helps to prolong the signal. On average, a given target spot can be irradiated for up to 1 min at 13 Hz before a spot is exhausted. If the laser is then moved successively to cover the whole target, a typical loading containing one pmole of sample can produce a signal for ~ 1 hour, at which point the whole matrix/analyte layer is removed from the tip of the probe.

Decoupling the ion source from the mass measurement

The above results indicate that the performance of the new MALDI configuration is comparable to conventional MALDI, but with the advantage of a mass-independent calibration and a simple calibration procedure. However, we believe that its most important advantages stem from the nearly complete decoupling of the ion production from the mass measurement. Optimum performance in conventional MALDI requires

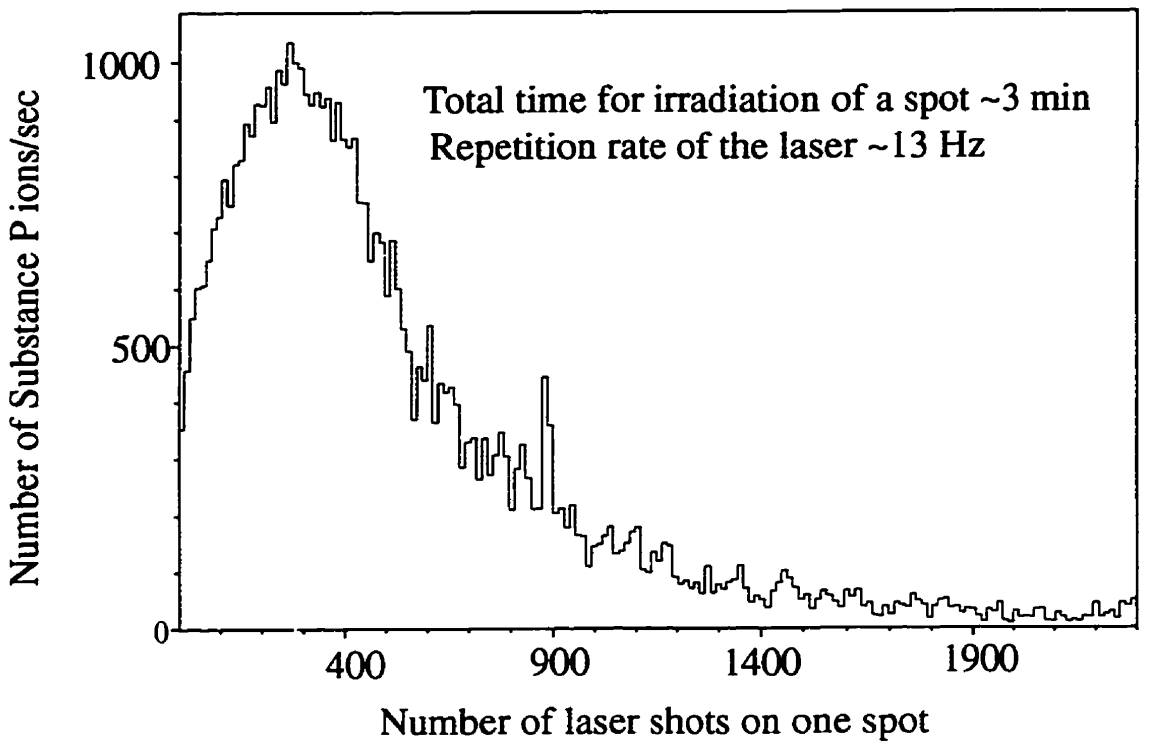

Figure 35. Dependence of the number of substance P ions desorbed per second from a given spot on the number of shots. One picomole of the peptide was applied on top of the α-cyano-4-hydroxycinnamic acid matrix and the laser was operated at 13 Hz.

that the laser fluence and location of the laser spot on the sample be carefully selected for optimum performance. These conditions are typically different for different matrices and even for different target preparation methods. The partial decoupling introduced by delayed extraction has made these adjustments less critical, but even so, commercial instrument manufacturers have found it useful to incorporate software to adjust laser fluence, detector gain, and laser position, and to reject shots in which saturation occurs.

None of this is necessary with the present technique. The performance obtained above shows no dependence on target or laser conditions. The detector is set for single-ion counting and the laser is simply set to any convenient fluence up to maximum. Although this may be several times the usual "threshold" value, no effect on sample fragmentation has been observed. The laser can be moved to a different spot on the target without any readjustment. As a result, the acquisition of MALDI spectra is extremely simple, requiring very little operator expertise and no need for software control of laser or detector conditions.

A major advantage of the decoupling is the ability to make both MALDI and ESI measurements on the same TOF instrument, as described below. In addition, several other potential advantages are evident. A decoupled MALDI source at a potential close to ground should be convenient for investigating new types of target, such as insulators or membranes, or lasers with different wavelengths or pulse widths. The effects of such changes can be evaluated readily, since the mass measurement is independent of these

conditions. The decoupling also permits selection of a parent ion for MS/MS measurements before entry into the TOF spectrometer.

MS/MS mode of operation

Complete decoupling of an ion source from a mass spectrometer provides an opportunity to perform various manipulations of the produced ions before mass measurement. One example of such manipulations is mass selection of a parent ion followed by collision-induced dissociation and mass analysis of the fragments (MS/MS experiment). This can be done most suitably in a tandem quadrupole-TOF system, which was mentioned earlier [Shevchenko et al., 1997], but even in the present instrument, it is possible to perform an MS/MS experiment. To evaluate this mode of operation, a few experiments were carried out.

Figures 36-38 show the MALDI mass spectra of a tryptic digest of citrate synthase (CS) obtained using the three different modes of operation shown in Figure 28. The spectrum shown in Figure 36A was obtained by using the RF-only mode of the quadrupole ion guide operation, i.e. it shows the full parent ion mass spectrum. Figures 36B and 36C show the mass filtering mode, which is analogous to a filtering mode implemented in conventional quadrupole mass filters. Here, small dc voltages are applied to the first section of the quadrupole ion guide to select the tryptic fragment peaks either at *m/z* 1265.63 or at *m/z* 1598.85 (see Fig 28 B); mass filtering mode of a quadrupole ion

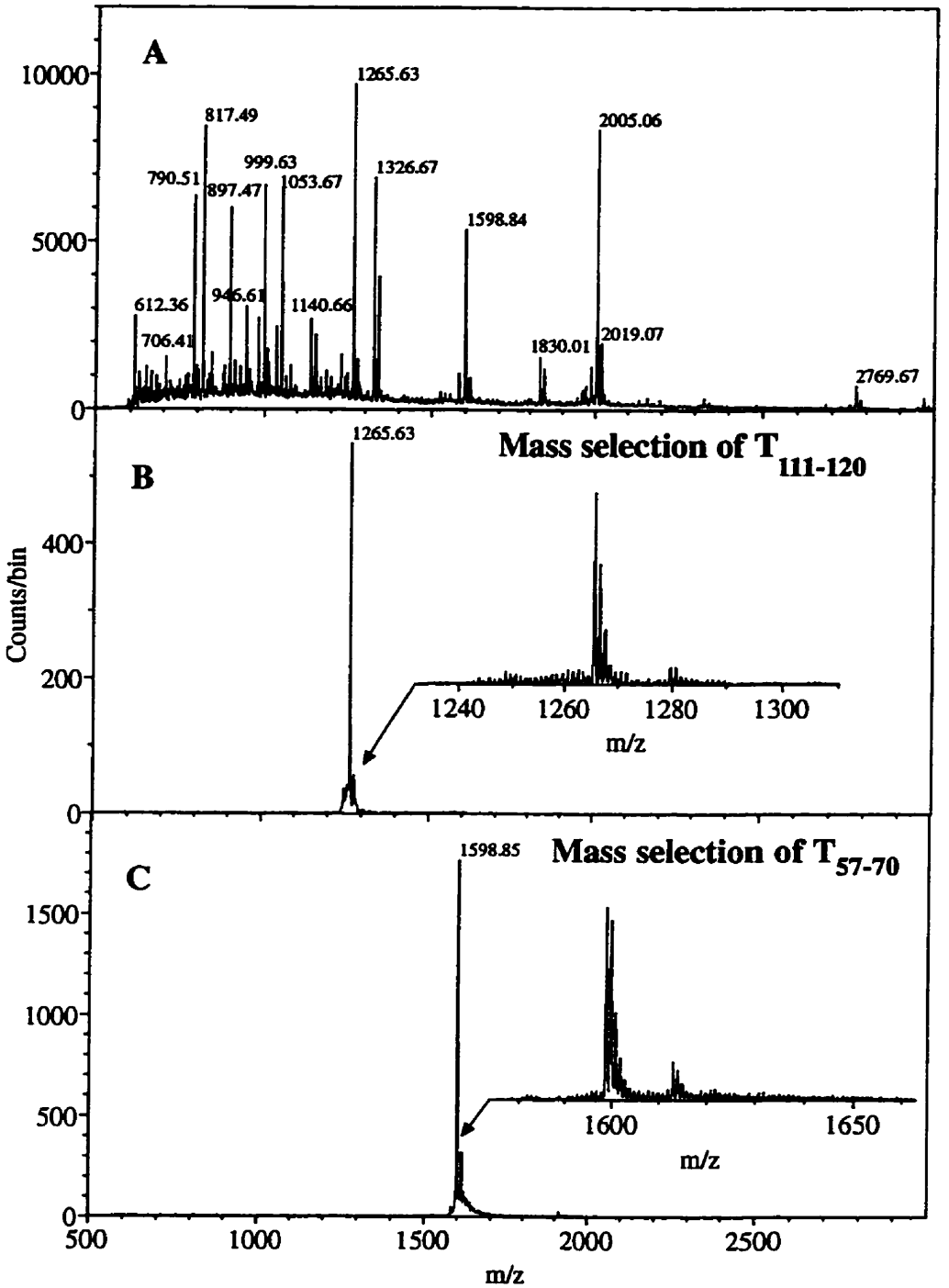

Figure 36. MALDI spectra of a tryptic digest of citrate synthase obtained in the different modes of collisional ion guide operation. (**A**) RF-only mode; (**B**) and (**C**) mass selection mode in which the first quadrupole is used as a mass filter. The CS tryptic fragment peaks identified previously as T111-120 and T57-70 (Fig. 34) were selected for the following MS/MS experiment.

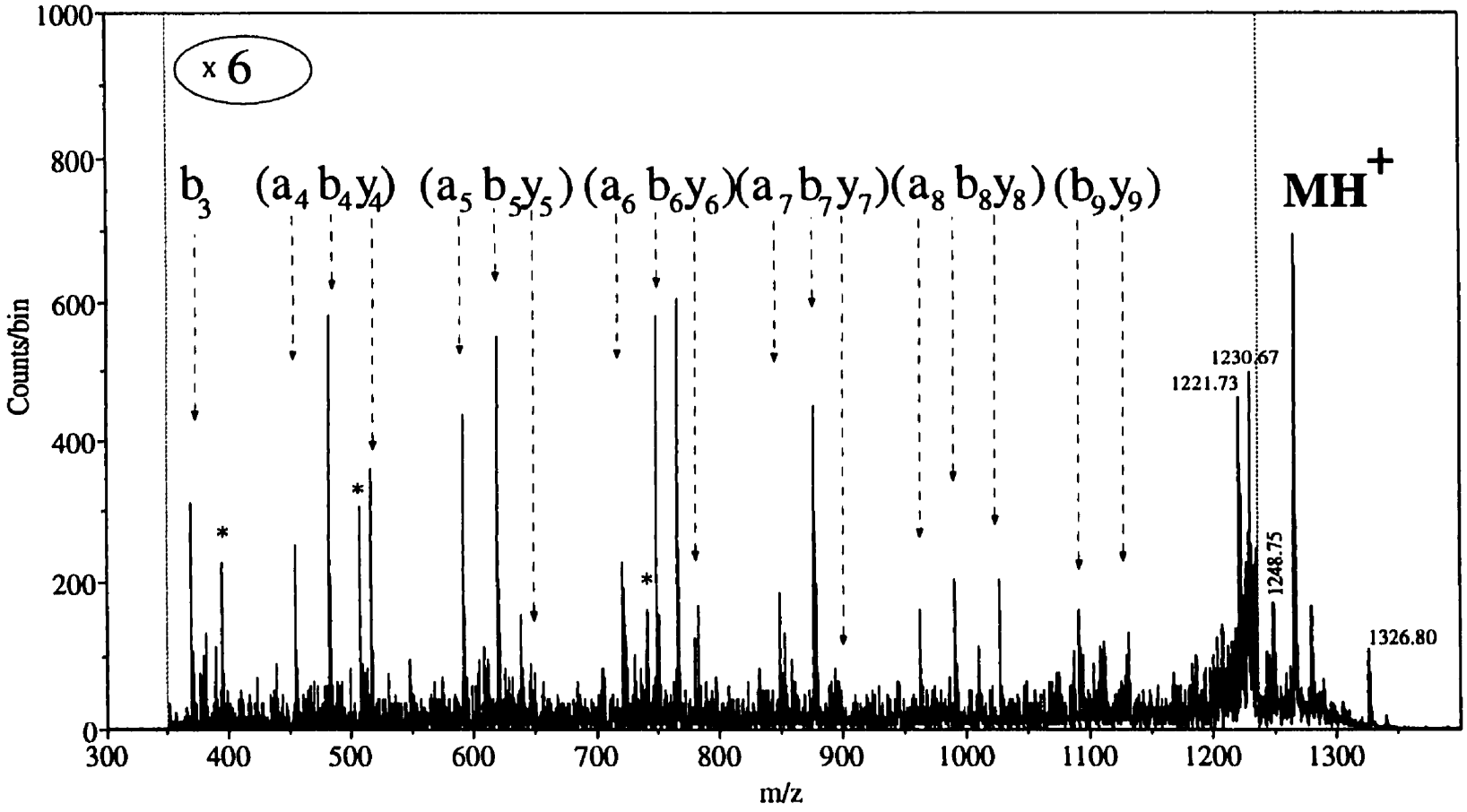

Figure 37. CID spectrum of the selected citrate synthase 111-120 tryptic fragment (HTMIHEQITR, theoretical m/z 1265.64) obtained at 100 eV collisional energy. Identified fragments of a sequence ladder are labeled according to Roepstorff's nomenclature (see Fig. 22). Some prominent mass peaks of internal fragments are labeled with asterisks.

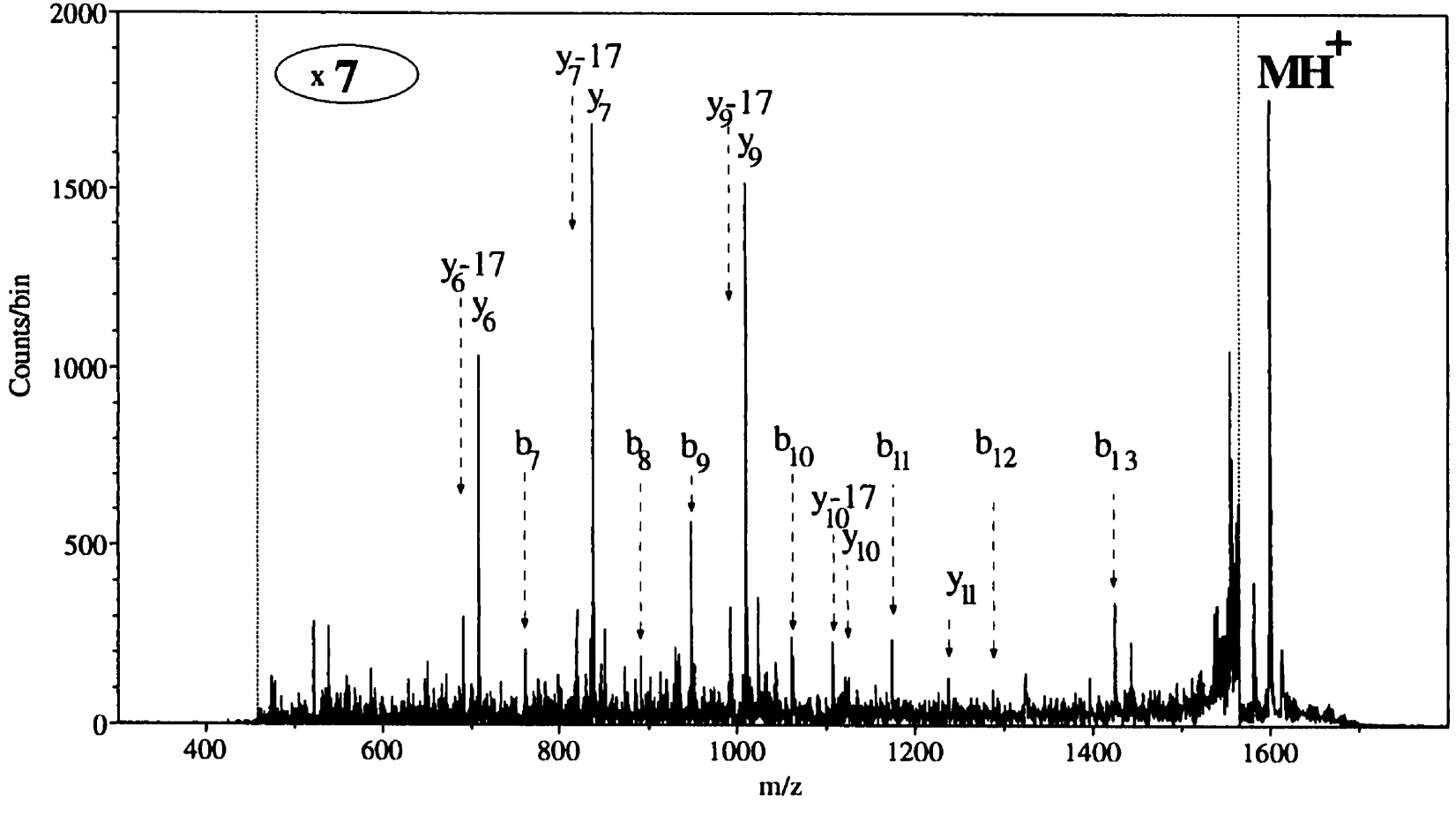

Figure 38. CID spectrum of the selected citrate synthase 57-70 tryptic fragment (ITFIDGDEGILLHR, theoretical m/z 1598.85) obtained at 120 eV collisional energy. Identified fragments of a sequence ladder are labeled according to Roepstorff's nomenclature (see Fig. 22).

guide operation was also demonstrated for electrospray ions). The second quadrupole section still acts as an ordinary ion guide. An approximately ~ 30 m/z window for a mass selection is rather wide, so the quadrupole resolution is not high (~ 40-50). The intensities of the selected peaks are also smaller than in the original spectrum, presumably because of losses while mass filtering at a high pressure (~70 mTorr). Nevertheless, both peaks could be selected for the following MS/MS experiment.

A collision-induced dissociation (CID) mass spectrum of the CS 111-120 tryptic fragment (sequence: HTMIHEQITR, 1265.64 m/z) is shown in Figure 37. To cause fragmentation of a parent ion, the potential difference between the quadrupole sections was increased to 100 V so that the ions selected by the first quadrupole could undergo acceleration in that region. This region acts as a collision cell. The second quadrupole still serves for collisional cooling of the fragment ions. The RF is the same in both quadrupoles, but the amplitude of the RF voltage in the second quadrupole is only one third of the amplitude of the RF voltage in the first one (as shown in Fig. 28C). This allows the daughter ions lighter than the parent ions to have stable trajectories and to be transmitted through the second quadrupole [Dawson, 1976]. As can be seen from the spectrum, not all selected parent ions suffer dissociation at 100 eV collisional energy. The spectrum is noisy (because of the wide mass selection window), but the fragmentation pattern consisting of a series of more prominent (a,b,y)-fragments is clearly recognizable. The intensities of fragment peaks are small in comparison with the intensity of the parent ion so the region inside dotted lines is expanded by a factor of 6. Fragmentation can be

enhanced by increasing the voltage between two quadrupoles, but the pattern becomes less informative because of increasing fragmentation of the daughter ions. A similar fragmentation pattern was observed in MS/MS analysis of CS tryptic fragment 57-70 (sequence: ITFIDGDEGILLHR, 1598.85 m/z), whose CID spectrum is shown in Figure 38. But in this case, some of the y-fragments are missing, only a few a-fragments are present (not labeled for this reason), and only seven b-fragments are present in an unbroken sequence.

Once MALDI ions of interest have been selected, they can be used for an MS/MS experiment. Although the fragmentation pattern looks similar to the one already known from PSD measurements [Spengler et al., 1992, 1995], it can be more controlled in the experiments described by changing CID energy. Partial identifications of a primary structure for a few other model peptides (substance P, and Arg-bradikinin) have been also performed. However, a more detailed investigation is needed to understand whether there is a common fragmentation pattern. Some preliminary results obtained in our QqTOF system coupled to a MALDI source indicate that structural information can be readily obtained from peptides presented in low femtomole amounts on the MALDI target [Loboda et al., 1998, preliminary results].

Observation of Electrosprayed Ions in the same Instrument

Because the collisional damping interface decouples the ion source from the TOF spectrometer, it is straightforward to insert an ESI source in place of the MALDI one. In the geometry of Figure 26, the MALDI probe of Figure 27 can be simply replaced by the ESI probe shown in Figure 39, which has a capillary (0.22 mm ID, 18.5 cm long) inside the probe shaft. Ions from a conventional electrospray source at the end of the probe pass through the heated capillary, together with the nitrogen used as a curtain gas. In this case the gas flow through the capillary determines the pressure in the first vacuum chamber. It is maintained at ~100 to 180 mTorr, depending on the temperature of the capillary. Interchange of the ESI probe and the MALDI probe can be done within a few minutes.

Figure 40 shows both MALDI and ESI *m/z* spectra of a mixture of two peptides, substance P and melittin, obtained from the same solution. To begin with, a 10^{-6} M solution was sprayed for 1 min to obtain the ESI spectrum shown in Figure 40A. Then the ESI probe was removed, a matrix layer on the tip of MALDI probe was prepared, 1 μL of the same solution was applied on top of the matrix, and the MALDI probe was put into the interface. The MALDI spectrum of the mixture obtained (also for 1 min acquisition time) is presented in Figure 40B. As expected, the *m/z* spectra look rather different because of the larger charge states produced in the electrospray process.

On the other hand, the *mass* spectrum from ESI, obtained by deconvolution, is very similar to the MALDI spectrum. Expanded regions of the spectra are shown in Figure 41. The resolution is again about 5000 for both sources. The intensities are

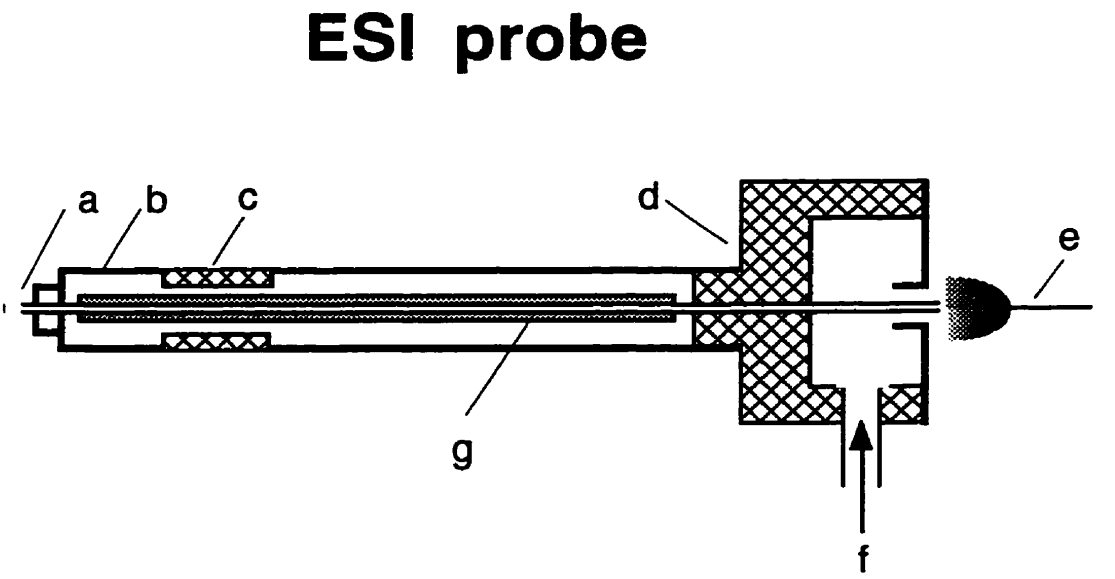

Figure 39. The ESI probe. It consists of a capillary (a) installed in the shaft (b). The tip is separated by insulator (c) from the rest of the shaft, which is mounted in a hollow knob (d). Ions obtained from an electrospray source (e) near the entrance to the capillary pass through a counter flow of a curtain gas introduced into the knob through the inlet (f). The heater (g) maintains the temperature of the capillary.

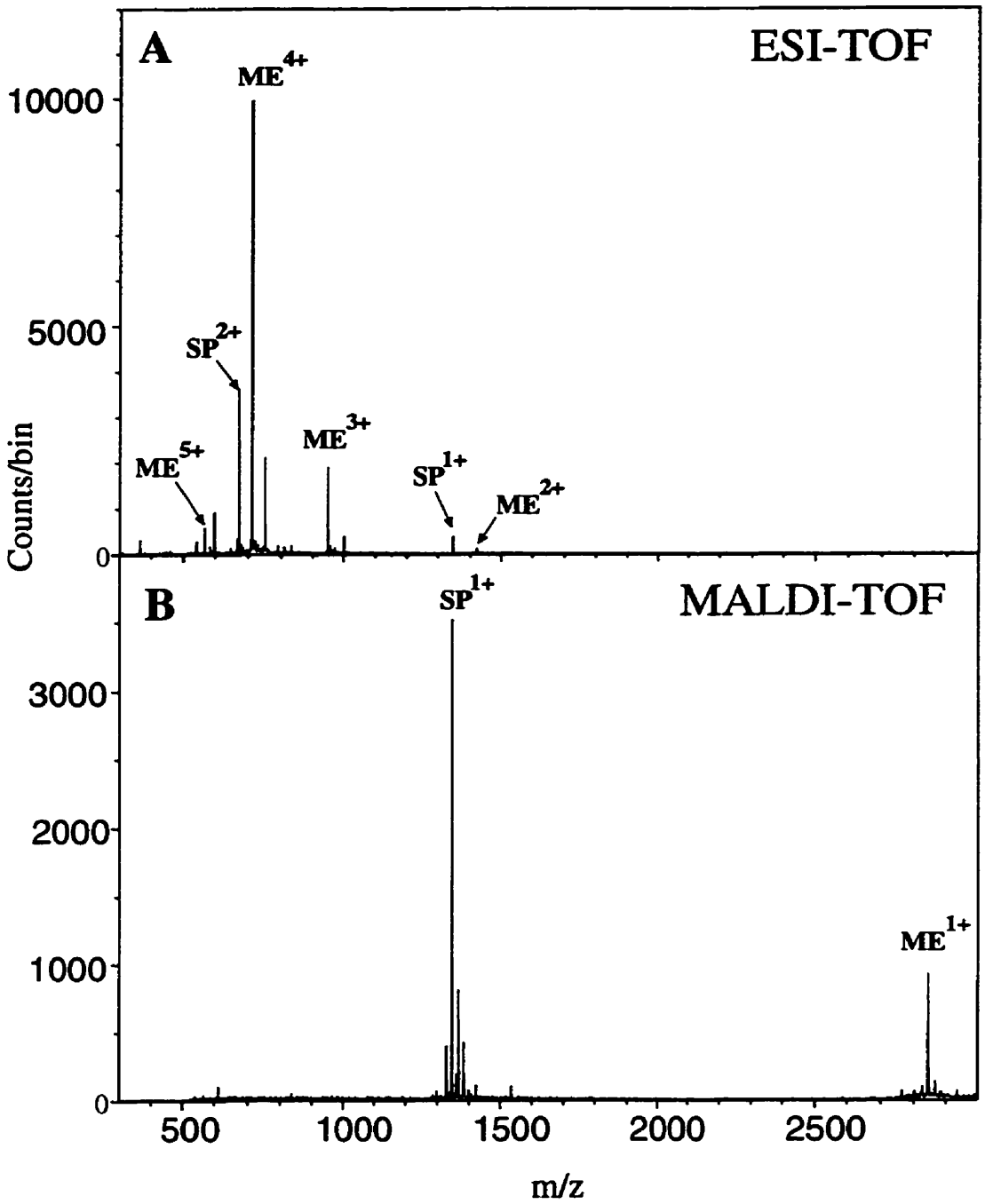

Figure 40. ESI and MALDI *m/z* spectra of an equimolar mixture of two peptides, substance P (SP) and melittin (ME). The spectra were obtained in the same TOF instrument (Fig. 26) a few minutes apart. The same 10-6 M solution was used for both peptides, and both spectra were acquired for 1 min.

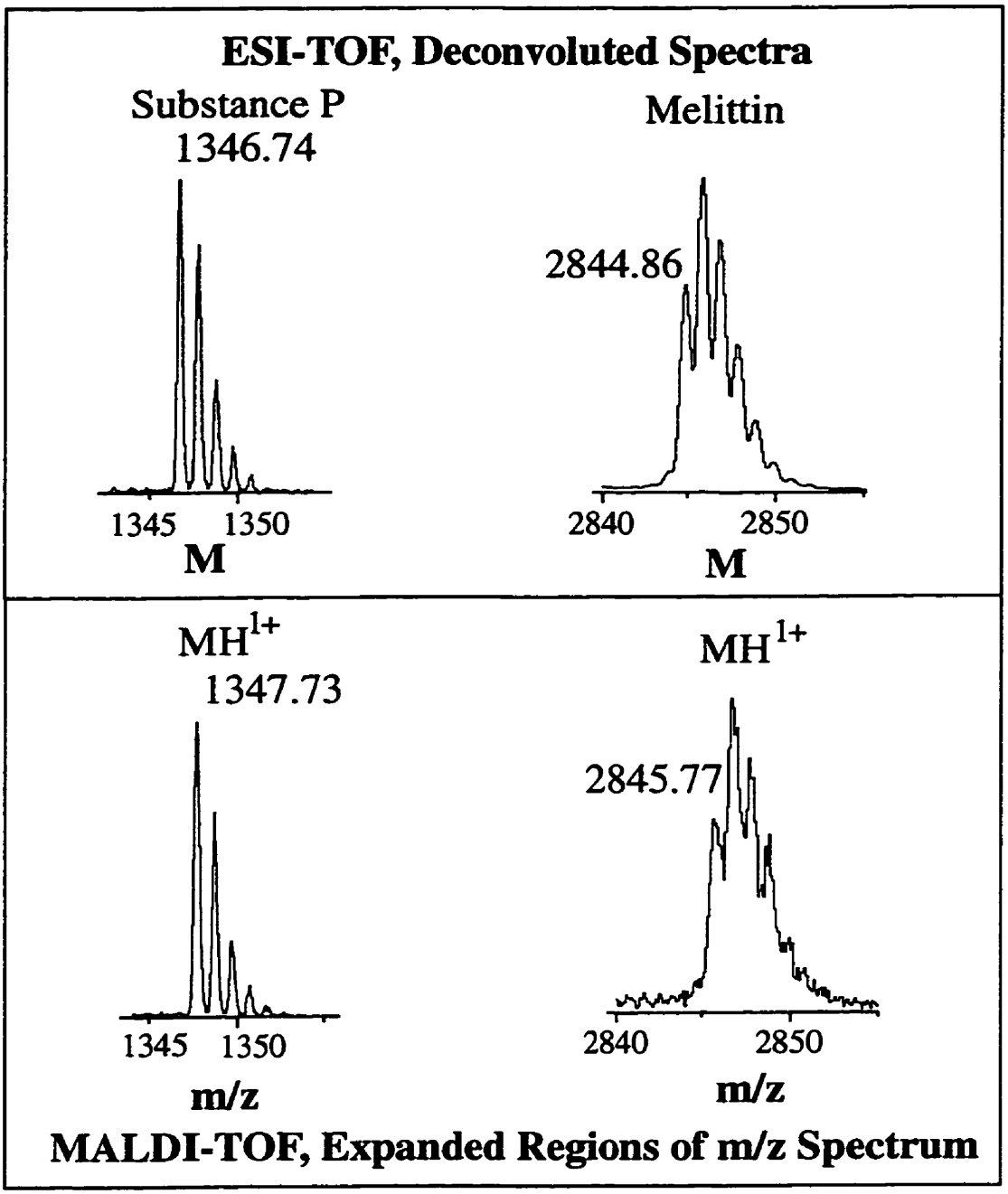

Figure 41. Expanded regions of the MALDI spectrum of Fig. 40 and the deconvoluted ESI spectrum obtained from the *m/z* ESI spectrum of Fig. 40. The same resolution (~5000) is obtained. Here the calibration was obtained from the *m/z* ESI spectrum, and the labels over the peaks indicate the values yielded by the calibration program for the peaks in the deconvoluted ESI spectrum and from the MALDI *m/z* spectrum.

comparable for substance P, but the intensity of melittin in the MALDI spectrum is smaller because of the lower detection efficiency. The accuracy of mass determination is within ~50 ppm.

Myoglobin is too large a molecule to be observed by MALDI with the present accelerating voltages, but it was examined by electrospray as a test of the operation of that source at higher mass. Its *m/z* spectrum is shown in Figure 42, with the deconvoluted mass spectrum as an insert. The ions were introduced directly from the atmosphere into vacuum through the capillary (unheated in the present case). Although the diameter of the capillary is much smaller and its length is larger than the capillary used in the previous collisional damping interface for electrospray ions, the intensities of the ion signals are comparable when spraying solutions of equal concentrations. Probably this is a result of more efficient ion collection from the supersonic jet when the ions enter the first section of the quadrupole ion guide directly from the capillary. Declustering of myoglobin was performed in the region between the two quadrupoles by setting a potential difference between them.

Conclusions

The collisional damping interface provides a satisfactory solution to the problem of orthogonal injection of MALDI ions into a TOF mass spectrometer. Resolution and sensitivity are competitive with the values found in the usual axial injection mode. Moreover, the configuration has a number of distinctive advantages. In particular, it

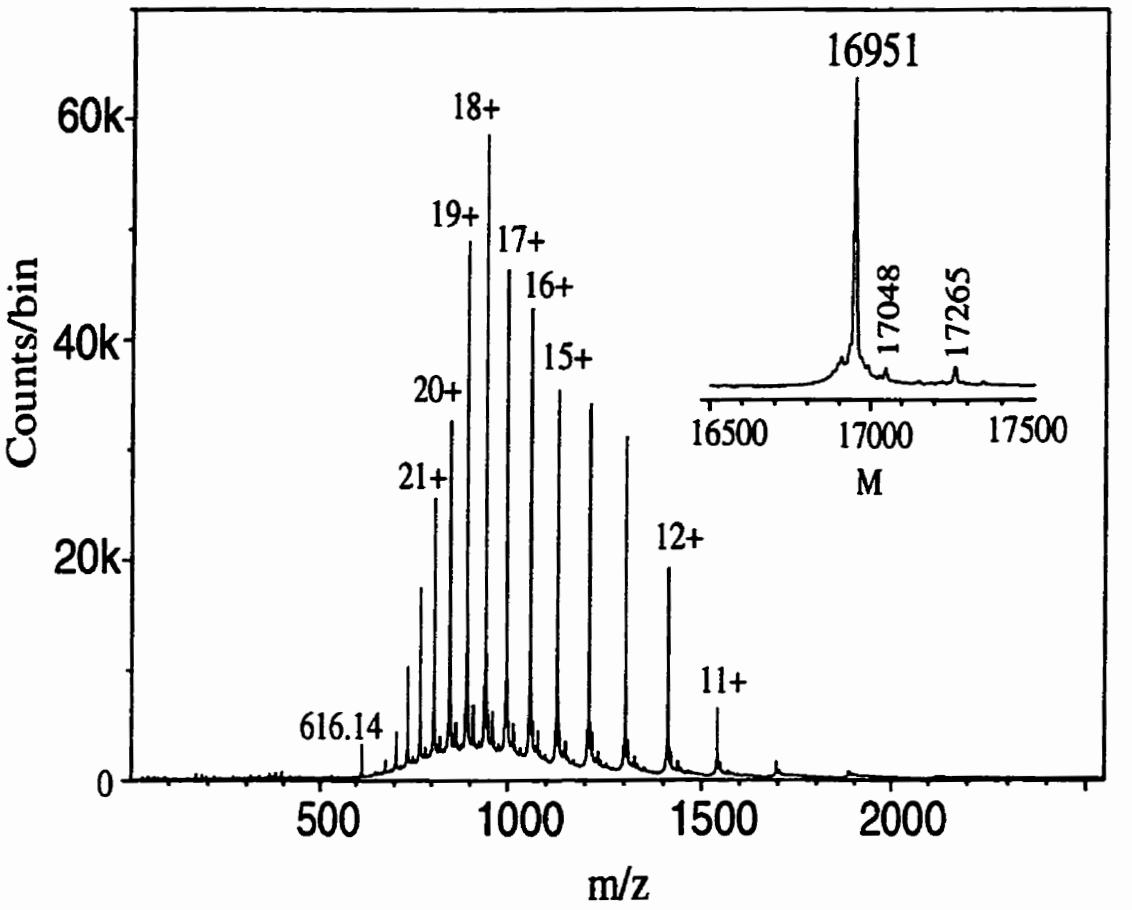

Figure 42. ESI spectrum of myoglobin obtained by using the ESI probe. Declustering of myoglobin ions was performed by setting a 40 V potential difference between the first and second quadrupoles in the collisional ion guide.

decouples the ion production process almost completely from the mass measurement, so various manipulations of the produced ions are possible prior to their orthogonal injection. The experiments in which the parent ion was selected for the following CID show that structural information can be obtained from the mass spectra of the fragment ions. However, such MS/MS measurements can be done most suitably in a QqTOF instrument and this work is in progress. Finally, another important consequence of decoupling is the ability to study the ions produced both by MALDI and by ESI in a single TOF spectrometer.

V. APPLICATION OF THE ESI-TOF III MASS SPECTROMETER FOR QUANTITATIVE EVALUATION OF PROTEIN-PROTEIN AND LIGAND-PROTEIN EQUILIBRIA OF A LARGE ALLOSTERIC ENZYME.

Introduction

The considerable improvements in sensitivity and mass resolution have advanced mass spectrometry (MS) as an important analytical tool for solution of many biochemical problems. Because of its unparalleled ability to distinguish species of different molecular masses, it has the potential to analyze macromolecular complexes with multiple components in equilibrium. MS can give unique insights into the formation and properties of these complexes, yielding information that is complementary to that obtained by other well established methods (X-ray crystallography, nuclear magnetic resonance spectroscopy, ultracentrifuge, gel electrophoresis etc.). The technique can be particularly valuable when the amount of sample is limited. In fact however, MS has not been applicable to the study of noncovalent complexes until fairly recently [Katta & Chait, 1991; Ganem et al., 1991], because these weakly bound entities were destroyed during transfer into the gas phase or in the subsequent ionization. This problem has been greatly alleviated by the development of electrospray, a very gentle ionization method, and an increasing number of measurements on noncovalent complexes are being carried out with this technique. In a number of cases ESI has been shown to preserve higher-order noncovalent interactions [Loo, 1997].

A serious practical problem for MS measurements is the limited m/z range of most commercial mass analyzers (usually <4,000 m/z); this is inadequate for the observation of many interesting but large complexes. The use of a time-of-flight mass analyzer combined with ESI provides an attractive solution to this problem, since TOF instruments have in principle an unlimited m/z range.

As shown previously, incorporation of a collisional quadrupole ion guide into our TOF III mass spectrometer considerably extended the analyzed mass range, an advantage that has been used for analyses of many large noncovalent complexes [Chernushevich et al., 1998]. One example of such a system studied is *Escherichia coli* citrate synthase (CS), the enzyme that initiates the citric acid cycle [Duckworth & Bell, 1982]. The enzyme plays one of the key roles in cellular metabolism and catalyzes the reaction between oxaloacetate and acetyl coenzyme A to produce citrate and coenzyme A. It also interacts with its inhibitor, the reduced form of nicotinamide adenine dinucleotide (NADH), and it is involved in simultaneous protein-protein and ligand-protein equilibria. Although an allosteric mechanism of inhibition has been proposed [Weitzman, 1966; Weitzman & Jones, 1968; Duckworth & Tong, 1976], exactly how this occurs has been unknown. In attempt to answer this and other questions, recombinant *E. coli* citrate synthases has been examined in our ESI-TOF III mass spectrometer with a collisional damping interface and the orthogonal injection of electrosprayed ions.

Experimental

Preparation of samples

The *E. coli* CS expression plasmid and host strain used were described previously [Anderson & Duckworth, 1988]. CS was purified from cell extracts by diethyl-aminoethyl-cellulose chromatography followed by size exclusion chromatography through Sepharose 6B, essentially as described [Duckworth & Bell, 1982]. For ESI-TOFMS, CS samples, initially in 20 mM TRIS-Cl, 1 mM EDTA, and 50 mM KCl, were washed 6 to 8 times with 2 ml aliquots of 20 mM NH_4HCO_3 in a Centricon 30 (30,000 molecular weight cut-off), and diluted to the appropriate protein concentration such that the buffer concentration was 5 mM. Stock CS concentration was determined spectrophotometrically using its known extinction coefficient of 47,000 M^{-1} cm^{-1} at 278 nm. The disodium salt of NADH was prepared by dialysis against 20 mM NH_4HCO_3 to remove sodium ions. The concentration of NADH was determined spectrophotometrically using its known extinction coefficient of 6,220 M^{-1} cm^{-1} at 340 nm. For each mass spectrum, a sample was prepared one day prior to the ESI-TOF experiment by mixing the appropriate components and diluting to 5 mM NH_4HCO_3.

Electrospray spectrum of citrate synthase under denaturing conditions.

An electrospray spectrum of citrate synthase obtained from an acidic solution (1/1 v/v methanol/deionized water, 5% acetic acid) is shown in Figure 43. The experimental mass determined after deconvolution of the m/z spectrum is 47,887 ± 2 Da, which is in

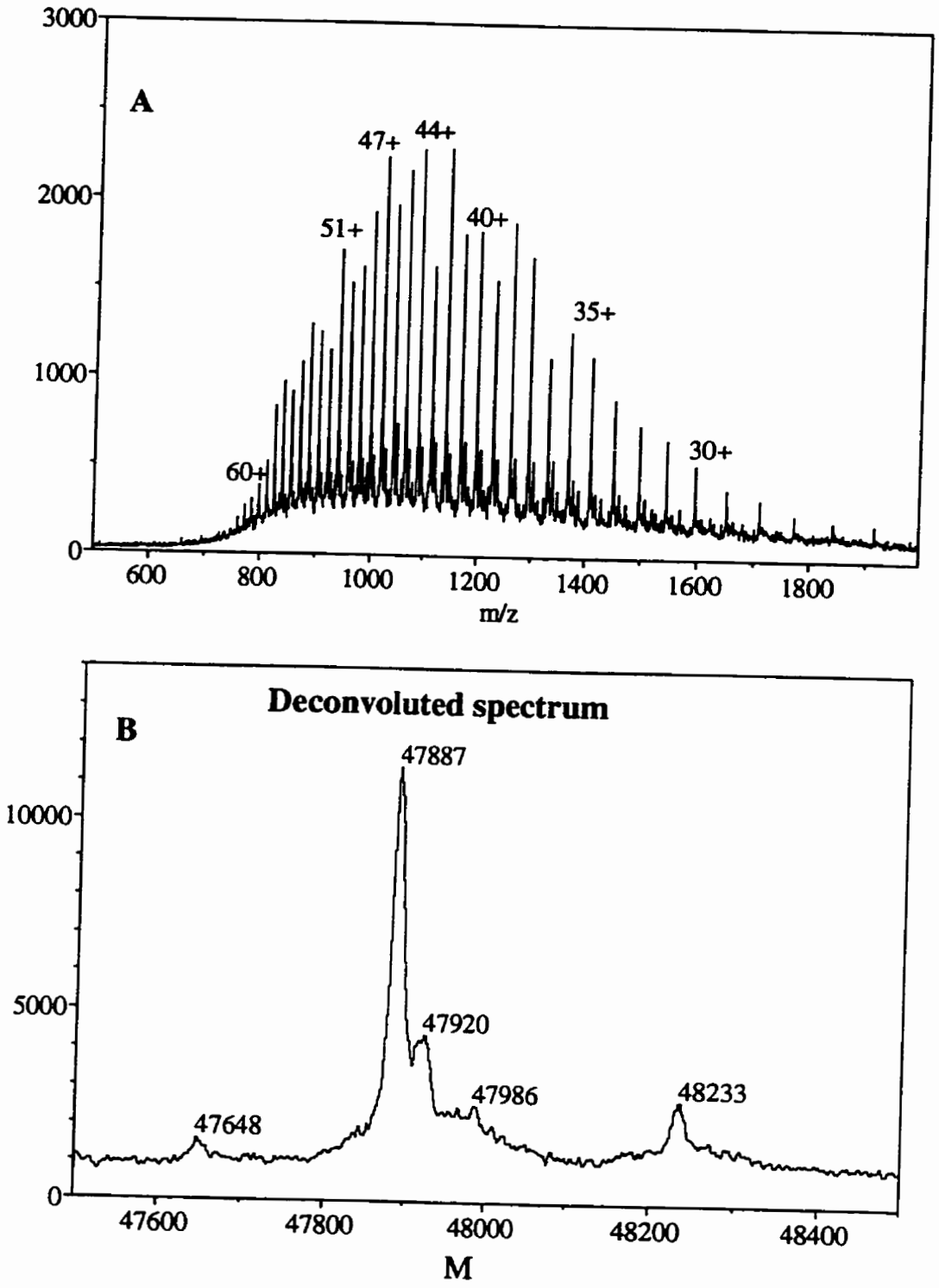

Figure 43. (**A**) Electrospray spectrum of recombinant *E. coli* citrate synthase obtained at the denaturing conditions (water/methanol 1/1 v/v +5% acetic acid). (**B**) mass spectrum obtained by deconvolution of the electrospray spectrum.

good agreement with the theoretical mass 47,885 Da, calculated from the amino acid sequence as inferred from the gene sequence [Ner et al., 1983], but correcting Phe-288 to Val [Donald et al., 1991] omitting Met-1, and replacing Asn-10 by Asp as found by N-terminal sequencing of the protein itself [Duckworth & Bell, 1982].

Electrospray spectra of citrate synthase under non-denaturing conditions

In their native form, most citrate synthases are dimers; formation of hexamers is confined to CS from gram-negative bacteria (such as *E. coli*), a group that also displays allosteric inhibition by NADH. With *E. coli* CS, previous equilibrium ultracentrifugation studies showed that aggregates greater than dimer are favored by lower pH or by high salt concentrations; a simple dimer-hexamer equilibrium could be demonstrated at relatively high ionic strength. At low ionic strength, where non-ideality effects distort concentration distributions in the ultracentrifuge, mixtures of different oligomeric forms were clearly present, with higher aggregation at lower pH, but it was not possible to decide exactly what species were present [Tong & Duckworth, 1975].

Measurements in our TOF III mass spectrometer on *E. coli* CS, in low ionic strength buffers, compatible with ESI , now clarify this question. As shown in Figure 44, only dimers (measured mass = 95,770 ± 10 Da) and hexamers (measured mass = 287,322 ± 30 Da) are present in significant amounts in the spectrum obtained from a 5mM ammonium bicarbonate buffer (pH ~7.5). Similar data were obtained at pH 6 (5 mM ammonium acetate buffer), except that more hexamer was present and no tetramer was

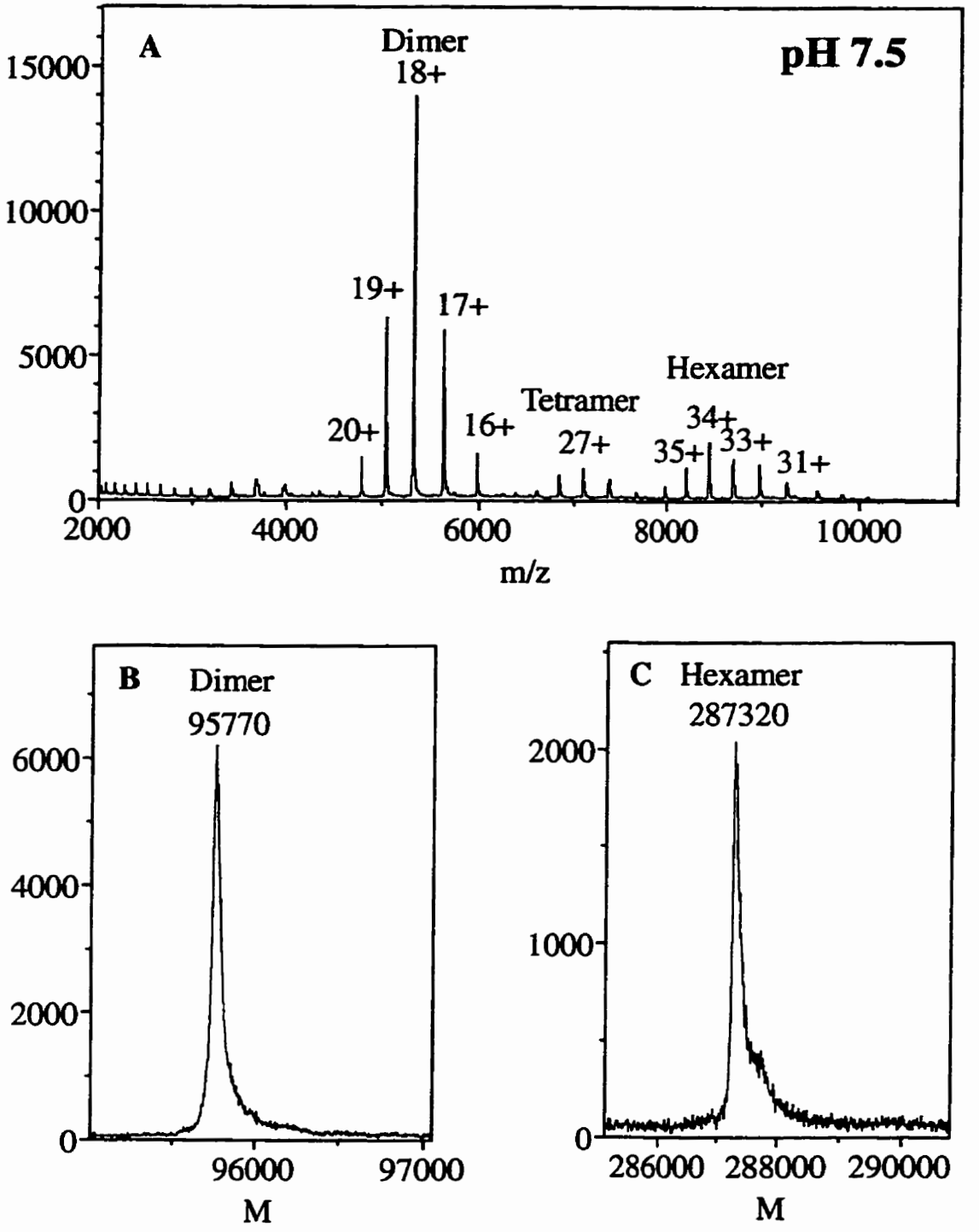

Figure 44. (A) Electrospray spectrum of citrate synthase obtained from 5 mM ammonium bicarbonate buffer (pH 7.5). (B) and (C) mass spectra of the dimer and the hexamer of citrate synthase obtained by deconvolution of the m/z spectrum.

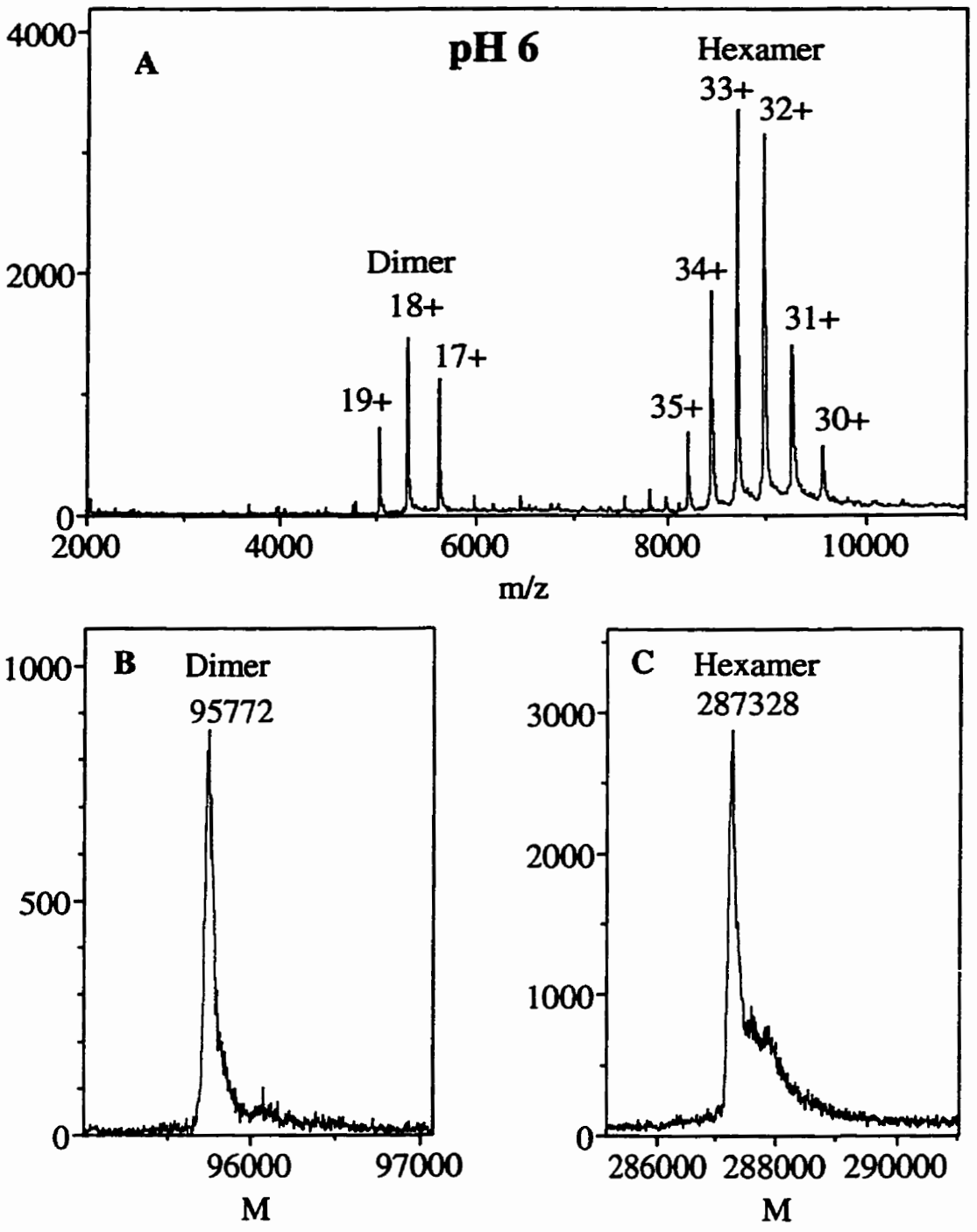

Figure 45. (A) Electrospray spectrum of citrate synthase obtained from 5 mM ammonium acetate buffer (pH 6). (B) and (C) mass spectra of the dimer and the hexamer of citrate synthase obtained by deconvolution of the m/z spectrum.

observed (Fig. 45). The advantage of being able to measure high *m/z* ratios is obvious - ions arising from CS dimers appear at *m/z* up to 5,500, and those arising from hexamers up to m/z ~10,000. These measured masses are in good agreement with the theoretical values of 95,770 Da (dimer) and 287,310 Da (hexamer). Some tetramers are also observed (Fig. 44A), but with considerably lower abundance. Their intensity appears to follow the dimer abundance (see Figure 48), suggesting that they arise from a nonspecific interaction between two dimers.

Dependence of the dimer/hexamer molar ratio on CS concentration

The dependence of the dimer/hexamer molar ratio on concentration of CS subunits in the solution was measured at pH ~7.5 and, the result is shown in Figure 46. This result can be quantitatively explained by assuming a simple equilibrium between dimers and hexamers and an association constant (K_A) of 6.9×10^{10} M^{-2} . The association constant was determined from the fit (shown by a solid line) of the equation:

$$[M] = \left(\frac{1}{K_A}\right)^{1/2} \frac{(2R+6)}{R^{3/2}}$$

where [M] is the subunit concentration of CS and,

R is the ratio of dimer to hexamer,

to the data shown in Figure 47 (the derivation of this equation and the detailed explanations are given in the Appendix IIIA). K_A values measured under comparable conditions are not available from equilibrium centrifugation, since convection and non-ideality effects prevent that method from being used effectively at such low electrolyte

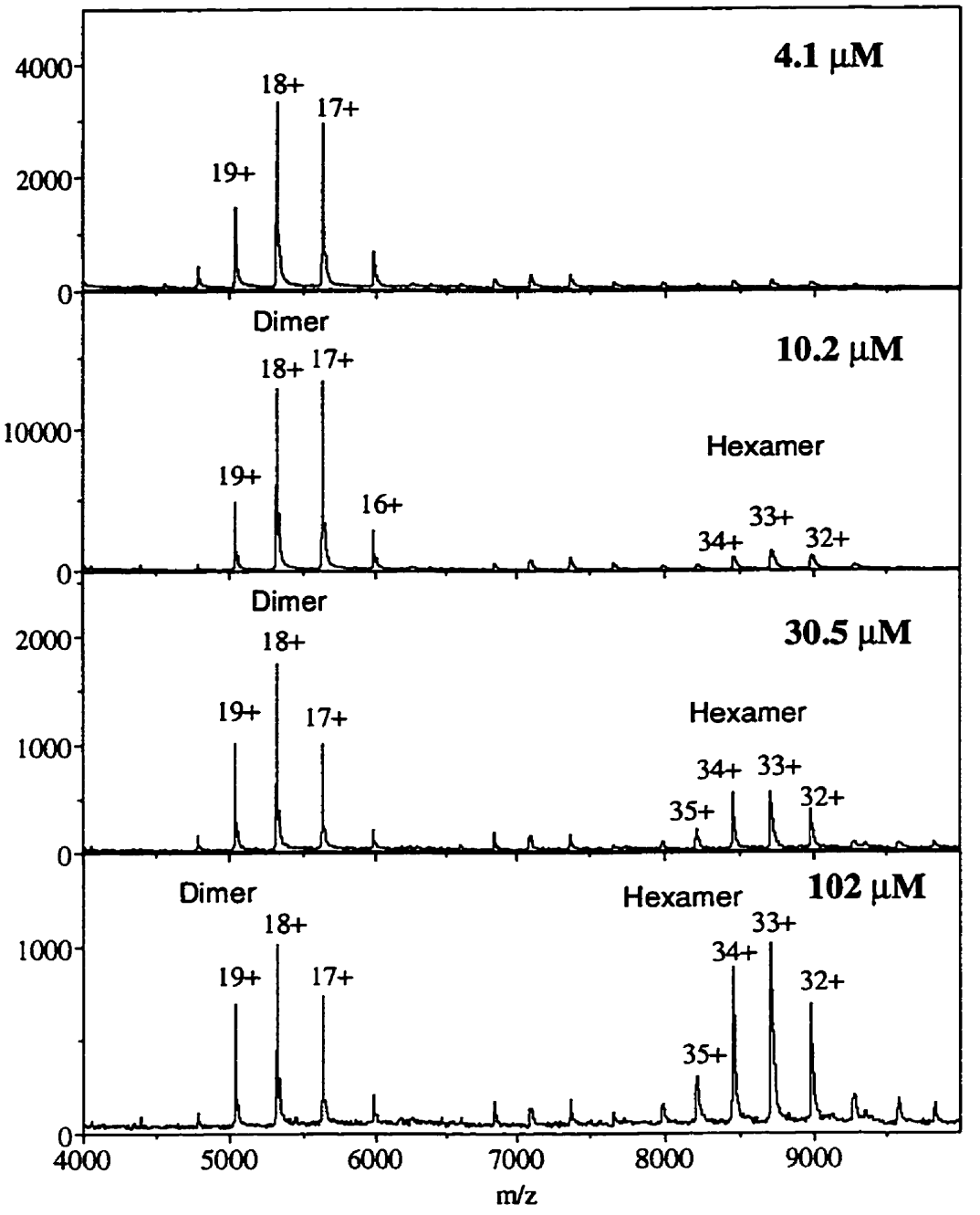

Figure 46. Selected electrospray spectra of CS (pH 7.5) obtained at the different concentrations of CS subunits in the solutions. The concentrations are indicated in each spectrum.

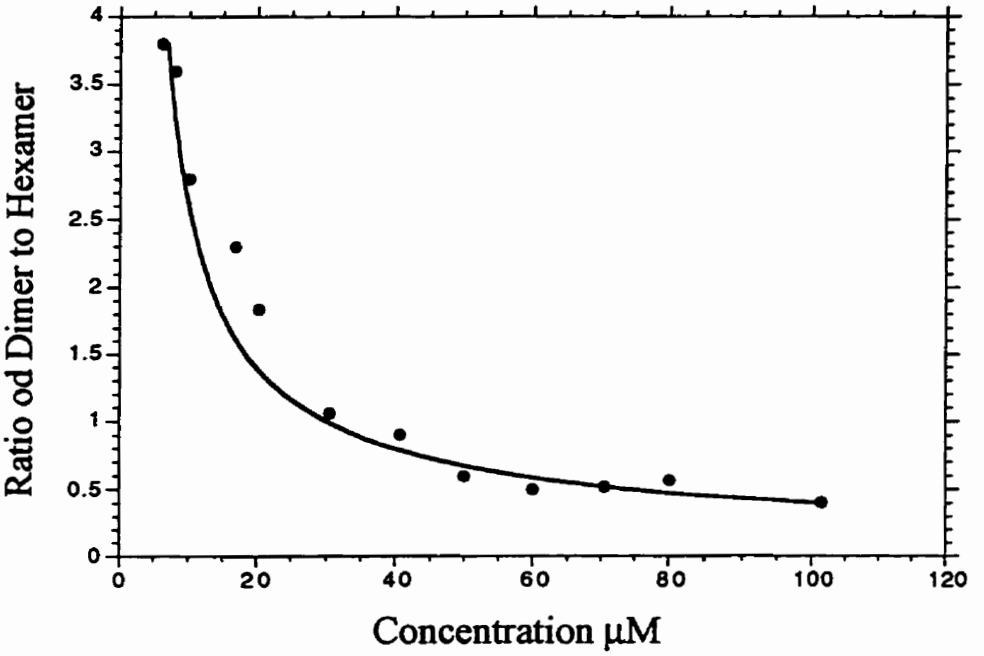

Figure 47. Dependence of dimer/hexamer molar concentration ratio, [D]/[H], on CS subunit concentration. Molar ratios, [D]/[H] were found from the electrospray spectra (Fig.45) by integrating the peak areas that correspond to the dimer and the hexamer, and then by finding the ratio of obtained values and correcting this ratio by factor 1/1.3 as explained in the Appendix III. Assuming that the [D]/[H] ratio is completely described by the equilibrium 3D = H, fitting the curve to the data gives $K_A=(6.9\pm 0.7)\times 10^{10}\ M^{-2}$.

concentrations [Yphantis, 1964]. The most similar conditions tried in the ultracentrifuge (20 mM TRIS-Cl buffers of pH 7.0 and 7.8) showed decided signs of non-ideal behavior [Tong & Duckworth, 1975] and data obtained in 50 mM KCl, 20 mM TRIS-Cl, pH 7.8, could be interpreted as showing a dimer-hexamer equilibrium; K_A value calculated from those data is $(4.1 \pm 0.5) \times 10^{11}$ M^{-2}. This is slightly larger than the value calculated from the present results by ESI-TOFMS at somewhat lower pH values and in the absence of salt; it is difficult to know how to use the ultracentrifuge value to estimate K_A in electrospray buffers, since KCl is an allosteric activator of CS [Weitzman, 1966] - and thus might well affect the strength of subunit interactions - as well as a source of ionic strength.

Complexes of citrate synthase with NADH

While it has been suggested previously that NADH inhibition involves the hexameric state of CS [Duckworth & Tong, 1976] no clear-cut evidence was available on this point. Electrospray spectra of CS in the presence of NADH now show that there is a most direct involvement: NADH shifts the oligomeric ratio towards hexamer (Figure 48). As NADH is added, the hexameric part of the spectra consists of a set of NADH-hexamer complexes, almost fully resolved from one another, and containing from 0 to as many as 18 NADH molecules. A set of NADH-dimer complexes also appears, but only at the higher NADH concentrations.

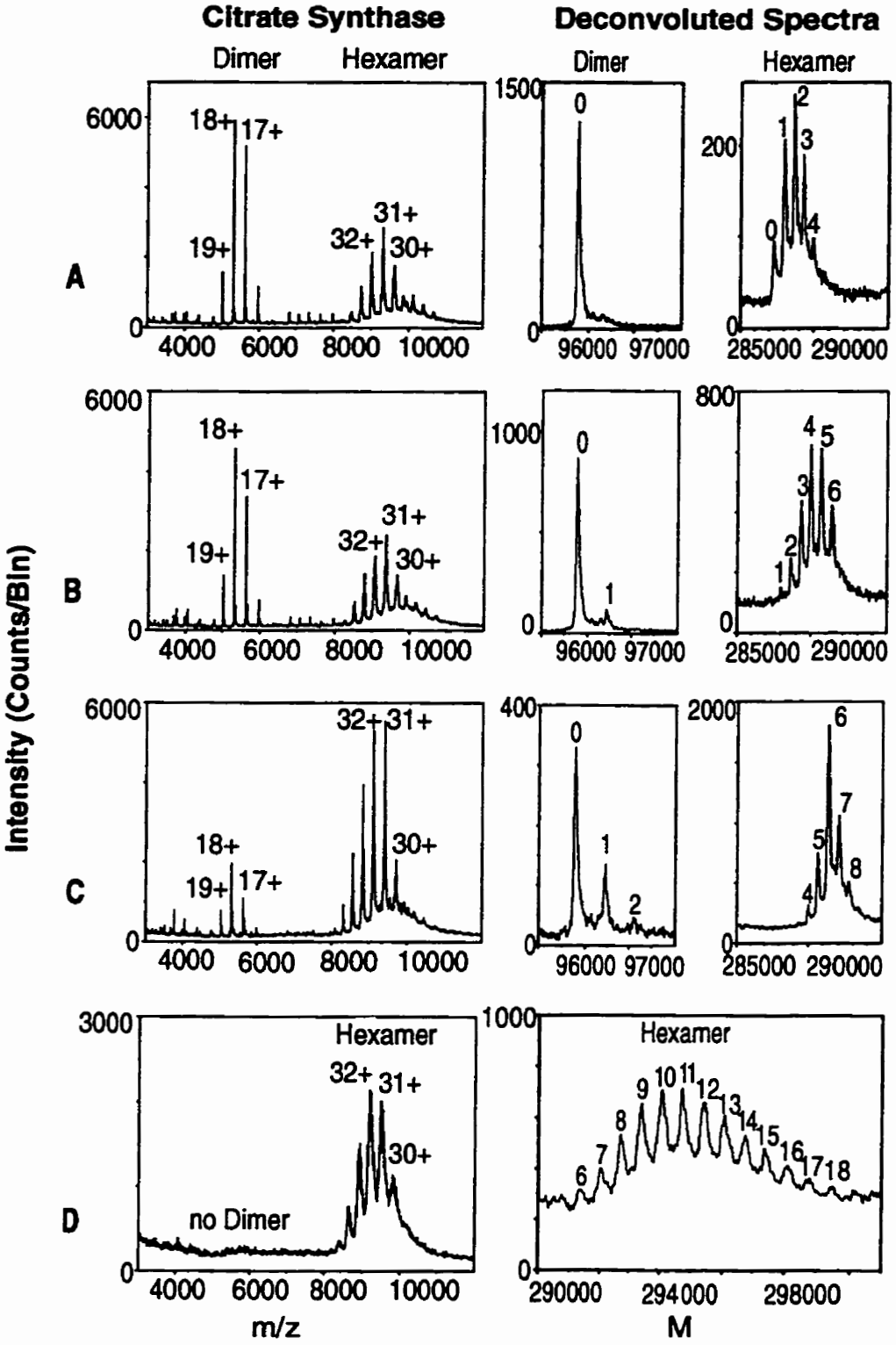

Figure 48. Selected electrospray and deconvoluted mass spectra of CS (9μM subunit concentration the presence of increasing concentrations of NADH in 5 mM ammonium bicarbonate at pH 7.5). NADH concentrations were (**A**) 4.5 μM, (**B**) 9 μM, (**C**) 18 μM, (**D**) 108 μM. The digits labeling the deconvoluted spectra correspond to the number of NADH molecules bound.

Summary on the titration experiment

The way in which these sets of complexes develop as NADH is added is shown in detail in Figure 49, where the average numbers of NADH molecules bound per subunit are plotted, for hexamers and dimers, as functions of free NADH concentration. Differences in binding specificity are immediately apparent. The hexamer binds NADH at very low concentrations, rapidly filling one site per subunit at about 10 mM NADH in a non-cooperative manner. At higher NADH concentrations, the number of bound molecules continues to increase, but gradually. This behavior is in sharp contrast to that exhibited by the dimer, where the increase in the number of NADH molecules bound is gradual throughout the entire NADH concentration range, and never reaches one site per subunit over the measured range. This suggests that non-specific binding occurs to both dimers and hexamers, but that specific binding is exclusive to hexameric CS.

Dissociation constants

In order to describe quantitatively the difference in NADH binding specificity for dimers and hexamers at pH 7.5, the data in Figure 49 were fitted to a hyperbolic function with two terms to describe different binding sites:

$$\bar{n} = \frac{[L]}{[L] + K_{D1}} + \frac{2[L]}{[L] + K_{D2}}$$

where $\bar{n}$ is the average number of NADH molecules bound to a subunit and,

$[L]$ is the concentration of unbound ligand.

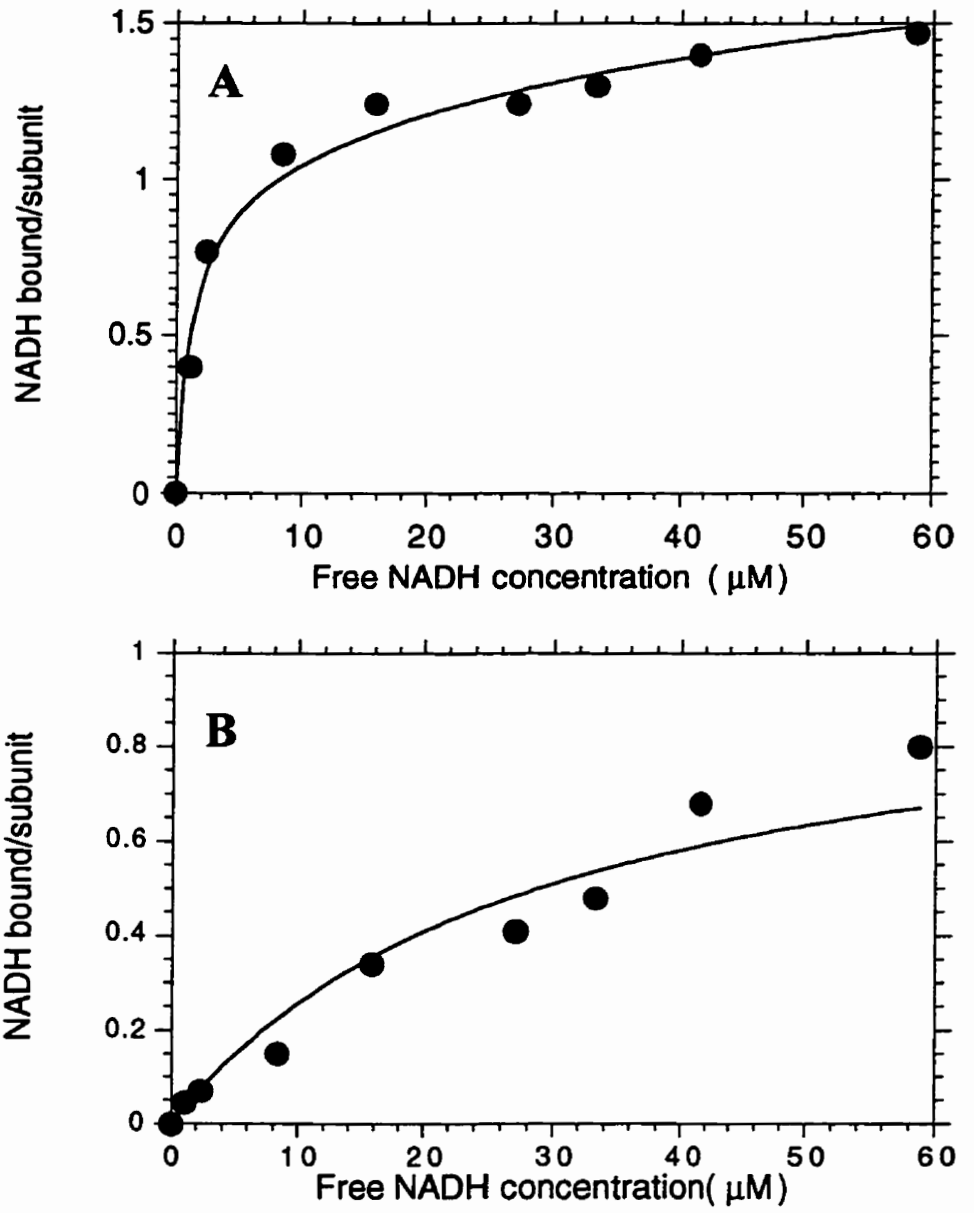

Figure 49. NADH binding to hexameric (**A**) and dimeric (**B**) CS in 5 mM NH_4HCO_3 (pH 7.5). The data were fitted to hyporbolae; to account for specific and non-specific binding to hexameric CS, two terms in the equation shown in the text were used - one term for binding to six 'tight' sites (one site per subunit) and the second term for binding to 12 weaker sites (two sites per subunit). The solid lines are the resultant fits and Table II shows the binding constants obtained.

The derivation of this equation and explanations are given in the Appendix III B. Binding to hexamer involves at least two classes of site - one set of six sites per hexamer with a dissociation constant (K_{D1}) of 1.1 ± 0.2 μM, and a second class of at least 12 weaker sites, 12 sites were assumed in calculating the K_{D2} value reported for this second or "loose" set of sites. The results are shown in Table II. Binding to dimer is also weak, and can be interpreted as a single class of two sites per dimer with a K_D of 28 ± 3 μM. Thus, NADH binds tightly and specifically only to hexamer. Weak binding of NADH molecules may be a genuine property of CS in solution, or it may be an artifact arising because all non-volatile species (including NADH) are greatly concentrated during evaporation of solvent in the electrospray source. That is, the weakly-bound NADH molecules may be analogous to the adducts of macromolecules with sodium or potassium ions that are constantly encountered in ESI if declustering voltages are insufficient to disaggregate them.

The K_{D1} value for tight binding of NADH to CS hexamers is the same as that previously determined for NADH binding in solution, 1.1 μM under similar conditions (20 mM TRIS-Cl, pH 7.8) by a fluorescence method [Duckworth & Tong, 1976]. In the earlier fluorescence study, the number of NADH sites measured was less than one per CS subunit, and increased towards lower pH [Duckworth & Tong, 1976]. The present results suggest a probable explanation for this trend: since tight binding occurs only to hexamers, and the proportion of hexameric CS increases as pH is lowered, the number of NADH

Parameter	Value
K_A = [hexamer]/[dimer]^3	$(6.9 \pm 0.7) \times 10^{10}$ M^{-2}
K_D for NADH binding to dimer	28.3 ± 3.4 μM
K_{D1} for NADH binding to hexamer, "tight" sites	1.1 ± 0.2 μM
K_{D2} for NADH binding to hexamer, "loose" sites	155 ± 19 μM*

* The K_{D2} value for the second or "loose" set of NADH binding sites was calculated by assuming that there are 12 of these sites per hexamer.

Table II. Equilibrium constants for CS dimer-hexamer-NADH system as determined from ESI-TOFMS data in 5 mM NH_4HCO_3.

sites would appear to increase at lower pH if re-equilibration between dimers and hexamers was slow.

Conclusions

There are distinct advantages to studying protein-protein and protein-ligand equilibria by the orthogonal injection ESI-TOF mass spectrometry. Some standard methods for investigating protein-protein equilibria, like ultracentrifuge or light scattering techniques, give average molecular weights, which must then be interpreted in terms of the components probably present, though not resolved from one another. Other methods, like gel permeation chromatography, frequently fail to resolve components, and always require calibrations that are built on assumptions. With mass spectrometry, each component in a mixture is clearly resolved and can be identified by its mass. Standard methods for studying protein-ligand equilibria, such as equilibrium dialysis, can give good K_D values, but the stoichiometry of a complex must be determined by extrapolating a series of measurements, each of which is the ratio of two experimentally determined numbers, so that the precision is low. Here we have shown that mass spectrometry of a very large macromolecule, the hexamer of CS, can resolve several closely related-complexes containing different numbers of ligand molecules, and give an exact stoichiometry for each. For tight, specific binding, the K_D value for a protein-ligand interaction has also been accurately determined. It will be interesting to extend this kind of study to other biochemical systems displaying multiple equilibria, and to see whether the

described approach will be generally applicable to the study of non covalent complexes of biological importance.

FINAL CONCLUSIONS AND PERSPECTIVES

Several collisional damping interfaces have been designed for our ESI-TOF spectrometer. Computer simulations and experiments performed in the instrument with the new interface indicate that collisional cooling of ions improves the quality of the primary ion beam orthogonally injected into the mass spectrometer. Very important characteristics of the instrument such as resolution and sensitivity were greatly improved. In addition, mass discrimination was reduced providing an observable mass range greater than 1MDa. The resulting instrument appears to be very useful for the study of large biological compounds and noncovalent complexes in particular. Many noncovalent complexes have been successfully studied in the TOF III with the new interface. One example of a such a system studied, that of *Escherichia coli* citrate synthase interacting with its allosteric inhibitor NADH, is reported in this thesis. The observation of large noncovalent complexes between citrate synthase dimers (M.W.= 95,770 Da) hexamers (M.W. ~287,320 Da) and a relatively small ligand (M.W. of NADH = 665 Da) demonstrates the capabilities of the mass spectrometer. Experience accumulated in the studies of these large macromolecular systems indicates that one of the major problems involved in observation of noncovalent complexes in an ESI-TOF instrument relates to the sufficient purification of a sample, and yet, not to the instrumental characteristics of the spectrometer. Many interesting macromolecular complexes have very large masses (for example, multi-component enzymes, intact viruses etc.) and the ways to achieve sufficient purity of the samples must be explored in the future.

Collisional cooling was also implemented for improving the ion beam quality of MALDI ions. High sensitivity and resolution have been achieved in the same TOF III mass spectrometer coupled to a MALDI source through a collisional damping interface. In addition, another interesting phenomenon was first predicted on the basis of computer simulations using the program described in the thesis, and then verified experimentally. This phenomenon is the formation of a quasi-continuous ion beam from an originally pulsed beam of MALDI ions. Thus, a rather novel concept of combining both very powerful ion sources, ESI and MALDI in the same TOF mass spectrometer has been introduced. It was shown that high performance can be achieved when both ion sources are coupled to the mass spectrometer through a collisional damping interface, which converts a pulsed beam of MALDI ions into an almost continuous beam, and leaves a beam of the electrosprayed ions as a continuous one. This approach appeared to be successful and the examples of electrospray and MALDI spectra obtained in the TOF III mass spectrometer have been shown. Recent results from the incorporation of a MALDI ion source in our tandem instrument (QqTOF) originally designed to operate with an ESI source, show competitive performance with the best axial MALDI instruments with delayed extraction. Resolution more than 10,000 and sensitivity in the attomole range for peptides with mass up to 5000 Da have been obtained in this instrument (these results will be published). Moreover, the MS/MS capabilities of the last instrument with both ESI and MALDI sources may be a great benefit especially when structural information is required. MS/MS mode of operation with MALDI ions is under investigation.

COMMENTS

The main results presented in this thesis have been published in several journals. The paper "A collisional damping Interface for an Electrospray Ionization Time-of-Flight Mass Spectrometer" by Krutchinsky, A.N.; Chernushevich, I.V.; Spicer, V.L.; Ens, W. and Standing, K.G. has been published in *Journal of American Society for Mass Spectrometry* **1998**, 9,569-579.

"Orthogonal Injection of Matrix-assisted Laser Desorption/Ionization Ions into a Time-of-Flight Mass Spectrometer Through a Collisional Damping Interface" by Krutchinsky, A.N.; Loboda, A.V.; Spicer, V.L.; Dworschak, R.; Ens,W. and Standing, K.G was published in *Rapid Communications in Mass Spectrometry*, **1998**, 12, 508-518.

Finally, the paper "Quantitative Evaluation of Protein-Protein and Ligand-Protein Equilibria of a Large Allosteric Enzyme by Electrospray Ionization Time-of-flight Mass Spectrometry" by Ayed, A.; Krutchinsky, A.N.; Ens, W.; Standing, K.G. and Duckworth, H.W. was published also in *Rapid Communication in Mass Spectrometry* **1998**, 12, 339-344.

Two patent applications related to results presented in "*Selective Collision-Induced Dissociation of Ions in the Quadrupole Ion Guide*" of the chapters II, and the chapter III have been submitted by the authors.

APPENDICES

I. Calculation of the Total Flight Time of Ions in the TOF Mass Spectrometer with orthogonal Injection.

Let's consider a special case only, when the mass spectrometer consists of one-stage accelerator, a field-free region and a simple one-stage mirror as shown in Figure 4. Then, the total ion flight time to the detector is the sum of three components:

$$t = t_1 + t_2 + t_3$$

where, t_1 is time an ion spends in the accelerator

t_2 is time an ion spends in the field-free region

t_3 is time an ion spends in the electrostatic mirror

Let's neglect the time an ion may spent in a post-acceleration region which, in some cases, is used to improve the detection efficiency of the detector. Since this region is usually small, the approximation is valid.

a. Computation of t_1

t_1 can be computed from the equation of ion motion in the accelerator:

$$d_a = at^2 / 2 + v_i t + z \qquad (1)$$

where, d_a is the length of the acceleration region measured relative to the origin, which coincides with the center of the orthogonally injected beam,

$$a = qV_a / md_a \qquad (2)$$

is acceleration of an ion with a charge q and mass m across a given potential V_a at the distance d_a.

$\upsilon_{\parallel}$ is an initial ion velocity along z-axis (can be negative and positive).

z is an initial ion position along z-axis.

Thus, t_1 is:

$$t_1 = \frac{\sqrt{\upsilon_{\parallel}^2 + 2a(d_a - z)} + \upsilon_{\parallel}}{a} \qquad (3)$$

neglecting a negative root of the quadratic equation.

Substituting the expression (2) for acceleration into (3) and making some re-arrangements gives:

$$t_1 = \frac{2d_a}{(2qV_a / m)}\left(\left(\upsilon_{\parallel}^2 + (2qV_a / m)\left(1 - \frac{z}{d_a}\right)\right)^{1/2} + \upsilon_{\parallel}\right) \qquad (4)$$

Introducing $\upsilon_a = (2qV_a / m)^{1/2}$ the velocity an ion gains after acceleration across the potential V_a,

$$t_1 = \frac{2d_a}{\upsilon_a^2}\left(\left(\upsilon_{\parallel}^2 + \upsilon_a^2\left(1 - \frac{z}{d_a}\right)\right)^{1/2} + \upsilon_{\parallel}\right) \qquad (5)$$

and finally,

$$t_1 = \frac{2d_a}{\upsilon_a}\left((1 - p)^{1/2} + \frac{\upsilon_{\parallel}}{\upsilon_a}\right) \qquad (6)$$

where,

$$p = \frac{z}{d_a} - \left(\frac{v_0}{v_a}\right)^2 \qquad (7)$$

is the energy deficit relative to the energy of the ion starting its movement at $z=0$ with no initial velocity v_0.

b. Computation of t_2

The velocity v_2 with which an ion leaves an acceleration column can be easily computed from:

$$v_2 = at_1 + v_0 \qquad (7)$$

Substitution of (2) and (6) into equation (7) gives:

$$v_2 = v_a(1-p)^{1/2} \qquad (8)$$

And thus, the time an ion spends in the field-free region of length D is:

$$t_2 = \frac{D}{v_2} = \frac{D}{v_a}(1-p)^{-1/2} \qquad (9)$$

c. Computation of t_3

In the electrostatic mirror, an ion undergoes first deceleration until it is totally stopped by a retarding potential and then re-acceleration back, toward a detector. Thus the time an ion spends in the mirror is

$$t_3 = 2(v_2 / a_m) \qquad (10)$$

where, a_m is acceleration of an ion in the mirror. It can be computed as:

$$a_m = qV_a / md_R = (2qV_a m)/ 2d_R = v_a^2 / 2d_R \qquad (11)$$

where, d_R is the depth of ion penetration into the mirror.

Substitution of (8) and (11) into (10) gives the time an ion spends in the mirror:

$$t_3 = \frac{4d_R}{v_a}(1-p)^{1/2} \tag{12}$$

Combining all terms, the total time is:

$$t = \frac{2d_a}{v_a}\left((1-p)^{1/2} + \frac{v_\parallel}{v_a}\right) + \frac{D}{v_a}(1-p)^{-1/2} + \frac{4d_R}{v_a}(1-p)^{1/2} \tag{13}$$

or,

$$t = \frac{D}{v_a}(1-p)^{-1/2} + \frac{2d_a + 4d_R}{v_a}(1-p)^{1/2} + \frac{2d_a}{v_a}\left(\frac{v_\parallel}{v_a}\right) \tag{14}$$

The parameter p is small comparative to unity because the width of the beam is small ($z \approx 0$) and, $v_\parallel << v_a$.

Then using Taylor expansion, some terms can be expressed as:

$$\begin{aligned}(1-p)^{-1/2} &= 1 + p/2 + 3p^2/8 + 5p^3/16 + \ldots\ldots \\ (1-p)^{1/2} &= 1 - p/2 - p^2/8 - p^3/16 - \ldots\ldots\end{aligned} \tag{15}$$

Keeping all terms up to the second order and collecting them in the final expression (14) for t, we get

$$t = \frac{D}{v_a}\left(1 + p/2 + 3p^2/8\right) + \frac{2d_a + 4d_R}{v_a}\left(1 - p/2 - p^3/8\right) + \frac{2d_a}{v_a}\left(\frac{v_\parallel}{v_a}\right) \tag{16}$$

The last expression can be re-written in more compact form:

$$t = \frac{Df_0}{v_a}\left[1 + f_1 p / f_0 + f_2 p^2 / f_0 + ...(2d_a / D)\left(v_{\parallel} / v_a\right)\right] \qquad (17)$$

where, $f_0 = 1 + (2d_a + 4d_R) / D$

$$f_1 = \frac{1}{2}\left[1 - (2d_a + 4d_R) / D\right]$$

$$f_2 = \frac{1}{8}\left[3 - (2d_a + 4d_R) / D\right]$$

The expression (17) was used in the text.

II. Computational Algorithm based on Monte Carlo Model for Simulation of Ion Motion in the Collisional Quadrupole Ion Guide.

Our simulation of the ion motion makes a number of simplifying assumptions. It is based on an iterative three step procedure:

1) We assume that the probability of having a collision in a distance *l* with a molecule of a buffer gas of density n is:

$$P(l) = e^{-\sigma n l} \tag{1}$$

The mean free path *fp* can then be computed as:

$$fp = -\frac{\ln(\xi_1)}{\sigma n} \tag{2}$$

where σ is the collision cross-section and ξ_1 is a random number between 0 and 1.

The time τ until the next collision is approximated as:

$$\tau = \frac{fp}{|\vec{v}_0|} \tag{3}$$

where $|\vec{v}_0|$ is the ion speed at the moment of collision.

2) Between collisions, the ion motion is modulated by the RF field and we numerically solve the Mathieu equation over a time interval τ using Euler's method [Press et al., 1988] with small time slices Δt (Δt<10 ns). The equations of motion in the x and y directions are defined by [Dawson, 1976]:

$$\frac{d^2x}{dt} + \frac{NeVx}{m_1 r_0^2}\cos\omega t = 0$$
$$\frac{d^2y}{dt} - \frac{NeVy}{m_1 r_o^2}\cos\omega t = 0 \qquad (4)$$

where: m_1 is the mass of the ion

e is the charge of an electron

N is the number of electronic charges on the ion

r_0 is half the spacing between opposite poles,

(3.5 mm in the present case)

w is the angular frequency of the RF field

V is the maximum amplitude of the RF field

The coordinate system is shown in Figure 7.

3) The ion's new velocity components $(v_{x'}, v_{y'}, v_{z'})$ after collision are computed based on a hard sphere collision model with stationary gas molecules.

In the coordinate system (x',y',z'), in which the direction of the z'-axis coincides with the direction of the initial velocity vector these components are:

$$v_{z'} = \frac{m_1 + m_2\cos\theta}{M}|\bar{v}_0|$$
$$v_{y'} = \frac{m_2}{M}|\bar{v}_0|\sin\theta\cos\phi \qquad (5)$$
$$v_{x'} = \frac{m_2}{M}|\bar{v}_0|\sin\theta\sin\phi$$

where m_1 is the mass of the ion

m_2 is the mass of the buffer gas molecule

$M = m_1 + m_2$

θ is the center-of-mass scattering angle.

ϕ is the azimuthal angle between the x'-axis and the plane of scattering.

For hard sphere collisions, the scattering is isotropic in the centre-of-mass system (CMS) [27], so the probability of scattering into the spherical polar element of solid angle $d\Omega = d\theta \sin\theta d\phi$ at angles (θ, ϕ) is:

$$P(\theta, \phi)d\Omega = \frac{d\theta \sin\theta d\phi}{4\pi} \tag{6}$$

Integrating over ϕ yields the probability of scattering through angle θ:

$$P'(\theta)d\theta = \frac{\sin(\theta)}{2} d\theta \tag{7}$$

For application of the Monte Carlo method we follow the standard procedure [see, for example, Sobol, 1974]] and set

$$\xi_2 = \int_0^{\theta} P'(\theta)d\theta = \frac{1 - \cos(\theta)}{2}$$

and, (8)

$$\xi_3 = \frac{\phi}{2\pi}$$

where ξ_2 and ξ_2 are random numbers between 0 and 1.

Figure 50 compares the distribution of scattering angles obtained in a typical run with the theoretical distribution given by equation (7) above.

Finally, all the velocity vector components are re-transformed into the original coordinate system (x,y,z) using a coordinate transformation [Beyer, 1987]. Then, we go back to step (1).

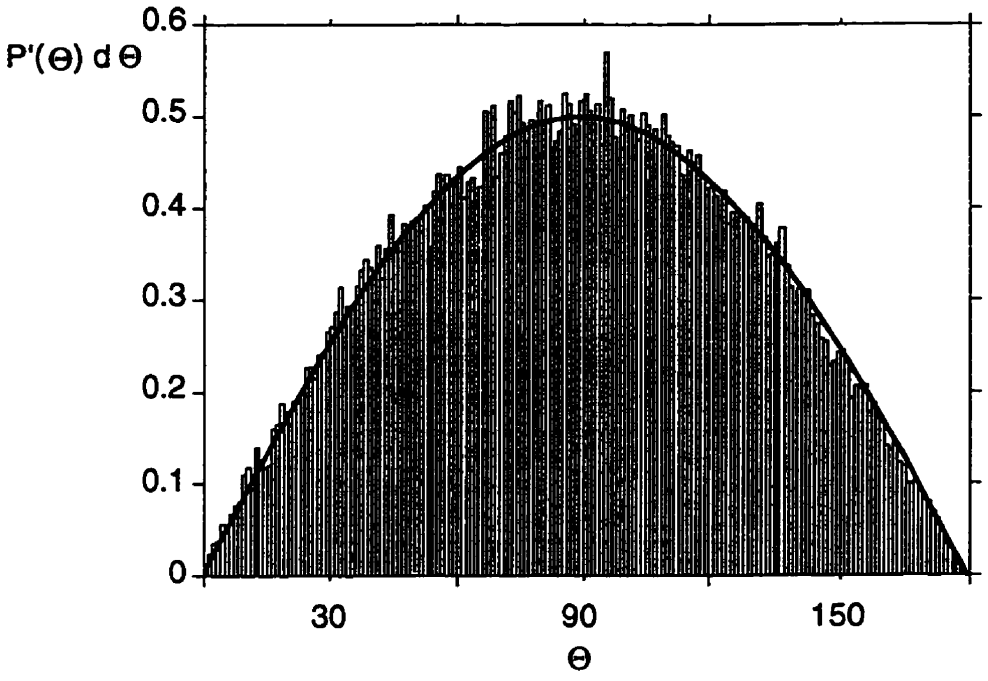

Figure 50. Comparison of the distribution of scattering angles obtained in a typical program run (histogram) with the theoretical distribution described by eq 7.

III A. Determinition of the Association Constant K_A for Dimer-Hexamer Equilibrium.

The association constant between dimers and hexamers of CS can be found if equilibrium between the two species is assumed:

$$[H] = K_A[D]^3 \qquad (1)$$

where $[H]$ is the concentration of the CS hexamer

$[D]$ is the concentration of the CS dimer, and

K_A is the association constant.

Assuming that only CS dimers and hexamers are present in the solution yields a simple equation:

$$[M] = 2[D] + 6[H] \qquad (2)$$

where $[M]$is the total concentration of CS monomer put into solution.

Parameters that can be measured rather precisely from experiment are the concentration of the CS monomers and *R*, the relative ratio of the dimer and the hexamer concentrations *(R=[D]/[H])* (corrected for the different sensitivity of the TOF mass spectrometer for dimers and hexamers, see below).

The above equations may then be rearranged:

$$[H] = K_A R^3 [H]^3 \qquad (1')$$

and,

$$[H] = [M]/(2R+6) \qquad (2')$$

Substitution of equation (2') into (1') gives:

$$[M]^2 = \left(\frac{1}{K_A}\right)\frac{(2R+6)^2}{R^3}$$

or,

$$[M] = \left(\frac{1}{K_A}\right)^{1/2}\frac{(2R+6)}{R^{3/2}} \qquad (3)$$

where $R=[D]/[H]$ is the relative ratio of the dimer and the hexamer concentrations. R was determined from each spectrum by integrating the relevant peaks, and correcting this value by some factor which takes into account different instrumental sensitivities for dimers and hexamers.

The correcting factor was found as follows: the sensitivity for "pure" hexamer was determined by using a sample of CS in excess NADH (10 μM CS subunits, 100 μM NADH, the latter being sufficient to shift CS completely to hexamer - see below). Sensitivity for "pure" dimer was determined using a sample of CS that had been alkylated at Cysteine-206 with 3,3,3-trifluoro-1-bromoacetone (TFBA); separate experiments showed that TFBA modification prevents hexamer formation in the concentration range we used (not shown). It was previously shown that TFBA alkylation of *E. coli* CS abolishes specific NADH binding [Weitzman, 1966]; the present finding, that TFBA-modified CS does not convert to hexamer, sufficiently explains why the modified enzyme

binds NADH only weakly. In TOF III mass spectrometer, the ratio of sensitivities for dimer and hexamer was found to be 1.3 ± 0.1, that is, an equimolar mixture of dimers and hexamers would give a peak area ratio of 1.3.

III B. Determinition of the Dissociation Constant K_D for NADH Binding.

A general treatment of the theory of multiple equilibria can be found in [Tanford, 1961]. However, it is informative to show the derivation of the equation for K_D explicitly.

Consider a protein (P) which has an N - identical independent binding sites to bind a ligand (L). A general expression describing the equilibrium between the protein with (n+1) bound ligands and one with n bound ligands, where n is some number between 0 and N, can be written as:

$$K_D[P \cdot (n+1)L] = [P \cdot nL]S \qquad (4)$$

where the statistical factor S is the ratio of the number of sites avalilable for binding $(N-n)$ and the number of ligands that can dissociate $(n+1)$.

K_D is the dissociation constant for an individual site.

For example, assuming 6 independent binding sites with equal K_D 's for the hexamer of CS, the equilibrium conditions for all 6 species can be written as:

$$\frac{K_D}{6}[H \cdot L] = [H] \cdot [L]$$

$$\frac{2K_D}{5}[H\cdot 2L]=[H\cdot L]\cdot[L]$$

$$\frac{3K_D}{4}[H\cdot 3L]=[H\cdot 2L]\cdot[L] \qquad (5)$$

$$\frac{4K_D}{3}[H\cdot 4L]=[H\cdot 3L]\cdot[L]$$

$$\frac{5K_D}{2}[H\cdot 5L]=[H\cdot 4L]\cdot[L]$$

$$6K_D[H\cdot 6L]=[H\cdot 5L]\cdot[L]$$

where $[L]$ is the concentration of free ligand, $[H]$ is the concentration of free hexamer, $[H\cdot L]$ is the concentration of the hexamer-(one ligand) complex etc.

Summing all equations and taking the denominator from the left hand site to the right hand site gives:

$$K_D([H\cdot L]+2[H\cdot 2L]+3[H\cdot 3L]+4[H\cdot 4L]+5[H\cdot 5L]+6[H\cdot 6L])=$$

$$=[L](6[H]+5[H\cdot L]+4[H\cdot 2L]+3[H\cdot 3L]+2[H\cdot 4L]+[H\cdot 5L]) \qquad (6)$$

The last equation can be rewritten as:

$$K_D\sum_{i=0}^{6} i[H\cdot iL]=[L]\left(6\sum_{i=0}^{6}[H\cdot iL]-\sum_{i=0}^{6} i[H\cdot iL]\right) \qquad (7)$$

noting that $i[H\text{-}iL]=0$ for i=0.

Introducing $\langle N\rangle$, the average number of occupied sites as:

$$\langle N \rangle = \frac{\sum_{i=0}^{6} i[H \cdot iL]}{\sum_{i=0}^{6} [H \cdot iL]} \tag{8}$$

the equation (7) becomes:

$$K_D \langle N \rangle = [L](6 - \langle N \rangle)$$

or,

$$\frac{\langle N \rangle}{6} = \frac{[L]}{[L] + K_D} \equiv \bar{n} \tag{9}$$

where $\bar{n}$ is the average occupancy or the average number of ligands bound per subunit of the haxamer.

The average number of ligands bound per subunit of an oligomercan be found directly from the mass spectra by measuring the average mass of the oligomer-ligand complexes formed:

$$\bar{n} = \frac{1}{N} \frac{\langle M \rangle - M_0}{m_L} \tag{10}$$

where N is a number of subunits in the oligomer

$\langle M \rangle$ is the average mass the oligomer-ligand complexes

M_0 is the average mass of the oligomer itself,

m_L is the average mass of the ligand.

Validity of this expression depends on the precision with which the bound species are resolved in the mass spectra, since we assume binding of only one type of ligand. In particular, undetected adducts such as sodium, potassium, water molecules of etc. would complicate the situation and lead to errors in determining K_D.

To express $[L]$, the concentration of free ligand, by measured parameters, consider the following equation:

$$[L]_{total} = [L]_{free} + [L]_{bound} \tag{11}$$

where the amount of bound ligandis given by:

$$[L]_{bound} = [L]_D + [L]_H \tag{12}$$

where $[L]_D = \langle N \rangle_D [D]$ and $[L]_H = \langle N \rangle_H [H]$. Here the subscripts indicate the oligomeric forms considered.

Using equations (2') and (12), the concentration of the free ligand can be calculated as:

$$[L]_{free} = [L]_{total} - [M]\frac{\langle N \rangle_D R + \langle N \rangle_H}{2R+6} \tag{13}$$

Note that in all expressions, R, which is the ratio of the dimers to the hexamers found from the spectra, was corrected by factor 1/1.3 because of the different sensitivity of TOF III mass spectrometer for the dimers and hexamers, as explained in the previous section.

REFERENCES

1. Aleksandrov, M. L.; Gall, L.N.; Krasnov, V.N.; Nikolaev, V, I.; Pavlenko, V.A.; Shkurov, V.A. *Dokl. Akad. Nauk.* SSSR **1984**, 277, 379-383.
2. Aleksandrov, M.L.; Gall, L.N.; Krasnov, V.N.; Nikolaev, V.I.; Pavlenko, V.A.; Shkurov, V. A.; Baram, G.I.; Gracher, M.A.; Knorre, V.D.; Kusner, Y. S. *Biorg. Kim.* **1984**, 10, 710-712.
3. Andersen, J.S.; Svenson B.; Roepstorff, P. *Nature Biotechnology* **1996**, 14, 449-457.
4. Anderson, D.A.; Duckworth, H.W. *J. Biol. Chem.* **1988**, 263, 3263-2169.
5. Annan, R.C.; Köchling,. H.J.; Hill, J.A.; Biemann K. *Rapid Commun. Mass Spectrom.* **1992**, 6, 298-302. 10
6. Ayed, A.; Krutchinsky, A.N.; Ens, W.; Standing, K.G.; Duckworth, H.W. *Rapid Commun. Mass Spectrom.* **1998**, 12, 339-344.
7. Bakker, J.M.B. *J. Phys. E* **1973**, 6, 785-789.
8. Bakker, J.M.B. . *J. Phys. E* **1974**, 7, 364-368.
9. Banks, J.F. Jr.; Shen, S.; Whitehouse, C M.; Fenn, J.B. *Anal. Chem.* **1994**, 66, 406-414.
10. Beavis, R.C.; Chait, B.T. *Chem. Phys. Let.* **1991**, 181, 479-484.
11. Beavis, R.C.; Chait, B.T. Rapid *Commun. Mass Spectrom.* **1989**, 3, 432-435.
12. Beavis, R.C.; Chaudhary, T.; Chait, B.T. *Org. Mass. Spectrom.* **1992**, 27, 156-158.
13. Beavis, R.C. in proceedings of the *Sanibel Conference on Mass Spectrometry*, Snibel Island, FL, 24-27 January, **1998**, p101.
14. Boyle , J.G.; Whitehouse, G.M; Fenn, J.B. *Rapid Commun. Mass Spectrom.* **1991**, 5, 400-405 .
15. Boyle, J.G.; Whitehouse, G.M. *Anal. Chem.* **1992**, 64, 2048-2089.
16. Brown R.C.; Lennon, J.J. *Anal.Chem.* **1995**, 67, 1998-2003.

17. Buchanan, M.V.; Hettich, R.L. *Anal.Chem.* **1993**, 65, 254A-259A.

18. Cameron, A.E.; Eggers, D.F., Jr., *Rev. Sci. Instr*um. **1948**, 19, 605-607.

19. Chait B. T.; Kent S.B.H, *Science* **1992**, 257, 1885-1894.

20. Chen, Y.-L.; Collings, B.A.; Douglas, D.J. *J. Am. Soc. Mass Spectrom.* **1997**, 8, 681-687.

21. Chernushevich, I.V. reported at the *Sanibel Conference on Mass Spectrometry*, Sanibel Island, FL, January 24-27, **1998**.

22. Chernushevich, I.V.; Ens, W.; Standing, K.G. in *New Methods for the Study of Biomolecular Complexes*, Kluwer Academic Publishers, Dordrecht, **1998**, pp. 101-116.

23. Chernushevich, I.V.; Ens, W.; Standing. K.G.; Loewen, P.C.; Fitzgerald, M.C.; Kent, S.B.H.; Werlen, R.C.; Lankinen, M.; Tang, X.-J.; Brewer, C.F.; Saha, S. *Proceedings of the 44th ASMS Conference on Mass Spectrometry and Allied Topics*; Atlanta, GA, May 21-26, **1995**, p. 1327.

24. Chernushevich, I.V.; Krutchinsky, A.N.; Ens, K.G.; Standing, K.G. *Proceedings of the 44th ASMS Conference on Mass Spectrometry and Allied Topics*; Portland, OR, May 12-16, **1996**, p. 751.

25. Chernushevich, I.V.; Ens, W.; Standing, K.G. In *Electrospray Ionization Mass Spectrometry*; Cole, R.B. (Ed.); Wiley & Sons Inc., NY, **1997**, pp. 203-234.

26. Chowdhury, S.K.; Katta, V.; Chait, B.T. *Rapid Commun. Mass Spectrom.* **1990**, 4, 81-87.

27. Cohen, S. L.; Chait, B.T. *Anal. Chem.* **1996**, 68, 31-37.

28. Colby , S.M.; King, T.B.; Reilly, J.P. *Rapid Commun. Mass Spectrom.* **1994**, 8, 865-869.

29. Cole, R.B.; Ed., *Electrospray Ionization Mass Spectrometry*, John Wiley& Sons, Inc. New York, **1997**.

30. Cotter, R.J. *Anal. Chim. Acta* **1987**, 195, 45-59.

31. Cotter, R.J. *Time-of-Flight Mass Spectrometry: Instrumentation and Applications in Biological Research*; ACS Professional reference books; American Chemical Society, Washington, DC, **1997**.

32. Covey, T. R.; Bonner, R.F.; Shushan, B. I.; Henion, J. D. *Rapid Commun. Mass Spectrom.* **1988**, 2, 249-256.

33. Covey, T.; Douglas, D.J. *J. Am. Soc. Mass Spectrom.* **1993**, 4, 616-623.

34. Cox, K.A.; Williams, J.D.; Cooks, R.G.; Kaiser Jr., R.E. *Biol. Mass Spectrom.* **1992**, 21, 226-241.

35. Cramer, R.; Hillenkamp, F.; Haglund, R.F., Jr., *J. Am. Soc. Mass Spectrom.* **1996**, 7, 1187-1193.

36. Dawson, P.H. In *Quadrupole Mass Spectrometry and its Applications*, Elsevier Scientific Publishing Company, Amsterdam, **1976**, p. 14.

37. Dodonov , A.F., Chernushevich, I.V.; Laiko, V.V. In *Time-of-Flight Mass Spectrometry*; Cotter, R.J., Ed.; ACS Symposium Series; American Chemical Society: Washington, DC, **1994**, p.108

38. Dodonov, A.F.; Chernushevich, I.V.; Dodonova, T.F.; Raznikov, V.V.; Tal'rose, V.L. (inventors), Inventors Certificate No. 1681340A1, February **1987**, USSR.

39. Dodonov, A.F.; Kozlovsky,V.I.; Loboda, A.; Raznikov, V.; Suleimenkov, I.; Tolmachev, A.; Kraft, A.; Wolnik, H. *Rapid Commun. Mass Spectrom.* **1997**, 11, 1649-1656.

40. Dole, M.; Mack, L.L.; Hines, R.L.; Mobley, R.C.; Ferguson, L.D.; Alice, M.B. *J. Chem. Phys.* **1968**, 49, 2240-2249.

41. Donald, L.J.; Crane, B.R.; Anderson, D.H; Duckworth, H.W. *J. Biol. Chem.* **1991**, 266, 20709-20713.

42. Doroshenko, V.M.; Cotter, R.J. *J. Mass Spectrom.* **1998**, 33, 305-318.

43. Duckworth, H.W.; Bell, A.W. *Can. J. Biochem.* **1982**, 60, 1143-1147.

44. Duckworth, H.W.; Tong, E.K. *Biochemistry* **1976**, 15, 108-114.

45. Duoglas, D.J.; French, J.B. *J. Am. Soc. Mass Spectrom.* **1992**, 3, 398-408.

46. Ehring, H.; Sundqvist, Bo U.R *J. Mass Spectrom.* **1995**, 30, 1303-1310.

47. Ens W.; Dworschak, R.; Spicer, V.; Standing, K.G.; Verentchikov, A. In *Proceedings of the 43th ASMS Conference on Mass Spectrometry and Allied Topics*; Atlanta, GA, May 21-26, **1995**, p. 1219.

48. Ens, W.; Standing. K.G.; Verentchikov, A. In *Proceedings of the International Conference on Instrumentation for Time-of-Flight Mass Spectrometry*; November 11-12, **1992**, Chestnut Ridge, NY, p.137-147.

49. Ens,W.; Mao, Y.; Mayer, F.; Standing K.G. *Rapid Commun. Mass Spectrom.* **1991**, 5, 117-123.

50. Ens,W.; reported at the *46th Conference on Mass Spectrometry and Allied Topics*, Orlando, FL, May31-June 4, **1998.**

51. Feng, R.; Konishi, Y. *Anal.Chem.* **1992**, 64, 2090-2095.

52. Fenn, J.B.; Mann, M.; Meng, C.K.; Wong, S.F.; Whitehouse, G.M. *Mass Spectrom. Rev.* **1990**, 9, 37-70.

53. Fenn, J.B.; Mann, M.; Meng, C.K.; Wong, S.F.; Whitehouse, M. *Science* **1989**, 246, 64-72.

54. Fuerstenau, S.D.; Benner, H.W. *Rapid Commun. Mass Spectrom.* **1995**, 9,1528-1538.

55. Gale, D.C.; Smith, R.D. *Rapid Commun. Mass Spectrom.* **1993**, 7, 1017-1021.

56. Ganem, B.; Li, Y-T.; Henion, J.D. *J. Am. Chem. Soc.* **1991**, 113, 6294-6296.

57. Gerlich, D. In *State-Selected and State-to-State Ion-Molecule Reaction Dynamics, Part 1: Experiment*; Ng, C-Y.; Baer, M. (Edts.); Advances in Chemical Physics Series, Vol. LXXXII.; John Wiley & Sons, New York, **1992**

58. Guevremont, R.; Siu, K.W.M.; Le Blank, J.C.Y.; Berman, S.S. *J. Am. Soc. Mass Spectrom.* **1992**, 3, 216-224.

59. Guilhaus, M. *J. Am. Soc. Mass Spectrom.* **1994**, 5, 588-595.

60. Henry, K.D.; Quinn, J.P.; McLafferty, F.W. *J. Am. Chem Soc.* **1991**, 113, 5447-5450.

61. Hillenkamp F.; Karas. M.; Beavis R.; Chait B.T., *Anal. Chem.* **1991**, 63, 1193A-1203A.

62. Hines, R.T. *J. Appl. Phys.* **1966**, 37, 2730-2736.

63. Ikonomou, M.G.; Kebarle, P. *J. Am Soc Mass Spectrom.* **1994**, 791-793.

64. Iribarne, J.V.; Dziedzic, P.J.; Thomson, B.A. *Int. J. Mass Spectrom. Ion Phys.* **1983**, 50, 331-337.

65. Johnson, R.E. *Int. J. Mass Spectrom. Ion Proc.* **1994**, 139, 25-38.

66. Johnson, R.E.; Sundqvist, Bo U.R. *Rapid Commun. Mass Spectrom.*, **1991**, 5 574-578.

67. Kaiser, R.E. Jr.; Cooks, R.G.; Stafford, G.C.; Syka, J.E.P.; Hemberger, P.H. *Int. J. Mass Spectrom. Ion Processes* **1991**, 106, 79-115.

68. Karas, M.; Glückman M. In proceedings of the *Sanibel Conference on Mass Spectrometry*, Sanibel Island, FL, January 24-27, **1998**, 12-17

69. Karas, M.; Hillenkamp, *Anal. Chem.* **1988**, 60, 2299-2301.

70. Katta, V.; Chait, B.T. *J. Am. Chem. Soc.* **1991**, 113, 8534-8535.

71. Kebarle, P.; Tang, L. *Anal.Chem.* **1993**, 65, 972A-986A.

72. Kofel, P.; Stöckli, M.; Krause, J.; Schlunegger, U.P. *Rapid Commun. Mass Spectrom.* **1996**, 10, 658-662.

73. Kriger, M.S.; Cook, K.D.; Ramsey, R.S. *Anal. Chem.* **1995**, 67, 385-389.

74. Krutchinsky A.N.; Ayed, A.; Chernushevich, I.V.; Ens, W.; Standing, K.G.; Duckworth, H. W. In *New Methods for the Study of Biomolecular Complexes*, Kluwer, Dordrecht **1998**, pp 135-140.

75. Krutchinsky A.N.; Dolgin, A.I.; Khodorkovski, M.A. *Anal. Chem.* **1995**, 67, 1963-1967.

76. Laiko, V.V.; Dodonov, A.F. *Rapid Commun. Mass Spectrom.* **1994**, 8, 720-726.

77. Liao, P-.C.; Allison, J. *J. Mass Spectrom.* **1995**, 30, 408-423.

78. Loboda A.V.; Krutchinsky, A.N; Ens, W.; Standing, K.G. some preliminary results on a MALDI QqTOF system have been reported at SCIEX Inc., July, **1998**.

79. Loo, J.A. *Mass Spectrom. Rev.* **1997**, 16, 1-23.

80. Loo, J.A.; Udseth, H.R.; Smith, R.D. *Anal. Bioch.* **1989**, 179, 404-412.

81. Loo, J.A; Edmonds, C.G.; Udseth, H.R.; Smith, R.D. *Anal.Chem.* **1990**, 62, 693-698.

82. Mack, L.L.; Kralik, P.; Rheude, A.; Dole, M. *J. Chem. Phys.* **1970**, 52, 4977-4986.

83. Mamyrin, B.A.; Karateav, V.I.; Schmickk, D.V.; Zagulin, V.A. *Sov. Phys. JETP* **1973**, 37, 45.

84. Mirza, U.A.; Chait, B.T. *Anal. Chem.* **1994**, 66, 2898-2904.

85. Mirza, U.A.; Cohen, S. L.; Chait, B.T. *Anal. Chem.* **1993**, 65, 1-6.

86. Mlynski, V.; Guilhaus, M. *Rapid Commun. Mass Spectrom.* **1996**, 10, 1524-1530.

87. Morris, H.R.; Paxton, T.; Dell, A.; Langhorne, J.; Berg, M.; Bordoli, R.; Hoyes, J.; Bateman, R.H. *Rapid Commun Mass Spectrom.* **1996**, 10, 889.

88. Ner, S.S.; Bhayana, V.; Bell, A.W.; Giles, I.C.; Duckworth, H,W.; Bloxham, P.D. *Biochemistry* **1983**, 22, 5243-5249.

89. Niu, S.; Zhang, W.; Chait, B.T. *J. Am. Soc. Mass Spectrom.* **1998**, 9, 1-7.

90. O'Halloran, G.J.; Fluegge, R.A. et al., *Determinition of Chemical Species Prevalent in a Plasma Jet*; Technical documentary report No. ASD-TDR-62-644, Bendix Corporation, April 1964.

91. Overberg, A.; Karas, M.; Hillenkamp, F. *Rapid Commun. Mass Spectrom.* **1991**, 5, 128-131.

92. Poppe-Schriemer, N.; Ens, W.; O'Neil, J.D.; Spicer. V.; Standing. K.G.; Westmore, J.B.; Yee, A.A. *Int. J. Mass Spectrom Ion Precesses* **1995**, 143, 65-85.

93. Price, D.; Milnes, G.J. *Int. J. Mass Spectrom. Ion Proc.* **1990**, 99, 1-39.

94. Purves, R.; Liang, Li. *J. Am. Soc. Mass Spectrom.* **1997**, 8, 1085-1093.

95. Qian, M.G.; Lubman, D.M. *Anal. Chem.* **1995**, 7, 234A-242A.

96. Qin, J.; Cait, B.T. *Anal. Chem.* **1996**, 68, 2102-2112.

97. Quist, A.P.; Huth-Fehre, T.; Sundqvist, Bo U.R. *Rapid Commun. Mass Spectrom.* **1994**, 8, 149-154.

98. Roepstorff, P.; Fohlman, J. *Biomed. Mass Spectrom.* **1984**, 11 601.

99. Schmelzeisen-Redeker, G.; Buttering, L.; Röllgen, F.W. *Int J. Mass Spectrom. Ion Proc.* **1989**, 90, 139-150.

100. Shevchenko, A.; Chernushevich, I.V.; Ens,W.; Standing, K.G.; Thomson, B.; Wilm, M.; Mann, M. *Rapid Commun. Mass Spectrom.* **1997**, 11, 1649-1656.

101. Sin, C.H.; Lee, E.D.; Lee, M.L. *Anal. Chem.* **1991**, 63, 2897-2900.

102. Siu, K.W.M.; Guevremont, R.; Le Blank, J.C.Y.; O'Brien, R.T.; Berman, S.S. *Org. Mass Spectrom.* **1993**, 28, 579-584.

103. Smith, R.D.; Barinaga, C.J.; Udseth, H.R., *Anal. Chem.* **1988**, 60, 1948-1952.

104. Smith, R.D.; Light-Wahl, K. J. *Biol. Mass Spectrom.* **1993**, 22, 493-501.

105. Smith, R.D.; Loo, J.A.; Ogorzalek Loo R.R.; Busman M.; Udseth H.R. *Mass Spectrom. Rev.* **1991**, 10, 359-451.

106. Spengler, B.; Cotter, R.J. *Anal. Chem.* **1990**, 62, 793-796.

107. Spengler, B.; Kirsch, D.; Kaufmann, R. *Rapid Commun. Mass Spectrom.* **1992**, 6, 105-108.

108. Spengler, B.; Kirsch, D.; Kaufmann, R.; Lemoine, J. *J. Mass Spectrom.* **1995**, 30, 782-795.

109. Stephens, W.E. *Phys. Rev.* **1946**, 69, p. 691.

110.Tanaka, K.; Waki, H.; Ido, Y.; Akita, S.; Yoshida, Y.; Yoshida, T. *Rapid Commun Mass Spectrom.* **1988**, 2, 151-153.

111.Tang X. Ph.D. Thesis, University of Manitoba, **1991**

112.Tang, X.-J.; Brewer, C.F.; Saha, S.; Chernushevich, I.V.; Ens, W.; Standing, K.G. *Rapid Commun. Mass Spectrom* **1994**, 8, 750-754.

113.Tang, X.; Beavis, R.; Ens, W.; Lafortune, F.; Schueler, B.; Standing, K.G. *Int. J. Mass Spectrom. Ion Processes* **1988**, 85, 43-67.

114.Thomson, B.A.; Douglas, D.J.; Corr, J.J.; Hager, J.W.; Joliffe, C.L. *Anal. Chem.* **1995**, 67, 1696-1704.

115.Thomson, B.A.; Iribarne, J.V. *J. Chem. Phys.* **1979**, 71, 4451-4463.

116.Tolmachev, A.V.; Chernushevich, I.V.; Dodonov, A.F.; Standing, K.G. *Nucl. Instr. and Meth. B.***1997**, 124, 112-119.

117.Tong, E.K.; Duckworth, H.W. *Biochemistry* **1975**, 14, 235-241.

118.Vachet, R.W.; Glish, G.L. *J. Am. Soc. Mass Spectrom.* **1996**, 7, 1194-1202.

119.Van der Bergh, P.; Franchoo, S.; Gentens, J.; Huyuse, M.; Kudryavtsev, Y.A.; Piechaczek, A.; Raabe, R.; Reusen, I.; Van Duppen, P.; Vermeeren, L.; Wöhr, A. *Nucl. Instr. and Meth. in Phys. Res. B* **1997**, 126, 194-197.

120.Verenchikov, A.; Ens, W.; Standing, K.G. *Anal. Chem.* **1994**, 66, 126-133.

121.Vertes, A. In *Methods and Mechanisms for Producing Ions from Large Molecules*; Standing, K.G and Ens, W., Eds.; NATO ASI Series B: Physics Vol 269.; Plenum Press, New York, **1991**, pp 275-291.

122.Vestal, M., in proceedings of the *Sanibel Conference on Mass Spectrometry*, Snibel Island, FL, 24-27 January, **1998**.

123.Vestal, M.; Juhasz, P.; Martin, S. A. *Rapid Commun. Mass Spectrom.* **1995**, 9, 1044-1051.

124.Vorm, O.; Roepstorff, P.; Mann, M. *Anal. Chem.* **1994**, 66, 3281-3287.

125.Wachs, T.; Henion, J. Proceedings of the *39th Conference on Mass Spectrometry and Allied Topics*; Nashville, TN; May 19-24, **1991**, p. 1358.

126.Wang, B.H.; Dreisewerd, K.; Bahr, U.; Karas, M.; Hillenkamp, F. *J. Am. Soc. Mass Spectrom.* **1993**, 4, 393-398.

127.Weitzman, P.D.J *Biochem J.* **1966**, 101, 44C-45C.

128.Weitzman, P.D.J. *Biochim. Biophys. Acta* **1966**, 128, 213-215.

129.Weitzman, P.D.J.; Jones, D. *Nature* **1968**, 219, 270-272.

130.Westmacott, G.; Ens, W.; Standing, K.G. *Nucl. Instr. and Meth. B* **1996**, 108, 282-289.

131.Wiley, W.C.; McLaren I.H. *Rev. Sci. Instrum.* **1955**, 26, 1150-1157.

132.Wiliams, P. *Int. J. Mass Spectrom. Ion Processes* **1994**, 131, 335-344.

133.Wilm, M.; Shevchenko, A.; Houthaeve, T.; Breit, S.; Schweigerer, L.; Fotsis, T.; Mann, M. *Nature* **1996**, 379, 466-469.

134.Wilm, M.S.; Mann, M. *Int. J. Mass Spectrom. Ion Proc.* **1994**, 136, 167-180.

135.Wiza, J.L. *Nucl. Instr. Meth.* **1979**, 162, 578-601.

136.Xiang, F.; Beavis, R.C. *Rapid Commun. Mass Spectrom.* **1994**, 8, 199-204.

137.Xu, H.J.; Wada, M.; Tanaka, J.; Kawakami, H.; Katayama, I. *Nucl. Instrum. Methods A* **1993**, 333, 274-281.

138.Yamashita, M.; Fenn, J. B. *J. Phys. Chem.* **1984**, 88, 4451-4459.

139.Yates III, J.R. *J. Mass Spectrom.* **1998**, 33, 1-19.

140.Yefchak , G.E.; Schultz, G.A.; Allison, J.; Enke, C.G.; Holland, J.F. *J. Am. Soc. Mass Spectrom.* **1990**, 1, 440-447.

141.Yphantis, D.A. *Biochemistry* **1964**, 3, 297-317.

142.Zhou, J.; Ens, W.; Standing, K.G.; Verentchikov, A. *Rapid Commun. Mass Spectrom.* **1992**, 6, 671-678.

143.Zhou, J.; Lee, T.D. *J. Am. Soc. Mass Spectrom.* **1995**, 6, 1183-1189.

IMAGE EVALUATION TEST TARGET (QA-3)

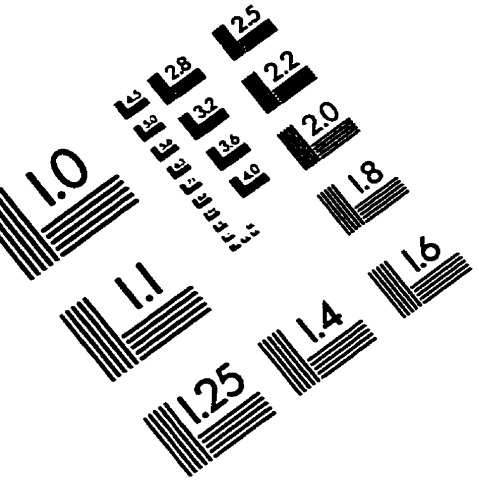

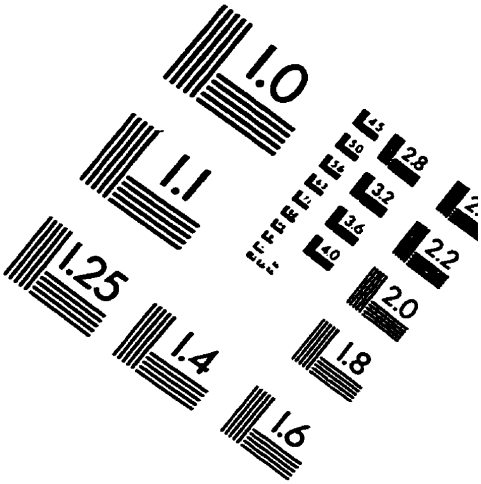

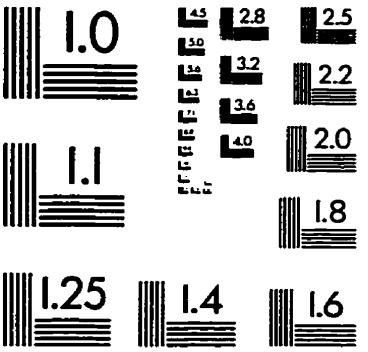

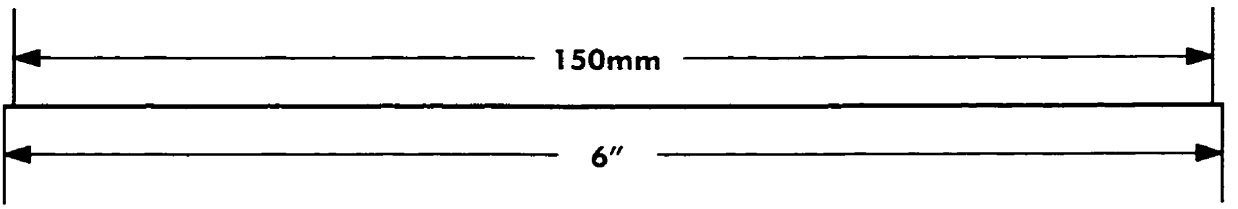

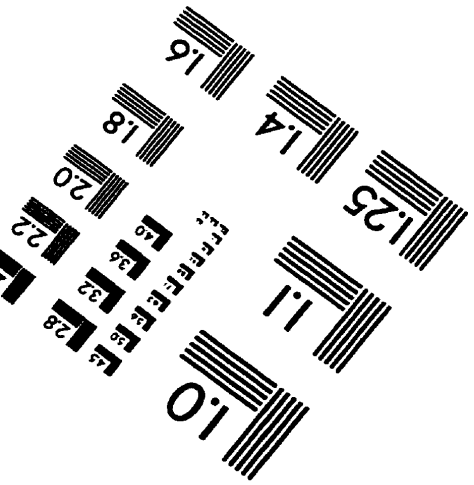

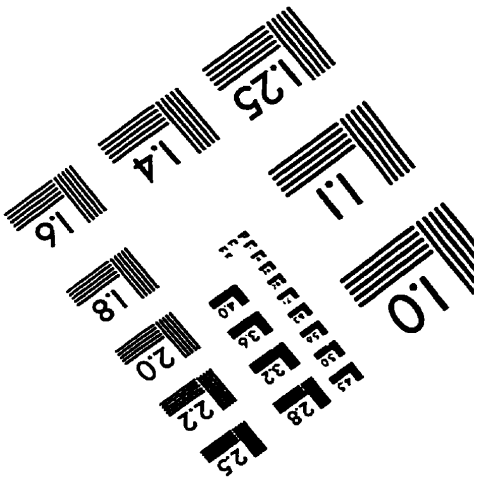

APPLIED IMAGE, Inc
1653 East Main Street
Rochester, NY 14609 USA
Phone: 716/482-0300
Fax: 716/288-5989